RECEIVED
LAWRENCE
RADIATION LABORATORY

NOV 17 1970

LIBRARY AND
DOCUMENTS SECTION

UCRL-19672

c.2

I. THE HEAT CAPACITY OF THE KONDO STATE IN COPPER-CHROMIUM AND COPPER-IRON
II. SEARCH FOR SUPERCONDUCTIVITY IN LITHIUM AND MAGNESIUM

Baylor Bunting Triplett
(Ph. D. Thesis)

September 1970

AEC Contract No. W-7405-eng-48

TWO-WEEK LOAN COPY

This is a Library Circulating Copy which may be borrowed for two weeks. For a personal retention copy, call Tech. Info. Division, Ext. 5545

UCRL-19672 c.2

LAWRENCE RADIATION LABORATORY
UNIVERSITY of CALIFORNIA BERKELEY

DISCLAIMER

This document was prepared as an account of work sponsored by the United States Government. While this document is believed to contain correct information, neither the United States Government nor any agency thereof, nor the Regents of the University of California, nor any of their employees, makes any warranty, express or implied, or assumes any legal responsibility for the accuracy, completeness, or usefulness of any information, apparatus, product, or process disclosed, or represents that its use would not infringe privately owned rights. Reference herein to any specific commercial product, process, or service by its trade name, trademark, manufacturer, or otherwise, does not necessarily constitute or imply its endorsement, recommendation, or favoring by the United States Government or any agency thereof, or the Regents of the University of California. The views and opinions of authors expressed herein do not necessarily state or reflect those of the United States Government or any agency thereof or the Regents of the University of California.

TABLE OF CONTENTS

I. THE HEAT CAPACITY OF THE KONDO STATE IN COPPER-CHROMIUM AND COPPER IRON

ABSTRACT ---------- v

LIST OF SYMBOLS ---------- viii

A. Introduction: Localized Moments and the Kondo State ------- 1

B. Experimental Techniques: 0.3K to 25K ---------- 13

1. Cryostat ---------- 13

2. Thermometry ---------- 14

3. Sample Holder ---------- 15

4. Superconducting Magnet ---------- 20

C. Experimental Techniques: 0.06K to 1.0K ---------- 22

1. Cryostat and Sample Holder ---------- 22

2. Thermometer Calibration ---------- 24

D. Sample Preparation and Analysis ---------- 29

1. Preparation ---------- 29

2. Analysis and Resistivity Measurements ---------- 31

E. Data Analysis ---------- 37

1. Addenda: Sample Holder and Pure Copper ---------- 37

2. The Nuclear Schottky Heat Capacity and Localized Moment Effects ---------- 41

3. Data ---------- 44

F. Results and Discussion ---------- 85

1. Kondo State Heat Capacity in Cu-Cr ---------- 85

2. Kondo State Heat Capacity in Cu-Fe ---------- 88

3. Interactions ---------- 99

4. Magnetic Degradation of the Kondo State in Cu-Cr ------- 103

G. Conclusion---------- 105

REFERENCES (I)---------- 111

FIGURE CAPTIONS (I)----------116

II. SEARCH FOR SUPERCONDUCTIVITY IN LITHIUM AND MAGNESIUM

A. Introduction---------- 143

B. Experimental----------147

1. Cryostat, Field and Susceptibility Measurements--------147

2. Nuclear Orientation Thermometry----------151

C. Results----------157

D. Conclusion----------160

APPENDIX: The Heat Capacity of Tungsten - Implications for the Cerium Magnesium Nitrate Temperature Scale----------161

TABLES----------166

REFERENCES (II)----------172

FIGURE CAPTIONS (II)----------175

ACKNOWLEDGEMENTS---------- 179

I. THE HEAT CAPACITY OF THE KONDO STATE IN COPPER-CHROMIUM AND COPPER-IRON

II. SEARCH FOR SUPERCONDUCTIVITY IN LITHIUM AND MAGNESIUM*

Baylor B. Triplett

Inorganic Materials Research Division, Lawrence Radiation Laboratory
Department of Chemistry, University of California
Berkeley, California 94720

ABSTRACT

I

Measurements of the heat capacities of 81.4, 195, 640, and 2560 at ppm solutions of Fe in Cu and 21.2, 33.6, and 51 at ppm solutions of Cr in Cu have been made in order to determine the concentration proportional heat capacity characteristic of the spin-compensated state. For Cu-Cr the results are in excellent agreement with the recent theoretical calculations of Bloomfield and Hamann above 0.1 T_K. The fit determines $T_K = 2.1$ K in agreement with the value 2.2 K derived from recent interpretation of the resistivity. The entropy associated with the formation of the Kondo state is $(1.05 \pm 0.10)R \ln 4$ in agreement with the value expected for a spin 3/2 system and in disagreement with an earlier report of a value significantly less than $R \ln 4$. The entropy as a function of temperature is used to represent the thermal destruction of the spin-compensated state.

---

*Submitted for publication in the Journal of Low Temperature Physics, UCRL-19650.

Heat capacity measurements on the Cu-Cr samples in magnetic fields up to 38 kOe indicate the Kondo state is destroyed more gradually in large magnetic fields than indicated in a recent NMR analysis.

The Cu-Fe data on the high temperature side of the anomaly are less accurate but are also consistent with an entropy of R ln 4 and the value $T_K \sim 34K$ obtained from the resistivity. The field dependence of the heat capacity suggests that the $T^{-1/2}$ term in the susceptibility, the poor agreement with T_K determined from the low temperature susceptbility and the anomalous NMR and Mössbauer measurements are associated with Fe-Fe interactions and are not representative of the spin-compensated state. The data suggest a new, simpler interpretation of these measurements. The application of fields ~30 kOe results in the suppression of interaction effects below ~3K while having little effect on the compensated state heat capacity.

II

Recent theoretical work suggests that magnesium and lithium should be superconducting in the millikelvin range of temperature. We have cooled samples of each of these metals to a temperature of 4 mK, measured by a gamma-ray anisotropy thermometer. Although the magnetic field was less than 10^{-2} Oe, no superconducting transitions were observed. The use of a nuclear orientation thermometer employing ^{60}Co in single-crystal (hcp) cobalt is described.

In view of the concern over the use of the susceptibility of powdered cerium magnesium nitrate to represent temperatures in the mK range,

we have accurately measured the heat capacity of a high-purity tungsten sample. The results are not in agreement with the recent thermodynamic analysis of the critical field curve for tungsten and imply a larger upper limit to Δ in the equation $T = T^* + \Delta$ where T^* is the magnetic temperature defined by setting $\chi(\mathrm{CMN}) = C/T^*$ for powdered CMN.

LIST OF SYMBOLS

	Quantities
$\mathcal{H}$	Hamiltonian
N	number of atoms
J	effective average of exchange integrals
$\vec{k}$	wavevector
$\vec{R}_n$	position vector of atom n in a periodic lattice
$a^*_{k\uparrow}, a_{k\uparrow}$	creation and destruction operators for itinerant electrons with wavevector $\vec{k}$ and spin $\uparrow$
$a^*_{n\downarrow}, a_{n\downarrow}$	creation and destruction operator for localized electrons on atom n with spin $\downarrow$
S_n	spin operator of magnitude 1/2 for electron localized on atom n
$\phi(\vec{r})$	Bloch function
$\omega(\vec{r}-\vec{R}_i)$	Wannier function
ϵ_F, k_F	Fermi energy, Fermi wavevector
ϵ_d	unperturbed energy of a localized d state on the impurity atom
U	Coulomb splitting between the spin up and spin down d states on the impurity atom
V_{sd}	Anderson mixing potential
Γ	half-width of the Anderson virtual level
$N(\epsilon)$	density of states at energy ϵ
$N(\epsilon_F)$	density of states at the Fermi level

$N_d(\epsilon)$	density of states of the virtual d level in the Anderson model
ρ	electrical resistivity
$\Delta\rho$	excess resistivity due to spin dependent scattering
ρ_m	spin dependent excess resistivity in the first Born approximation
ρ_0	unitarity limit resistivity
c	impurity concentration
k_B	Boltzman's constant
T	temperature
2D	width of the conduction band assumed in Kondo state calculations
N(0)	approximate density of states assumed to be constant in the band of width 2D (Kondo state calculations)
T_K	the Kondo temperature--usually defined as the point at which a divergence appears in the vertex function of the many body s-d exchange theory--T_K also appears as a parameter in physical quantities calculated from theory
τ_0	the lifetime of localized spin fluctuations

I. THE HEAT CAPACITY OF THE KONDO STATE IN COPPER-CHROMIUM AND COPPER-IRON

A. INTRODUCTION: LOCALIZED MOMENTS AND THE KONDO STATE

In recent years considerable effort has yielded some progress toward understanding the nature of the magnetic moment on a localized impurity in a metal and its interactions with the itinerant electrons surrounding it. The theoretical prediction of the formation of a singlet bound state resulting from the interactions in the s-d exchange model has been paralleled by the development of a spin fluctuation theory which concerns itself with the lifetimes of localized spin fluctuations in a metal. The s-d exchange Hamiltonian is the limit of a general problem and is presumably valid only when the lifetimes of localized spin fluctuations are long. It is this hard moment model that has yielded the most detailed calculations and has enjoyed considerable success to date in explaining the resistance minimum phenomenon and related experiments. However, recent spin fluctuation papers[1, 2] have suggested that the Kondo effect as described by the s-d model[3, 4, 5] and localized spin fluctuations are the same, and spin fluctuation theory has also recently yielded predictions of the resistance minimum! The s-d exchange Hamiltonian first proposed by Zener[6] as a model for ferromagnetic transition metals has been discussed in the recent theoretical review by Kondo[5] and only a summary of the current situation will be given here.

The Hamiltonian represents the exchange interaction between the localized and conduction electrons where consideration of the effects of finite lifetimes of the localized electrons has been implicity

ignored. The s-d Hamiltonian can be written

$$\mathcal{H}_{sd} = - N^{-1} \sum_{kk'n} J \exp\left[i(\vec{k}'-\vec{k})\cdot \vec{R}_n\right]\left[(a^*_{k\uparrow} a_{k'\uparrow} - a^*_{k\downarrow} a_{k'\downarrow})S_{nz}\right.$$

$$\left. + a^*_{k\uparrow} a_{k'\downarrow} S_{n-} + a^*_{k\downarrow} a_{k'\uparrow} S_{n+}\right] \tag{1}$$

where $a^*_{k\uparrow}$ and $a_{k\uparrow}$ are the creation and annihilation operators of the electron with wave vector $\vec{k}$ and spin $\uparrow$ and J denotes some average exchange integral. The Bloch function for the localized electron has been introduced in terms of its Wannier expansion

$$\phi_k(\vec{r}) = N^{-1/2} \sum_i \exp(i\vec{k}\cdot \vec{R}_i)\, \omega(\vec{r} - \vec{R}_i) \tag{1a}$$

assumed to be singly occupied

$$a^*_{n\downarrow} a_{n\downarrow} + a^*_{n\uparrow} a_{n\uparrow} = 1 \ . \tag{1b}$$

Equation (1b) allows us to write

$$1/2\,(a^*_{n\downarrow} a_{n\downarrow} - a^*_{n\uparrow} a_{n\uparrow}) = S_{nz}, \quad a^*_{n\downarrow} a_{n\uparrow} = S_{n+}, \quad a^*_{n\uparrow} a_{n\downarrow} = S_{n-} \tag{1c}$$

The diagonal part of Eq. (1) represents a uniform ferromagnetic coupling between the local spins independent of the separation between them. Hart[7] pointed out that this result contradicts Friedel's theorem[8] and indicates the necessity of considering higher-order terms.[5]

Equation (1) is of the same form as the Fermi interaction of the nucleus with metallic electrons; Ruderman and Kittel[9] and Kasuya[10] and Yosida[11] made second order perturbation calculations of the energy for nuclear spins and the electronic system respectively.

The RKKY interaction obtained by them is expressed

$$\mathcal{H} = \sum_{n<m} \vec{S}_n \cdot \vec{S}_m \; I(|\vec{R}_n - \vec{R}_m|) \tag{2a}$$

where

$$I(|R|) = \frac{9\pi J^2}{2\epsilon_F} \left[\frac{\cos 2k_F R}{(2k_F R)^3} - \frac{\sin 2k_F R}{(2k_F R)^4} \right] \tag{2b}$$

ϵ_F is the Fermi energy.

and k_F is the Fermi wavevector.

The uniform spin polarization given by the diagonal elements of the Hamiltonian has changed to an oscillating structure that decreases as R^{-3} for large distances from the local spin.

In Eq. (1b) the existence of a localized moment has been assumed without giving any theoretical justifications or conditions for its existence. Anderson[12] proposed a mixing model in the Hartree-Fock approximation which qualitatively describes the localized moment and indicated that if the localized levels were close enough to the Fermi level or the interaction with the free electron states strong enough, the resulting broadening of the virtual level would result in complete collapse of the localized moment into a nonmagnetic state.

The Anderson model is shown schematically in Fig. 1. The starting point of the model is a singly occupied d↑ localized state split from the spin down state of the same orbital by a repulsive Coulomb interaction U (see Fig. 1a). In the Anderson model these split states are "mixed" with the free-electron band by an s-d interaction potential. The resulting density of states curve (Fig. 1b) shows humps below and above the Fermi surface due to the appearance

of virtual levels consisting of the appropriate mixture of localized d state and opposite spin free electron states. The mixing has the effect of broadening the localized d level into a continuum distribution while decreasing the effective separation between the two levels (as more and more opposite spin character is mixed into the levels). As the occupation numbers of the two levels begin to differ appreciably from 0 and 1, a "collapse" of the split levels results in the symmetric nonmagnetic state shown in Fig. 1c.

The condition favorable for the formation of the magnetic state is shown in Fig. 2 and expressed

$$\epsilon_F - \epsilon_d \gg \Gamma = \pi V_{sd}^2 N(\epsilon_F) \text{ and } \epsilon_d + U - \epsilon_F \gg \Gamma \tag{3}$$

where Γ is the half-width of the virtual level and a representation of the s-d interaction derived from the mixing potential V_{sd} and $N(\epsilon_F)$ is the density of states at the Fermi level. The change in the density of states is expressed by

$$N_d(\epsilon) = \frac{\Gamma}{\pi} \frac{1}{(\epsilon - \epsilon_d)^2 + \Gamma^2} \quad ; \tag{4a}$$

at the Fermi level (4a) reduces to

$$N_d(\epsilon_F) = \frac{\Gamma}{\pi} \frac{1}{(\epsilon_F - \epsilon_d)^2 + \Gamma^2} \quad . \tag{4b}$$

It was quickly demonstrated that if the condition Eq. (3) is assumed, the Anderson Hamiltonian can be canonically transformed[13] into a Hamiltonian whose leading terms are equivalent to the s-d Hamiltonian with

$$J = V_{sd}^2 \left[\frac{1}{(\epsilon_d - \epsilon_{k'})} + \frac{1}{(\epsilon_k - \epsilon_d - U)} \right] < 0 \qquad (5)$$

As Kondo[5] has pointed out, this does not prove the equivalence of the two Hamiltonians until the effect of higher order terms is analyzed, but a fundamental relationship between the two models has been demonstrated.

The s-d exchange model assumes the existence of a localized moment and represents it with a spin operator without attempting to construct it from one-electron theory which does not allow localized states coincident in energy with a free electron band.

The Anderson model on the other hand is an attempt to describe this moment and conditions for its existence in terms of a virtual (finite lifetime) level built up from one electron states.

Sarachik et al.[14] established a one-to-one correspondence between the existence of dilute magnetic impurities in metals as implied by a strongly temperature dependent susceptibility and the appearance of a minimum in the resistance versus temperature curve. Kondo[15] then calculated the scattering amplitude of the s-d exchange model in the second Born approximation and obtained a logarithmic divergence in the electrical resistivity for an antiferromagnetic s-d interaction ($J < 0$).

His result can be expressed by

$$\Delta\rho = c\rho_m \left[1 + 4N(0)J \ln \left(\frac{k_B T}{D} \right) + \cdots \right] \qquad (6)$$

where c is the impurity concentration, and $N(0)$ is the density of states

in a flat band of width 2D. ρ_m is the spin dependent part of the resistivity calculated from the first Born approximation. Hamann[16] has obtained Eq. (6) directly from the Anderson model where the anomalous term appears in the sixth order of the scattering probability expanded in powers of V_{sd}.

The logarithmic form of Eq. (6) was an exciting theoretical development that implied the s-d Hamiltonian represents a true many-body problem which cannot be explicitly solved by a perturbation theory approach. It was recognized immediately that the anomalous term results from a situation analogous to that encountered in superconductivity. Electrons scattered by the localized moment (by the phonon field) are not properly treated in a one-electron approximation, but an effective electron-electron interaction comes into play because the spin dependent scattering probability (wavevector dependent scattering probability) depends on whether a previous event of the opposite sign has taken place. There is a kind of pairing between itinerant electrons of opposite spin analogous to the pairing of electrons with opposite wavevectors which takes place in the BCS theory of superconductivity. Further theoretical studies of the Kondo singularity showed that perturbational approaches fail below a characteristic temperature T_K and that below this temperature a many-body bound state appears with a nonanalytic binding energy of order kT_K where

$$k_B T_K \cong D \exp\left[\frac{-1}{2\,N(0)|J|}\right] \quad , \quad J < 0 \tag{7}$$

analogous to the BCS equation for the superconducting transition temperature. The state so formed is commonly called a spin

compensated state because a coherent mixing takes place between the spin up and spin down states localized on the impurity through interactions with the itinerant electrons in such a way as to remove the degeneracy and the spin-flip scattering process associated with the levels. This is a nonmagnetic ground state and there is considerable speculation[1, 2, 3, 17] that it is the nonmagnetic impurity state in the Anderson model (see Fig. 2). If this is the case, then systems traditionally considered nonmagnetic in the Anderson sense are those with very high Kondo temperatures. This view is consistent with Eq. (7) because small changes in $N(0)|J|$ can result in large variations in T_K. However, there are objections to applicability of the s-d exchange model to describe these high Kondo temperature systems. If the picture of a transition to a nondegenerate ground state is accepted, the transition must necessarily be broad because the condensation will be localized in real space around the impurity, and therefore a small number of degrees of freedom will be operative in the transition.

Early perturbation calculations showed that the Kondo divergence appears in other physical quantities in a manner similar to its appearance in the resistivity. When it became obvious that the divergence was appearing in such fundamentally significant functions as the free energy, theoretical workers split into three groups.

The first group has approached the problem by assuming the "normal" high temperature state of the metal when perturbed by the s-d Hamiltonian should provide an adequate representation of the low temperature ground state. The application of sophisticated mathematical techniques has allowed these workers to make an analytic continuation

of the "normal state" solution valid at high temperatures across T_K where perturbation theory diverges. This approach offers no guarantee that the continued solution is the one of lowest free energy but calculations of this type have yielded detailed calculations in increasingly better agreement with experiment.

The three most significant techniques are 1) Abrikosov's representation of the spin operators in a form making it possible to diagrammatically analyze an infinite perturbation series, 2) Suhl's application of Chew-Low scattering theory, and 3) the Nagaoka-Hamman-Bloomfield theory based on the Nagaoka truncation of an infinite series of double time Green's functions. For a discussion of these theories and a complete list of references the reader is referred to the excellent theoretical review by Kondo.[5] For our purposes it is sufficient to note that the two most refined techniques (2 and 3) are non-perturbative and give the same answer in so far as the leading terms of physical quantities are concerned. Although these leading terms are not divergent at low temperatures and give results (such as the entropy) that are thermodynamically possible, they are still considered unphysical by most authors in the limit $T \rightarrow 0$. In general these theories fit the experimental results such as the g shift, the electrical resistivity, and (as we shall see) the heat capacity very well down to at least T_K ($0.1\ T_K$ in the case of our heat capacities). At lower temperatures, however, small deviations appear and get progressively worse. Analytic solutions of physical parameters still have powers of $\ln(T/T_K)$

appearing in them.

A second group of theorists has approached the problem by trying to guess the ground state, often by analogy to the reasonably well understood superconducting state and Cooper pairs. The proposed ground state models are limited to $T \ll T_K$ and fall into two categories: namely, those that have powers of $\ln(T/T_K)$ appearing in all physical parameters derived from them and those that have only powers of T/T_K appearing.

The third group[1, 2] has suggested that it is possible to start from the Anderson (or Wolff) model in the limit where it is nonmagnetic in the Hartree-Fock sense (Fig. 1c) and describe the destruction of the "nonmagnetic" ground state by the lifetime τ_0 of localized spin fluctuations. The postulate of this approach is

$$kT_K = \alpha/\tau_0 \tag{8a}$$

where α is a constant of order unity and the representation of τ_0 is conventional

$$\tau_0 = \frac{\pi N_d(0)}{1 - U N_d(0)} \tag{8b}$$

where $N_d(0)$ is defined by Eq. (4b). The localized spin fluctuation is described as the repeated scattering between an electron and hole of opposite spin on the impurity site.[2] This picture implies that when the lifetime of this resonant scattering is long at $kT \ll 1/\tau_0$ the moment cannot be "seen", but as $kT \sim \frac{1}{\tau_0}$ thermal fluctuations gradually break up, the resonance and the moment on the impurity "appears" and shows increasingly magnetic character.

The only justification for Eq. (8a) is contained in the fact that resistivities calculated numerically from spin fluctuation theory[1] are similar to Hamann's calculation[18] based on the s-d exchange model and the experimental resistivities. Recently, very accurate measurements[19] on the resistivity of Cu-Fe at very low concentrations have indicated

$$\Delta\rho = \rho_0 (1 - \alpha T^2) \qquad T \ll T_K \tag{9}$$

in agreement with the spin fluctuation predictions. Unfortunately no detailed specific heat predictions have been made by the spin fluctuation groups, but it is noted that all ground state proposals which give resistivities and susceptibilities of the same form as those of the spin fluctuation theories also give a specific heat proportional to T/T_K. All the spin fluctuation predictions are well behaved in the limit of low temperatures.

In Table I selected theoretical results[4, 5] of the three groups are summarized for the resistivity, the specific heat, and the magnetic susceptibility. The resemblance of the Celli-Zuckermann-Klein (CZK) model[20, 21] to spin fluctuation theory is striking considering the very different approaches involved, but it should be remembered that the NHB theory has been derived from three apparently unrelated approaches. The Kondo-Appelbaum variational model for the ground state[22] appears to be closely related to the NHB theory.

The original (NHB) calculation by Nagaoka[23] yielded results of this same form for the resistivity, specific heat, and susceptibility.

It was later pointed out that he had neglected the spin-flip component of the anomalous scattering. When calculations with this component included were made,[18, 24] the theory assumed its present form. Suhl[25] has pointed out that far below T_K spin-flip scattering is impossible because the spin is quenched. On the other at $T \sim T_K$ spin-flip scattering presumably plays an essential role in the quenching. This argument implies that the result orginally obtained by Nagaoka neglecting the spin-flip component should also be obtained from the theories including this component at $T \ll T_K$. The fact that a small discrepancy exists and gets worse as $T \rightarrow 0$ suggests that the difficulty results from the fact that the full (NHB) calculation includes only the most divergent logarithmic terms and these do not uniquely determine the low-temperature properties when continued across T_K.

For a more extensive discussion of the various theoretical results and comparison with experiment the reader is referred to the recent review by Heeger.[4]

The detection of an additional contribution to the heat capacity of a metal which is proportional to the impurity concentration at all temperatures would be an important verification of the nondegenerate ground state theories. We have measured this contribution for the systems Cu-Cr and Cu-Fe. The verification was not achieved earlier because of two significant difficulties.

One problem is associated with the fact that the spin degeneracy can be removed by other mechanisms. Work on the more concentrated solutions of magnetic impurities in metals showed that the additional heat capacity was linear in temperature and independent of impurity

concentration at low temperatures.[26, 27, 28] Marshall[29] has shown that the well-known RKKY spin-spin coupling produces a distribution of effective fields on the localized moments. This produces a distribution of Schottky type interactions which, when integrated, yield a heat capacity that is linear in temperature and independent of concentration. At higher temperatures the behavior is more complex and a discussion will be delayed until section F. 3.

The heat capacity measurements of Franck et al.[30] on samples of 0.2, 0.1, and 0.05 at. % Fe in Cu suggests that below about 0.05 at. % the heat additional heat capacity is proportional to concentration and characteristic of the spin-compensated state.

The second difficulty associated with the measurement of the heat capacity of the spin compensated state is inherent in the large temperature range covered by the transition. Theroretical calculations by Bloomfield and Hamann[24] which have been substantially confirmed by this work show that the additional heat capacity associated with the condensation is still 40% of its peak value a decade in temperature above and below the temperature at which the peak occurs. The necessity for working at very low concentrations and the interference of the rapidly increasing lattice heat capacity at higher temperatures makes high precision measurements in a wide temperature range essential to the experiment.

B. EXPERIMENTAL TECHNIQUES: 0.3K to 25K

1. Cryostat

The He^3 cryostat used for heat capacity measurements in the temperature range 0.3K to 25K was similar to the one first described by N. M. Senozan,[31] and the reader should consult his work for design details.

Care has been taken to reduce vibrational heat input to the system: the cryostat system itself is isolated from the room by Barry Isolation Mounts;[32] the pumping lines are connected to the system through flexible metal bellows.

The cryostat consists of two concentric dewars containing liquid nitrogen and liquid helium and the all-metal cryostat "rig" used for cooling the sample to 0.3K and then breaking thermal contact. The sections of the dewar system and rig are shown schematically in Fig. 3. We use a Kinney pump Model KT-300 to pump the liquid He^4 bath down to below 1.2 K and a Consolidated Vacuum MCF-300 diffusion pump for subsequent pumping of liquid He^3 down to ~0.3 K. Thermal-contact and isolation is achieved inside the rig vacuum space in three stages:

a. Nitrogen exchange gas is pumped out of the vacuum space at 77 K.

b. Mechanical heat switch No. 1 is opened at 1.1K to isolate the He^3 pot and sample support cage from the liquid He^4 bath.

c. Mechanical heat switch No. 2 is opened at 0.3K to isolate the sample-sample holder for heat capacity measurements.

Heat capacities were taken with the heat pulse technique in which a measured amount of energy was put into a resistance heater attached to the sample-holder and the rise in temperature recorded potentiometrically from the resistance of a germanium thermometer.

2. Thermometry

Calibrated germanium resistance thermometers are used exclusively in our laboratory for heat capacity measurements above 0.3K. All our thermometers are calibrated against our temperature scale as represented by resistance vs. temperature calibration (R-T) tables for two standard germanium thermometers.

The R-T tables for these thermometers is based on the following:

a. 1958 He^4 vapor pressure scale 1.0 to 4.2K.

b. Extrapolation to lower T using the magnetic susceptibility of single-crystal cerium magnesium nitrate (CMN) assuming a Curie law.

c. Constant volume gas thermometer based on the H_2 boiling point above 4.2K.

The germanium thermometers currently in use were calibrated in a calibrator rig of improved design[33] to be used for additional work on our temperature scale at a later date. The lead system from room temperature to the interior of the vacuum space at 1K consists simply of two 1/8"stainless steel tubes filled with 34 - .005" Formvar insulated copper wires cast in the epoxy Stycast 2850 GT,[34] which has almost the same thermal expansion properties as copper as well as excellent

thermal conductivity. Each of the lead tubes was fitted with a 31 pin Amphenol Series 48 connector at the room temperature terminal. With this system we obtain noise levels down to .01 microvolt and very constant thermals of a few tenths of a microvolt.

The calibrator block consists primarily of 2.2 kilograms of copper and was thermally connected to the He^3 chamber via gold plated brass bolts. The long thermal relaxation time of this arrangement resulted in cooling times on the order of three days to reach 0.3K, but provided excellent thermal stability. We used an electronic temperature regulator to hold the temperature constant to within 1 part in 10^4.

The thermometer calibration data is normally fit to a fourteen term equation

$$1/T = A_0 + A_1 \log R + A_2(\log R)^2 + \cdots A_{13}(\log R)^{13} \qquad (10)$$

by a computer and the temperature scale is assigned by drawing a smooth curve through the fractional deviations Δ from Eq. (10). The Δ values have peak-to-peak oscillations of approximately 0.001 for fits covering the range 0.3K to 25K. Temperatures are calculated from our germanium thermometer by multiplying the right side of Eq. (10) by $(1 + \Delta)$. It was necessary to do double precision calculations with an improved fitting routine[35] in order to get good fits over the entire two decade temperature range.

3. Sample Holder

The sample holder was certainly the key to success in these experiments and is a considerable improvement over earlier designs.

Previous experiments[30, 36, 37] had shown that the Kondo condensation occurs over a very broad range of temperature (at least three decades) and impurity-impurity interactions severely limit the maximum concentration in which one can hope to measure a dilute impurity effect. In addition, the work of Heeger et al.[38] indicated the desirability of doing measurements in various magnetic fields for the purpose of suppressing interaction effects at low fields and degrading the Kondo state itself at higher fields.

In designing the calorimeter the following requirements were kept in mind:

a. Samples should be easy to mount and remove--preferably without removing the sample holder from the cryostat.

b. The thermometer should be positioned in a region of low magnetic field in order to maintain its calibration during in-field measurements.

c. The need for precise measurements requires that the heat leak be minimized and that excellent thermal contact between the sample, heater, and thermometer be maintained.

d. The sample must be held rigid with respect to the magnetic field for in-field measurements in order to avoid eddy current heating induced by spatial displacement in a magnetic field.

e. The experiments place a premium on reproducibility. The calorimeter should be durable and mounted permanently so that no alteration is required during the experiments.

The sample holder shown in Figure 4 met the above requirements. The stalk is a .0808" Formvar insulated copper wire. There are three

sections to the calorimeter:

a. The heater bobbin, which was hard soldered to the bottom of the stalk. A 1/4"-20 thread 3/16" long was both the support and thermal contact element for the threaded samples. This design for making thermal contact has been discussed by Suomi et al.,[39] and we have found it possible to make excellent thermal contact to samples with either larger or smaller expansion coefficients. Just prior to an experimental run the samples were etched, washed, dried, and weighed before being screwed finger tight on the bobbin (which was held steady with a special spanner wrench). We used no grease of any kind to facilitate contact between the sample and calorimeter. In addition to improving our reproducibility, this technique made excellent thermal contact resulting in relaxation times instantaneous compared with the relaxation time of the chart recorder (less than 0.3 seconds). A heater with about 7,000 Ω resistance was noninductively wound from roughly 14 feet of .0009" platinum-9% tungsten alloy wire. Thermal contact to the bobbin was obtained with Stycast 2850 GT. The heater was further anchored by adding 4" leads of .0063" Formvar insulated copper wire (several inches were cast in the epoxy on the bobbin and several inches attached to the stalk immediately about the bobbin with General Electric 7031 insulating varnish.)[40] The bobbin has six .040" holes drilled in its upper rim to allow rigid mounting of the calorimeter.

b. The germanium thermometer, Solitron No. 1609, was fitted snugly into a copper sleeve at the upper end of the stalk where the magnetic field would be about 100 Oe at our highest operating field (38 kOe). The magnetic field at the thermometer site was further reduced, to less than 1 Oe, by positioning the thermometer inside a mu-metal shield 3/8" diameter by .030" wall, 1-1/4" long. The shield was attached to the He^3 pot.

We feel that shields of this type may be important--not only to preserve the thermometer calibration but also to eliminate pickup caused by vibrational motion of the thermometer with respect to magnetic fields of 50 Oe and more. These shields will nominally exclude 300 Oe and can be redesigned to handle up to 1000 Oe--beyond this region the ratio of the volume of mumetal required to the enclosed volume starts to go up quite rapidly because of the field distortion and the rapidly dropping permeability of the mu-metal as it approaches its saturation magnetization (about 8000 gauss).

Thermal contact to the thermometer element was made through the four leads which were attached to four 4" long, .0063" Formvar insulated copper wires wound around the stalk and anchored with G. E. varnish.[40]

c. The third and last part of the calorimeter is a .0508" bare copper wire hard soldered near the middle of the stalk. The mechanical heat switch jaws open and close on this wire for the purpose of making and breaking thermal contact. A disk with six .040" holes has been hard soldered above the heat switch wire to facilitate rigid mounting.

The calorimeter was mounted with .0086" nylon monofilament. The bridge structure was to provide durability as well as to minimize vibrational heating. No grease or glue was used on any point where the monofilament contacted the calorimeter. After mounting it was possible to push on the calorimeter hard enough to move it by stretching the monofilament and watch it relax back to near its original position with a time constant of seconds. The temperature drifts with the heat switch open were very close to flat or slightly cooling even at the lowest experimental temperature of 0.3K.

On the runs in the He^3 rig, the samples were secured with additional monofilament strung through .040" holes drilled near the edge of the samples. In the adiabatic runs to be discussed later, we dispensed with this procedure with no ill effects. It now seems possible to screw on any threadable sample and do a heat capacity run. The calorimeter weighed about 17.24 gms.

All measurements were taken without removing or altering the calorimeter in any way. 0.0009" Pt – 9% W wire was used to make electrical contact to the calorimeter leads while still assuring satisfactory thermal isolation. A three-lead heater was used. The heat developed in the leads was assumed to divide equally between the sample and surroundings.

4. Superconducting Magnet

The superconducting magnet used in these experiments and shown in Fig. 5 was designed and built by Mr. R. Hintz at the Lawrence Radiation Laboratory, Berkeley.

This magnet has a maximum field inside its 2.015" bore of 38 kOe and homogeneity of ± .01% in the 2" by .75" diameter cylindrical space in which samples were mounted (see Fig. 6). It was necessary to operate the magnet in the persistent mode--with only a small current through the leads--in order to reduce the superfluid liquid He^4 loss to a rate that would allow experimental run times of six hours. In addition the persistent mode operation improved the field stability and resulted in lower noise levels on our thermometers.* We will discuss only the last (and most successful) of three persistent mode switches built during the Kondo state experiments.

The persistent mode switch shown in Fig. 5 was made from Norton Nb -25% Ti T48S superconducting wire from which the copper plate had been removed. The bare 0.016" conductor was coated with Stycast 2850 GT and wrapped with dacron woven insulation. The insulated wire was non-inductively wound over a bakelite spool in two layers. A 100 Ω heater of .006" Formvar insulated manganin was

---

*This improvement was most noticeable on the adiabatic runs to be described later where the magnet in use had a low inductance and the sample was at low temperatures where heating effects produce more severe experimental problems.

wound between the two layers. The resulting switch had a normal state resistance of 11 Ω and allowed rapid charging of the magnet with acceptable heat inputs to the helium bath. The switch could carry 50 amperes but was not tested at currents higher than this. In order to assure non-resistive contacts all joints in the persistent current loop were spot welded and then wound with bare copper wire and soldered for mechanical strength.

The magnetic fields were determined by measuring the current flowing through a known resistance with a Hewlett Packard 2401C integrating digital voltmeter. The field per ampere characteristic for the magnet was determined from the program "Coils" used by the Accelerator Study Group, UCLRL, Berkeley for calculating the field-current ratio more accurately than can usually be determined with flux integrating devices. The probe of a Bell 120 Hall-effect gaussmeter was mounted external to the dewar system and was used as a rough monitor of the field. Subsequent analysis of the nuclear Schottky anomaly from the copper nuclei indicated that, at least for the 38 kOe runs, the magnetic field was always set to better than 0.5 percent.

C. EXPERIMENTAL TECHNIQUES: 0.06K to 1.0K

1. Apparatus and Sample Holder

The adiabatic demagnetization cryostat used for the experiments down to 0.060K was similar to those described by Ho[41] and O'Neal.[42] Figures 7 and 8 show the cryostat. The major changes included a 2.56" outer diameter vacuum can fitted with a superconducting solenoid allowing application of magnetic fields up to 10 kOe. The magnet was operated in the persistent mode at currents up to 30 amperes. A mu-metal shield was used (see Fig. 7) to exclude the residual magnetic field at the thermometer site. All electrical lead systems carrying less than 2 amperes were fitted with Amphenol Series 48 or Bendix Pigmy Type PC connectors (see Section B. 2).

The isothermal magnetization and demagnetization procedures have been described elsewhere,[41] and we will confine our discussion to the problems associated with using adiabatic demagnetization techniques for measurements to be made in a magnetic field.

The salt magnetization field is applied with a room temperature iron core magnet having a maximum field of 12 kOe. It is not possible to apply the demagnetization field and the sample field simultaneously because of the large force of the magnetic fields interacting with one another. The solenoid field on the sample is applied near the end of the demagnetization of the cooling salt.

The sample solenoid was mounted with the bottom of its windings 3.35" above the top of the demagnetization cooling salt; nevertheless, calculations indicated that the fringing field of the solenoid would warm

the cooling salt in the highest solenoid fields. For this reason a superconducting trimmer solenoid was centered about 1" above the top of the cooling salt for the purpose of compensating the fringing field.

Unfortunately, the major limitation in attempting to reach low temperatures with this type of apparatus turned out to be eddy-current heating caused by raising the magnetic field on the sample after demagnetizing the cooling salt. It should be noted that the eddy currents were generated in the copper shield surrounding the sample as well as the sample itself. After additional warming which took place during opening of the superconducting heat switch, the lowest temperature points were limited to .060K in zero field, .085K in 3kOe, and .13 K in 9kOe.

The calorimeter itself was similar to the one described in Section B. 1 except that it was constructed of high-purity silver.[43] (The low average nuclear moment of silver would make possible studies in high magnetic fields where the relatively large nuclear Schottky anomaly in copper might prove troublesome.) Except for the silver construction the only significant difference between this calorimeter and the one previously described is the replacement of the (mechanical) heat switch wire with a superconducting high-purity lead wire. The .012" diameter by 1" long lead wire acts as a heat switch because of the very high normal state thermal conductivity of lead compared to the very low thermal conductivity of the superconducting state far below the transition temperature. Application of a magnetic field with the

superconducting heat switch solenoid shown in Fig. 7 closes the heat switch by driving it normal--removal of this field allows the lead wire to go superconducting thus opening the switch.

2. Thermometry: 0.06K to 1.0K

The thermometer used in the experiments with the adiabatic demagnetization calorimeter was a germanium thermometer, Cryocal No. 1751. calibrated against the magnetic susceptibility of cerium magnesium nitrate (CMN) which was in turn calibrated on the 1958 He^4 vapor pressure scale.

Prior to this series of experiments only carbon resistance thermometers[44] had been used in this laboratory below 0.1K. These thermometers did not retain their calibrations on thermal cycling to the accuracy required by our experiments and it was found necessary to calibrate on a given experiment and take the heat capacities without allowing the thermometer to warm above 4.2K. After each warming to room temperature it was necessary to recalibrate by closing the superconducting thermal switch to make contact between the resistance thermometer mounted on the sample and the cerium magnesium nitrate magnetic thermometer mounted beneath the cooling salt (see Fig. 8).

For some time we have been interested in extending the low temperature range of our calibrated germanium thermometers but there were two persistent problems that are discussed below.

First, we were not able to find germanium thermometers that had R-T characteristics that would make them usable below 0.1K, and it was difficult to pick promising candidates from high temperature

characteristics such as the resistance at 77K and 4.2K. All thermometers tested in early experiments had resistances that would either rise far too rapidly or tend to a constant value in the temperature range between 0.1 - 0.5K. In recent years germanium thermometers have been obtained from Cryocal, Inc.,[45] that have almost ideal R-T characteristics. It is speculated that this is because the germanium sensing elements have been made more homogeneous. In Table II resistances for various temperatures and thermometers are listed and the usefulness of these thermometers is characterized. The criteria for defining a useful operating range for the thermometer is based partly on the fact that too large a sensitivity will cause the thermometer resistance to increase to a point where it is not possible to measure the small current necessary to prevent heating effects in the thermometer with a potentiometric system. Other measuring systems--bridges, etc.--could be used to eliminate this problem but high sensitivity thermometers would still be inconvenient for measurements over large temperature ranges because of the necessity of changing the operating current often and because of zero shifts in our null detectors[46] that occur for high input impedances.

On the low sensitivity side it is simply not possible to determine the change in resistance accurately without using so much power that the thermometer runs hot.

Of the thermometers listed in Table II only the Cryocal No. 986 and the Cryocal No. 1751 are satisfactory for use below 0.1K and both of them can be used down to much lower temperatures than the 0.060K region necessary for these experiments.[47] The thermometer

Solitron No. 1477 displays a rapidly decreasing sensitivity below 0.10K and is apparently approaching a constant resistance in a manner similar to the Cryocal No. 985. A characteristic that appears to indicate the behavior of these thermometers is the ratio of the resistance at 4.2K to the resistance at 77K--values in the 5.0 to 7.0 range serve notice that the thermometer may be useful over a very wide range of temperature.

The second problem related to the use of calibrated resistance thermometers at very low temperatures is that of obtaining an accurate calibration free from heating effects in the thermometer due to the measuring power input or rf pickup. The thermometer is normally electrically insulated from the sample and the thermal contact to the sample is limited by a boundary resistance proportional to T^{-3}. This problem by itself would not be too severe, as long as good, relatively reproducible thermal contact to the sample is maintained (so that heat generated in the thermometer will not produce an appreciable temperature gradient between the thermometer and sample holder--sample system). Moreover, heating effects in the thermometer due to rf pickup[48, 49] has not been a problem in this laboratory as long as the thermometer resistance remains below about 5,000 Ω. Consequently, it was felt that the problem reduced to that of determining the calibration and proving that it was retained a) when the thermometer was mounted on the sample holder and b) under repeated thermal cycling.

With these considerations in mind we calibrated Solitron No. 1477 and Cryocal No. 1751 by attaching them directly to the copper thermal link as shown in Fig. 8. The thermometer leads consisted of 8" of .0063" Formvar insulated copper wire anchored non-inductively around

the thermal link with GE 7031 varnish. In this way it was possible to assure much better thermal contact between the CMN crystals and the thermometer than would be possible through the .012" lead thermal switch. As previously mentioned, the Solitron No. 1477 was not usable at very low temperatures, but its known R-T curve above 0.3K was used to establish the constants A, B for the equation relating the magnetic susceptibility of a dilute paramagnetic salt to temperature,

$$\chi = A + B/T \tag{11}$$

Extrapolation of this equation served to define the temperatures from 0.058K to 3.0K used in the calibration of the Cryocal No. 1751. This thermometer was then mounted in the silver sample holder described in Section C.1 and was recalibrated in a different adiabatic demagnetization rig with a different CMN salt. Care was taken on both runs to assure the magnetic susceptibility was independent of the measuring power at all temperatures.

Excellent thermal contact to the sample holder was obtained by fitting the thermometer tightly into its silver mounting sleeve and anchoring the .0063" copper leads with Stycast 2850 GT. It is assumed that this epoxy, which seals superfluid leak tight to copper, resulted in thermal contact which does not decay with thermal cycling (this assumption will be checked in later experiments). Thermal contact between the sample holder and the thermal link was made with the lead switch and a copper clamp which connected the thermal leak to a dummy copper sample screwed on the sample holder. This calibration run agreed with the former to 1 part in 10^3 below 0.1K and got increasingly

better at higher temperatures. The scatter in both runs was less than 2 parts in 10^4 and the peak to peak noise level of .2 microvolt at .06K is more than an order of magnitude better than our best carbon thermometer at this temperature. The low noise level made it possible to avoid running the thermometer hot within our detection limits down to .08K and only 1% hot at .06K* The R-T curve was fit with an equation similar to Eq. (10) in Section B.2.

Why did it work so well? It seems probable that the answer lies in a combination of the following suggestions:

a) A germanium single crystal is inherently superior to carbon resistance elements.

b) Lower resistance thermometers (both carbon and germanium) appear to be less susceptible to transient effects. Cryocal No. 1751 has the lowest resistance at .06K of any nonmetallic thermometer used in this laboratory.

---

*The carbon thermometers used previously were often run hot in order to obtain maximum sensitivity over the noise in the measuring circuit.

D. SAMPLE PREPARATION AND ANALYSIS

1. Preparation

Dr. J. C. F. Brock and Mr. Gary P. Schwartz did the preliminary work on the Cu-Fe system and these samples were made under their direction. After melting the Cu and Fe under vacuum in an inducation furnace, the samples were chill cast, homogenized by annealing at 900°C for ~24 hours, and quenched to prevent precipitation of the Fe from solution. Microprobe analysis of the samples failed to show any evidence for precipitation of Fe.

The work of these investigators and other communications[50, 51] indicated that high quality control and standard procedures were essential to ensure good homogeneous alloys free from extraneous impurities. For instance, careful wet analysis of the 99.999% "pure" Cominco copper used in the Cu-Fe samples showed the presence of 8.9 at ppm Fe. Cominco claimed less than 1 ppm in any impurity and this discrepancy was not noted until after the samples were made.

Dilute Cu-Cr alloys are even more difficult to prepare than Cu-Fe alloys. Particularly troublesome is the high vapor pressure of Cr and its pronounced tendency to react with refractory materials, carbon, oxygen, and especially nitrogen.[52] Moreover, it has an even lower solubility in copper (less than 0.2% at 800°C) than Fe (approximately 1% at 800°C).[52] Both Cr and Fe have room temperature solubilities in copper of less than 10 ppm, but rapid quenching from high temperatures yields samples with solution concentrations up to the 800°C solubility.

The Cu-Cr alloys were all prepared by Mr. Stanley Ross of UCLRL, Berkeley, The Cu and Cr were melted in an induction furnace in a vacuum of $\sim 1 \times 10^{-6}$ mm. The copper used came from a single Asarco 99.999+% rod with a resistivity ratio of 950 indicating total magnetic impurities of about 2 ppm -- presumably mostly Fe. The Cr source was a 99.98% pure sample obtained from the U. S. Bureau of Mines and previously studied in this laboratory.[41] The sample melt was contained in high purity alumina crucibles,[53] covered to prevent loss of the volatile Cr. The Cr or master alloy chips with high Cr content were positioned between the Cu slugs contained inside the crucible to further minimize any loss of the Cr.

Attempts to prepare a homogeneous master alloy with 0.5% Cr content were checked with x-ray fluorescence techniques.[54] The masters so prepared were consistently inhomogeneous until melt temperatures of 2000°C were held for 20 minutes. After obtaining a master with top and bottom concentration agreeing to within 5%, the master was cut in half. The interior showed Cr content about 10% higher than the outside and chips were cut from the center of the master and used to prepare the 150 g. samples with nominal Cr concentrations of 50, 30, 20, and 13 at ppm. Concentration analysis accurate to ± 5% later showed that the Cr content in the samples differed from the nominal Cr content by 0.5, 3.2, 1.2, and 2.9 at ppm, respectively, for the four samples. The true Cr content was always higher than the nominal value, presumably because the master chips were taken from the highest Cr content section of that alloy.

The four samples were sealed in quartz tubes evacuated to 10^{-6} mm at 400°C, homogenized at 950°C for 24 hours, and quenched by breaking the tube in a drop from the annealing furnace into water. At all stages of the preparation the sample surfaces remained shiny.

After slices and turnings were cut from the samples for analysis, the 1/4-20 mounting hole was tapped $\frac{1}{4}$" deep. The samples weighed from 90 to 60 g when the heat capacity measurements were taken.

Evidence pertaining to the sample homogeneity and the extent of which the Cr is completely in solution is discussed in the next section. Heat capacities were measured for the samples with 50, 30, and 20 ppm nominal concentrations and the 13 ppm sample will not be discussed further.

2. Analysis and Resistivity Measurements

Wet chemical analysis, neutron activation analysis, and resistivity measurements were used to determine the concentrations of the samples.[55, 56] In Tables III and IV the concentration found for the Cu-Fe and Cu-Cr samples and the accuracy of the measurements are reported. Neutron activation analysis was not used for Cu-Fe because conventional use of the technique does not give results approaching the accuracy of the wet chemical analysis.

The wet chemical analysis carried out by Mr. T. Morrison on Cu-Fe owes its accuracy to the fact that it was possible to chemically separate the Fe completely from the bulk of the Cu by standard analytical techniques. Analysis results for slices cut from the top and bottom of

the samples indicate that they were homogeneous to within a 4% and this limits the accuracy of our concentration values.

Cu-Fe Analysis by Mr. T. Morrison

Chemistry Dept., U. C., Berkeley

1) The samples were etched with HNO_3.

2) Weighed samples were dissolved in HNO_3 which was destroyed by boiling with 12 M HCl.

3) After evaporation to small volume, the sample was transferred to a 50 ml volumetric flask with 6 M HCl.

4) The $FeCl_3$ was selectively separated from the 6-8 M HCl solution with isopropyl ether.

5) After complexing the Fe with o-phenantholine the optical density was read with a Coleman Junior spectrophotometer.

The estimated accuracy of ± 2% was based on the ability to correctly determine the Fe concentration in standard samples of Fe and Cu in solution.

Some problems with the stability of the Fe complex were attributed to the extraction of small amounts of Cu from the acid solution.

The wet chemical analysis for Cr in Cu was done by Mr. Robert Giauque.[55] Chemical separation of the Cu and Cr was not achieved and the expected accuracy of 5% is estimated from the scatter and reproducibility of the optical density calibration curve. The calibration was done with standard samples of known Cr concentration taken into solution from Cu wire and Cr powder. The optical calibration points were

measured for standard samples with Cr concentrations of 6.2, 12.5, 18.6, 24.8, 32.3, 43.5, and 62.1 at ppm Cr. The Cu background was kept constant by using solutions of the same Cu concentration and the optical density contributed by the Cr was ~2% per at ppm. The blank used for pure Cu had a resistivity ratio of 2500.

Cu-Cr Analysis by Mr. Robert Giauque

UCLRL, Berkeley

1) The samples were etched with HNO_3.

2) Weighed samples were dissolved in a minimum of hot HNO_3 and made to volume. Aliquots containing 250 mg of sample were used for the analysis.

3) After adding 3.0 ml of a 10% solution of H_2SO_4 solution and chilling in an ice bath, the Cr is oxidized to the +6 state with an excess of AgO.

4) The excess AgO is reduced by heating and diluting the solution.

5) The Cr^{+6} is complexed with a solution of a-diphenylcarbazide and the optical density read at 540 mμ on a Beckman Model B spectrophotometer. The readings must be taken within 2 minutes because the complex is unstable with the Cu present.

Neutron activation analysis[55] gave values for the concentrations that were 30% to 40% lower than the wet concentration results and concentrations inferred from the resistivity (based on the concentration values determined by other workers). Apparently, a systematic error is present in these measurements and further investigation with neutron

activation analysis is planned in an attempt to resolve the discrepancy.

The nominal concentration for the samples are listed. The concentrations inferred from the analysis work are from 1 to 10% higher than the nominal values.

The electrical resistivity at low temperatures and low enough concentrations is a direct measure of the Kondo condensation and is proportional to the concentration of a single magnetic species in solid solution. It is necessary to know the proportionality constant which characterizes the given impurity and this value can only be known to the accuracy of somebody else's analysis, but the resistivity can always be used to determine the ratio between sufficiently dilute concentrations. It is important to measure the resistivity to see whether significant precipitation or oxidation of the magnetic species has occurred. In Table III the concentrations listed are obtained from the equation

$$\rho(4.2\ \mathrm{K}) = 1.085 \times 10^{-3}\ \frac{\mu\Omega\text{-cm}}{\mathrm{ppm}} \times c(\mathrm{ss.}) \qquad (12)$$

$$c(\mathrm{ss.}) = \text{concentration in solid solution}$$

which is in agreement with our data and that of Knook[57] who determined his solid solution concentrations from the temperature coefficients α of the resistance at 0°C and 100°C.[57, 58] The accuracy of the resistance measurements was initially poor but the difficulty was shortly traced to the necessity of using point contact current leads to the cylindrical samples which had lengths comparable to their diameters. Guarded circuitry was used with 2 volt storage batteries connected in parallel. An integrating digital voltmeter was used to measure the current and our

resistance thermometer circuitry to measure the voltage. Because of shrink holes in the samples it was not convenient to measure the resistivity for the 81.4 and 195 ppm Cu-Fe samples and the Cu-Cr samples, and it was derived from the resistance ratio R(300K)/R(4.2K) using small corrections to the room temperature resistivity obtained from other works.[59]

A plot of the 4.2 K resistivity versus concentration (wet analysis) for the Cu-Cr samples gave a straight line to within 5%. A small correction to the resistivity for the resistivity measured for "pure" copper at 4.2 K did not make any noticeable difference in the scatter of the points or significantly change the slope of the line drawn through them. The resistivities of Daybell and Steyert[60] (as estimated from their graph) do not agree well with out graph except for the 50 ppm sample in which they report interaction effects. We see no evidence for deviation from a concentration proportional resistance in our 51 ppm sample and suspect Daybell and Steyert must have underestimated the concentration values for their lower concentration samples by about 15% (they only claim 10% accuracy). Neutron activation analysis was one of the analytical techniques used by these authors and use of this same technique on our samples gave results that were ~40% low.

Since the resistivity measurements were more precise than the wet analysis, the relationship

$$\rho(4.2K) = (1.08 \pm .05) \times 10^{-3} \frac{\mu\Omega\text{-cm}}{\text{ppm}} \times c(\text{ss.}) \qquad (13)$$

obtained from the graph of $\rho(4.2K)$ vs. wet analysis and nominal concentration was used to assign c(ss.). Eq. (13) implies the Cu-Cr resistivity reported in Ref. 60 saturates near $1.7 \frac{\mu\Omega\text{-cm}}{\text{ppm}}$.

E. RESULTS AND DATA ANALYSIS

1. Addenda and Pure Copper

In order to determine the heat capacity due to the formation of the Kondo state, the heat capacity of the sample holder and the background contributed by the copper matrix must be subtracted from the measured value. The heat capacities of the sample holder and Cominco copper were measured in zero magnetic field and 27.9 kOe in the He^3 cryostat. An eight term fit ($T^{0.5}$, T, $T^{1.5}$, T^2, T^3, T^5, T^7, T^9) with a fractional deviation (Δ) plot (see section B. 2) was used to represent the heat capacity of the sample holder in all magnetic fields and the nuclear contribution (proportional to the square of the magnetic field) was subtracted separately.

After subtraction of the contribution from the sample holder, the heat capacity of the Cominco copper sample was fit with a computer to the equation

$$C(\mathrm{mJ/mole\text{-}K}) = \gamma T + a_3 T^3 + a_5 T^5 + a_7 T^7 + a_9 T^9 \qquad .3\ \mathrm{K} < T < 25\mathrm{K} \quad . \tag{14}$$

The fit with $\gamma = 0.6947$, $a_3 = 0.0492$, $a_5 = -1.146 \times 10^{-5}$, $a_7 = 1.326 \times 10^{-7}$, and $a_9 = -1.404 \times 10^{-10}$ still had fractional deviations of ~0.5% from a perfect fit. Previous efforts to fit the heat capacity of pure copper in this laboratory had experienced similar difficulties. Although there are some small bumps in our temperature scale, it was felt that the major problem could be traced to small amounts of magnetic impurities that resulted in Kondo state anomalies in the copper. For these reasons and also

because we wished to compare the fractional deviations of several copper samples with different purities, it was found convenient to use Δ plots together with Eq. (14) to represent the heat capacity of all copper samples (0.3K - 25K).

For the silver adiabatic empty, the nuclear contribution was negligible, but the heat capacity showed deviations that were magnetic field dependent by as much as 6% below 0.2 K. This sample holder was represented with a three term fit (T, T^3, T^5) and different deviation plots in different fields.

Since the nuclear spin contribution for pure copper agreed with that calculated from theory and could be represented by a single term proportional to H^2/T^2 where H is the applied magnetic field, it was possible in principle to subtract out all contributions to the heat capacity not associated with the localized moment and its interactions to the precision of our data (about ± 0.1% of the total heat capacity above 0.4 K in the He^3 rig -- more like ± 1% below 0.1 K in the adiabatic rig).

The heat capacity of pure copper was measured for two samples, Cominco and Asarco. The Cominco sample was melted from the Cominco copper used to make the Cu-Fe samples. The Asarco sample was cut from our highest purity Asarco copper rod and was measured as cut and then remeasured after annealing for 1 hour at 1000°C under a vacuum of $\sim 1 \times 10^{-6}$ mm.

There were two significant anomalies present in these "pure" copper samples. First, the Cominco copper contained 8.9 ppm Fe which contributed a Kondo state anomaly to the heat capacity. Measurements on the 81.4 and 195 ppm Cu-Fe samples were analyzed by subtracting the Cominco copper sample and dividing by the effective

concentrations, 72.5 and 184.1 at ppm Fe. The molar excess heat capacity derived in this way was concentration independent within the scatter of the data. Finally, the heat capacity contribution due to 8.9 ppm Fe was subtracted from the Cominco copper to obtain a heat capacity representative of the copper matrix and impurities other than Fe.

The Asarco rod contained only about 2 ppm Fe (estimated from the resistivity ratio and the assumption that Fe is the major magnetic impurity in this sample, as it is in most copper), but the unannealed rod exhibited a 10% anomaly sharply peaking near 1 K. This anomaly has been reported previously by Martin[61] and attributed to the presence of hydrogen in solution with the copper. The rod was then annealed and remeasured (this time in the adiabatic rig). The anomaly had been reduced to less than 1% but not completely eliminated. The rod was then melted and remeasured in another He^3 rig by Howard Simon of this group. No trace of the original anomaly was found.

In Fig. 9 the fractional deviations Δ from Eq. (14) are shown for the three heat capacity runs done by this author. The four sets of Δ values plotted are as follows:

1) Δ (Cominco, 0 ppm Fe) -- the Δ value for the sample prepared from the Cominco copper after correction for the 8.9 ppm Fe present in the sample.

2) Δ (Cominco, 2 ppm Fe) -- the Δ value for the Cominco copper sample plus the heat capacity contribution of 2 ppm Fe.

3) Δ (Asarco, 2 ppm Fe, unannealed) -- the Δ value for the Asarco copper sample containing ~2 ppm Fe as estimated from the resistivity ratio.

4) Δ (Asarco, 2 ppm Fe, annealed) -- the Δ value for the Asarco copper sample after annealing.

Δ (Cominco, 0 ppm Fe) -- the Δ value representing the copper matrix for the Cu-Fe samples and the smooth curve drawn through these points was used in conjunction with Eq. (14) to define the matrix heat capacity subtracted from the data for the Cu-Fe sample.

Δ (Asarco, 2 ppm Fe, unannealed) and Δ (Asarco, 2 ppm Fe, annealed) are in excellent agreement with Δ (Cominco, 2 ppm Fe) except for the 1 K anomaly which was neglected and except for small deviations at high temperatures -- perhaps due to other magnetic impurities in the Cominco sample in addition to Fe. The curve drawn through these points (using the Asarco Δ values at high T) represents the material from which the Cu-Cr samples were made. This curve was used with Eq. (14) to subtract out the matrix heat capacity for these samples.

For the Asarco copper sample containing ~2 ppm Fe, the heat capacity data below 0.3 K show no deviations within the scatter from the equation $C = \gamma T + \alpha T^3$ and this equation was used to represent pure copper for the runs done in the adiabatic rig. The coefficient of the T term of the heat capacity, $\gamma = 0.690$ mJ/mole - K^2, is in excellent agreement with the values $\gamma = 0.6915 \pm 0.034$ (mJ/mole - K^2) reported by Martin[62] on a number of very pure samples.

It was necessary to follow the self-consistent procedure described above in order to follow the concentration proportional contribution from the Kondo state up to the highest temperatures allowed by the $\pm 0.1\%$ scatter in our data. For instance, the use of a heat capacity appropriate

to 0 ppm or 8.9 ppm Fe to represent the Cu-Cr matrix (which contained ~2 ppm Fe) would lead to significant errors in the data above 5 K.

2. The Nuclear Schottky Heat Capacity and Localized Moment Effects

The application of magnetic fields up to 9 kOe in the adiabatic runs and 38 kOe in the runs in the He^3 calorimeter produces a heat capacity contribution from the removal of the spatial degeneracy of the nuclear spin I as each nuclear level is split into its 2I+1 components by the applied magnetic field. In pure copper there is no hyperfine interaction and the expected nuclear heat capacity is[63]

$$\frac{C_N}{R} = \frac{1}{3}\left\langle \frac{I+1}{I}\mu^2 \right\rangle \left(\frac{H}{kT}\right)^2 - \frac{1}{240}\left\langle \frac{(2I+1)^4 - 1}{I^4}\mu^4 \right\rangle \left(\frac{H}{kT}\right)^4 \ldots \quad (15)$$

where R is the gas constant, and

$$\left\langle \frac{I+1}{I}\mu^2 \right\rangle = \sum_i A_i \frac{I_i+1}{I_i}\mu_i^2 \quad (15a)$$

with A_i, I, and μ_i the fractional natural abundance, the nuclear spin, and the nuclear moment, respectively, of isotope i of the element. The higher order terms are negligible for our measurements, and even the second term can be neglected unless μ is very large. For copper where I = 3/2 for both naturally abundant isotopes Eq. (15a) reduces to

$$\langle\ \rangle = \frac{4}{3}\sum_{i+2} A_i\mu_i^2 = \frac{4}{3}\times(2.2746\ \mu_N)^2$$

where μ_N is the nuclear magneton. The second term of Eq. (15) is negligible and we observed no deviation from the value caculated from

the first term to 0.3% in a test run on pure copper at 27.9 kOe.

Complications arise when the simple picture described above is applied to Cu-Fe or Cu-Cr. Firstly, there is the question of a "Knight shift" alteration of the field seen by the copper nuclei. Such shifts are observed for systems with dilute magnetic impurities and have not been satisfactorily explained. In general the Knight shift on a given nucleus can be related to the local electronic spin density at that nucleus. In the case of the dilute magnetic impurity, Knight shifts in the surrounding matrix and their temperature dependence are due to the changes in the spin density of the itinerant electrons resulting from interactions with the localized moment. Sugawara[64] has measured the Knight shifts for Cu with dilute Fe and Cr impurities and found they are negative and less than 1% at all temperatures. It should be kept in mind that the NMR techniques used to measure the Knight shift see only nuclei that are relatively far from any impurity atom and exposed to a reasonably homogeneous field.

Generally the localized moment will have some magnetization associated with it, either due to spin-spin interactions or from the application of an external magnetic field. This magnetization induces spin density oscillations in the itinerant electrons of the RKKY type above the Kondo temperature, and at lower temperatures a modified structure appears in which an oscillatory contribution persists far below T_K (see Ref. 38 and other references discussed there).

In any case it is necessary to consider spin polarization and electric-field gradient effects from the oscillations and Kondo structure.

The electric-field gradient effect has been calculated for Fe impurities[65] to be of order 10^{-2} of the magnetic hyperfine contribution and this sum will be referred to as a single component. These important effects are also small except for $T < 0.1$ K in low fields. For our runs in magnetic fields > 20 kOe, the nuclear heat capacities of our samples exceeded those calculated for pure copper by less than 1% for all Cu-Fe and Cu-Cr samples.

The nuclear heat capacity calculated for pure copper in the applied magnetic field was subtracted from our data. Any remnant contribution was considered to be a reflection of the localized moment and its interactions and is therefore dealt with in the discussion sections.

The last contribution to the nuclear heat capacity that we might consider troublesome is a large hyperfine interaction on the impurity atoms due to spin-orbit coupling -- the spin on the impurity moment appearing as the externally applied magnetic field or spin-spin interactions destroy correlations with the electron gas. Because of the small nuclear moments of the naturally abundant Fe and Cr isotopes, the hyperfine interaction would have to be $\approx 10^{10}$ Oe for Fe or $\approx 3 \times 10^{7}$ Oe for Cr in order to be detected. The expected hyperfine fields on Cr or Fe should be $< 10^{6}$ Oe and the possibility of contribution from this source can be discounted.

3. Data

This section contains the heat capacity points taken by this author on the Cu-Cr and Cu-Fe samples. In addition the data taken by Dr. J. C. F. Brock on the 640 ppm Cu-Fe sample in zero magnetic field are listed. The width of the data points is about T/10.

The temperature scale for the runs in the He^3 rig is not well defined, for heat capacity purposes, below 0.4 K. This situation results from rapid oscillations in the computer fit to the R-T characteristic curve near the end of the calibrated region. For this reason heat capacities are reported for $T < 0.4$ K in this rig only for runs where an overlapping adiabatic run was not made. The effect of this errors is most noticeable for runs in high magnetic fields where the excess heat capacity is very small due to the large nuclear contribution. The error is on the order of 0.5% of the total heat capacity below 0.4 K.

Three heat capacities are presented:

a) ΔC(mJ/mole-K) is the excess molar heat capacity of the sample after subtraction of the heat capacity of the copper matrix (for runs in a magnetic field the nuclear contribution C_N calculated for pure copper has been subtracted out).

b) $\Delta C/c$ (J/K-mole impurity) is the excess heat capacity calculated from ΔC by dividing by concentration. This reduced heat capacity is the quantity which is presumably due to the formation of the Kondo state if the concentration is low enough.

c) C_{Cu} (H=0) (mJ/mole-K) is the heat capacity used for the copper matrix as discussed in the previous section.

Data Section Contents

1.	Cu-Cr	51.04 ppm	.06 K - .6 K	Zero Field	----------	48
2.	"	"	.3 K - 12 K	"	----------	49
3.	"	"	.08 K - .9 K	3 kOe	----------	50
4.	"	"	.2 K - .9 K	9 kOe	----------	51
5.	"	"	.3 K - 12 K	10 kOe	----------	52
6.	"	"	"	20 kOe	----------	53
7.	"	"	"	30 kOe	----------	54
8.	"	"	"	38 kOe	----------	55
9.	"	33.62 ppm	.3 K - 12 K	Zero Field	----------	56
10.	"	"	"	38 kOe	----------	57
11.	"	21.160 ppm	.06 K - .6 K	Zero Field	----------	58
12.	"	"	.3 K - 7 K	"	----------	60
13.	"	"	.08 K - .9 K	3 kOe	----------	61
14.	"	"	.3 K - 7 K	38 kOe	----------	62
15.	Cu-Fe	81.4 ppm	.3 K - 25 K	Zero Field	----------	63
16.	"	"	.3 K - 2.5 K	20 kOe	----------	65
17.	"	"	"	30 kOe	----------	66
18.	"	"	.3 K - 25 K	38 kOe	----------	67
19.	"	195 ppm	"	Zero Field	----------	68
20.	"	"	.3 K - 2.5 K	20 kOe	----------	69
21.	"	"	"	30 kOe	----------	70
22.	"	"	"	38 kOe	----------	70
23.	"	640 ppm	.06 K - 1 K	Zero Field	----------	71
24.	"	"	.3 K - 25 K	"	----------	73
25.	"	"	.3 K - 1 K	1 kOe	----------	74

26.	Cu-Fe	640 ppm	.3 K - 8 K	3 kOe	---------- 75
27.	"	"	.3 K - 25 K	10 kOe	---------- 76
28.	"	"	.3 K - 1 K	18 kOe	---------- 77
29.	"	"	.3 K - 3 K	24 kOe	---------- 78
30.	"	"	.3 K - 2 K	30 kOe	---------- 79
31.	"	"	"	33 kOe	---------- 80
32.	"	"	.3 K - 25 K	36 kOe	---------- 81
33.	"	"	.3 K - 2 K	38 kOe	---------- 82
34.	"	2560 ppm	.3 K - 25 K	Zero Field	---------- 83
35.	"	"	"	38 kOe	---------- 84

Summary

T(K) = mean temperature

C_N (mJ/K-mole Cu) = $3.19733\ H^2 \times 10^{-5}$ H in kOe

ΔC (mJ/mole-K) = C(raw) - C(sample holder)-C_N-C_{Cu}(H=0)

$$\Delta C/c \text{ (J/K-mole impurity)} = \frac{\Delta C(\text{mJ/mole-K})}{c(\text{at.ppm}) \times 10^{-3}}$$

1. Cu-Cr 51.04 ppm .06 K - .6 K Zero Field

N	T	ΔC	ΔC/c	$C_{Cu}(H=0)$
2	.07147	.08131	1.59300	.04957
3	.08477	.07429	1.45558	.05874
4	.10004	.08140	1.59479	.06926
5	.11301	.08579	1.68094	.07821
6	.12531	.09046	1.77237	.08671
7	.07436	.07280	1.42630	.05156
8	.08441	.07359	1.44185	.05849
9	.10701	.08345	1.63494	.07407
10	.13041	.09114	1.78556	.09022
11	.14467	.09557	1.87237	.10006
12	.16903	.10049	1.96888	.11686
13	.19441	.10541	2.06527	.13438
14	.15234	.09767	1.91364	.10536
15	.17847	.10311	2.02016	.12337
16	.20338	.10682	2.09290	.14059
17	.22722	.11168	2.18807	.15714
18	.25274	.11561	2.26514	.17488
19	.28914	.11789	2.30971	.20028
20	.22029	.11038	2.16269	.15232
21	.24640	.11538	2.26060	.17047
22	.27731	.11542	2.26141	.19201
23	.29473	.12023	2.35566	.20419
24	.33370	.12312	2.41231	.23155
25	.37308	.12303	2.41039	.25937
26	.41537	.12524	2.45374	.28942
27	.46344	.12984	2.54384	.32384
28	.31354	.12126	2.37582	.21738
29	.35607	.12390	2.42751	.24734
30	.39713	.12497	2.44843	.27643
31	.44315	.12699	2.48808	.30928
32	.49494	.12691	2.48648	.34656
33	.52115	.13095	2.56567	.36558
34	.59089	.13211	2.58828	.41670
41	.08141	.07422	1.45416	.05643
42	.09502	.07842	1.54621	.06580
43	.10929	.08521	1.66942	.07565
44	.12216	.08792	1.72266	.08453
45	.13352	.09401	1.84180	.09237
46	.06243	.09384	1.83862	.04333
47	.07011	.08487	1.66286	.04863
48	.06274	.10786	2.11321	.04354
49	.06487	.07979	1.56323	.04501

2. Cu-Cr 51.04 ppm .3 K - 12 K Zero Field

N	T	ΔC	ΔC/c	$C_{Cu}(H=0)$
5	.39355	.12761	2.50017	.27428
6	.44425	.12804	2.50856	.31045
7	.50459	.13022	2.55125	.35392
8	.56277	.13113	2.56907	.39632
9	.61072	.13192	2.58470	.43166
10	.67756	.13109	2.56840	.48158
11	.75405	.13057	2.55823	.53977
12	.83921	.13025	2.55184	.60603
13	.93706	.12909	2.52918	.68431
14	1.05392	.12584	2.46557	.78121
15	1.17403	.12148	2.38006	.88528
16	1.30762	.12112	2.37304	1.00722
17	1.42944	.11855	2.32276	1.12535
18	1.54763	.11465	2.24623	1.24632
19	1.70342	.11516	2.25629	1.41577
20	1.87619	.11290	2.21205	1.61800
21	2.09829	.11148	2.18425	1.90256
22	2.36095	.10623	2.08134	2.27831
23	2.64578	.10492	2.05569	2.74125
24	2.96245	.09586	1.87820	3.32982
25	3.29834	.08969	1.75731	4.04990
26	3.64825	.08611	1.68707	4.91638
27	4.02311	.07910	1.54980	5.98985
28	4.44373	.06786	1.32949	7.39023
29	4.91717	.06940	1.35977	9.23714
30	5.43167	.06271	1.22869	11.58091
31	6.01085	.05259	1.03027	14.71323
32	6.56144	.05463	1.07026	18.26560
33	7.16186	.05103	.99983	22.80219
34	7.76307	.04268	.83619	28.10803
35	8.47133	.03481	.68210	35.41922
36	9.33220	.02821	.55274	46.09652
37	10.25340	.05932	1.16227	60.07934
38	11.25231	-.05336	-1.04548	78.39818

3. Cu-Cr 51.04 ppm .08 K - .9 K 3 kOe

$C_N = 0.00028776/T^2$ (mJ/K-mole Cu)

N	T	ΔC	ΔC/c	$C_{Cu}(H=0)$
3	.09608	.09901	1.93991	.06654
5	.12906	.09206	1.80363	.08929
9	.11615	.08970	1.75746	.08038
10	.13362	.09701	1.90064	.09244
11	.13727	.09595	1.87989	.09496
12	.15405	.10472	2.05174	.10653
13	.17258	.11110	2.17681	.11931
14	.19381	.11451	2.24362	.13397
15	.21599	.12250	2.40016	.14934
16	.14398	.10102	1.97929	.09958
17	.16313	.10618	2.08027	.11279
18	.18528	.11265	2.20706	.12807
19	.20596	.11948	2.34095	.14238
20	.22873	.12306	2.41100	.15819
21	.25037	.12835	2.51470	.17323
22	.27548	.12861	2.51984	.19073
23	.21876	.12044	2.35978	.15126
24	.23848	.12413	2.43208	.16496
25	.26295	.12928	2.53282	.18199
26	.29080	.13771	2.69801	.20144
28	.33331	.14165	2.77518	.23128
29	.36697	.14368	2.81500	.25504
30	.40129	.14645	2.86939	.27939
31	.45052	.14989	2.93677	.31456
32	.50585	.15099	2.95819	.35446
33	.54745	.15639	3.06412	.38476
34	.62242	.15799	3.09544	.44009
35	.70533	.15753	3.08635	.50249
36	.80087	.16024	3.13955	.57618
37	.90029	.16069	3.14835	.65504

4. Cu-Cr 51.04 ppm .2 K - .9 K 9 kOe

$C_N = 0.002590/T^2$ (mJ/K-mole Cu)

N	T	ΔC	ΔC/c	C_{Cu}(H=0)
23	.30508	.11346	2.22302	.21144
24	.36473	.13380	2.62150	.25346
25	.42372	.14244	2.79085	.29538
26	.48960	.15697	3.07552	.34270
27	.54041	.15669	3.06985	.37962
28	.53120	.16183	3.17073	.37290
29	.62582	.17422	3.41346	.44262
30	.72590	.18625	3.64907	.51819
31	.83117	.19763	3.87206	.59997
35	.21817	.09991	1.95755	.15086
36	.26563	.11313	2.21656	.18386
39	.22070	.09801	1.92035	.15261
40	.25935	.10782	2.11249	.17949
41	.29710	.11775	2.30700	.20585
42	.34293	.12677	2.48382	.23806
43	.38942	.13704	2.68497	.27096
44	.44113	.14805	2.90067	.30783
45	.49919	.15606	3.05756	.34964
46	.53795	.16534	3.23950	.37782
47	.60388	.17534	3.43530	.42631
48	.66522	.18076	3.54151	.47212
49	.72705	.18800	3.68341	.51907
50	.79698	.19154	3.75268	.57314
51	.86895	.19834	3.88603	.62993

5. Cu-Cr 51.04 ppm .3 K - 12 K 10 kOe

$C_N = 0.0031973/T^2$ (mJ/K-mole Cu)

N	T	ΔC	ΔC/c	C_{Cu}(H=0)
1	.34517	.12512	2.45137	.24001
2	.37847	.13216	2.58926	.26357
3	.41743	.13957	2.73450	.29128
4	.46161	.14772	2.89417	.32291
5	.50808	.15308	2.99920	.35645
6	.55637	.16220	3.17799	.39163
7	.60675	.16817	3.29492	.42871
8	.67372	.17149	3.35983	.47870
9	.74876	.17598	3.44779	.53571
10	.82582	.18179	3.56176	.59550
11	.89224	.18313	3.58789	.64815
12	.98010	.18146	3.55519	.71954
13	1.03364	.17649	3.45793	.80651
14	1.19773	.17613	3.45073	.90636
15	1.31579	.17491	3.42700	1.01494
16	1.46056	.16981	3.32710	1.15658
17	1.63915	.16692	3.27031	1.34446
18	1.84472	.16207	3.17544	1.57996
19	2.05063	.15354	3.00827	1.83902
20	2.25831	.14510	2.84296	2.12637
21	2.47041	.13961	2.73527	2.44948
22	2.69121	.13176	2.58159	2.82067
23	2.92475	.12193	2.38882	3.25536
24	3.18638	.11037	2.16238	3.79828
25	3.45176	.10740	2.10422	4.41447
26	3.74785	.10399	2.03745	5.18639
27	4.09900	.09169	1.79644	6.22680
28	4.47661	.08012	1.56977	7.50885
29	4.87823	.06388	1.25157	9.07316
30	5.28067	.07236	1.41768	10.85638
31	5.78924	.05556	1.08850	13.44775
32	6.31945	.05437	1.06515	16.63896
33	6.91397	.06919	1.35563	20.83776
34	7.49013	.03203	.62751	25.60739
35	8.14225	.05309	1.04022	31.86623
36	8.93583	.03362	.65861	40.91843
37	9.83950	.04422	.86641	53.44554
38	10.87009	.04418	.86563	70.99405
39	11.89308	.00431	.08440	92.03593

6. Cu-Cr 51.04 ppm .3 K - 12 K 20 kOe

$C_N = 0.0127893/T^2$ (mJ/K-mole Cu)

N	T	ΔC	ΔC/c	$C_{Cu}(H=0)$
1	.33829	.08051	1.57743	.23516
2	.37038	.08471	1.65976	.25784
3	.41094	.09320	1.82592	.28665
4	.45772	.10303	2.01859	.32011
5	.51133	.11584	2.26958	.35881
6	.56500	.12707	2.48958	.39796
7	.61411	.13637	2.67177	.43417
8	.68065	.14698	2.87963	.48391
9	.76309	.15899	3.11503	.54673
10	.84975	.17136	3.35728	.61434
11	.92807	.18019	3.53033	.67701
12	1.03757	.18844	3.69204	.76741
13	1.16569	.19606	3.84128	.87785
14	1.29272	.20262	3.96980	.99324
15	1.43555	.20696	4.05484	1.13145
16	1.56169	.21111	4.13617	1.26115
17	1.71477	.21306	4.17436	1.42857
18	1.88368	.21418	4.19628	1.62712
19	2.07550	.20749	4.06533	1.87201
20	2.33644	.20204	3.95845	2.24175
21	2.63151	.19770	3.87335	2.71664
22	2.90321	.18550	3.63447	3.21336
23	3.19423	.17102	3.35069	3.81554
24	3.48846	.15613	3.05889	4.50517
25	3.79141	.15405	3.01827	5.30786
26	4.15739	.13366	2.61869	6.41375
27	4.54831	.11779	2.30773	7.77183
28	5.00061	.10813	2.11846	9.59516
29	5.50876	.10766	2.10924	11.96455
30	6.08712	.06579	1.28890	15.17684
31	6.64960	.08762	1.71669	18.88577
32	7.30461	.06633	1.29953	23.99374
33	8.08139	.09406	1.34286	31.23905
34	8.87799	.04247	.83204	40.20124
35	9.76835	.09416	1.84479	52.36369

7. Cu-Cr 51.04 ppm .3 K - 12 K 30 kOe

$C_N = 0.028776/T^2$ (mJ/K-mole Cu)

N	T	ΔC	ΔC/c	$C_{Cu}(H=0)$
1	.34716	.05504	1.07835	.24142
2	.37906	.05859	1.14797	.26399
3	.41795	.06481	1.26985	.29165
4	.46551	.07318	1.43376	.32571
5	.53287	.08641	1.69290	.37447
6	.59119	.09684	1.89734	.41722
7	.64592	.10563	2.06964	.45785
8	.70546	.11455	2.24441	.50267
9	.76586	.12311	2.41212	.54886
10	.83519	.13417	2.62875	.60286
11	.91706	.14602	2.86085	.66811
12	.99347	.15614	3.05910	.73059
13	1.07874	.16504	3.23356	.80232
14	1.17591	.17341	3.39763	.88690
15	1.28836	.18546	3.63357	.98918
16	1.41812	.19816	3.88241	1.11410
17	1.56147	.20747	4.06480	1.26091
18	1.71971	.21817	4.27458	1.43417
19	1.89224	.22565	4.42097	1.63760
20	2.07124	.23365	4.57778	1.86633
21	2.26209	.23329	4.57064	2.13186
22	2.49286	.23103	4.52652	2.48555
23	2.73444	.23250	4.55530	2.89777
24	3.00146	.22087	4.32747	3.40817
25	3.32804	.21455	4.20349	4.11866
26	3.65776	.21808	4.27271	4.94170
27	4.02324	.20193	3.95630	5.99026
28	4.40352	.18779	3.67929	7.24736
29	4.85818	.18851	3.69336	8.98954
30	5.36144	.15472	3.03139	11.23972
31	5.90897	.15146	2.96743	14.12301
32	6.46104	.12882	2.52386	17.57743
33	7.07061	.15276	2.99291	22.06330
34	7.72026	.12633	2.47512	27.70512
35	8.41123	.15144	2.96711	34.74963
36	9.22067	.16588	3.25009	44.59191
37	10.11289	.17572	3.44272	57.76196
38	11.06893	.18767	3.67699	74.77974

8. Cu-Cr 51.04 ppm .3 K - 12 K 38 kOe

$C_N = 0.0461694/T^2$ (mJ/K-mole Cu)

N	T	ΔC	ΔC/c	C_{Cu} (H=0)
1	.35169	.05441	1.06607	.24462
2	.38855	.05637	1.10434	.27072
3	.42788	.05853	1.14669	.29874
4	.46934	.06346	1.24340	.32847
5	.51479	.06918	1.35543	.36132
6	.56051	.07589	1.48681	.39466
7	.60609	.08276	1.62154	.42823
8	.67004	.09069	1.77693	.47593
9	.74059	.09897	1.93904	.52945
10	.81697	.10904	2.13645	.58857
11	.89370	.11849	2.32153	.64932
12	.96890	.12690	2.48625	.71033
13	1.05996	.13596	2.66380	.78632
14	1.15008	.14568	2.85432	.86410
15	1.25252	.15888	3.11290	.95602
16	1.37438	.17194	3.36872	1.07114
17	1.52448	.18488	3.62225	1.22211
18	1.68042	.19904	3.89973	1.39001
19	1.85074	.21264	4.16619	1.58719
20	2.03851	.22361	4.38114	1.82309
21	2.23965	.22906	4.48777	2.09941
22	2.45741	.23841	4.67112	2.42876
23	2.69813	.24320	4.76496	2.83292
24	2.96785	.24556	4.81106	3.34058
25	3.27624	.23945	4.69149	3.99929
26	3.64480	.24916	4.88161	4.90722
27	4.01533	.23192	4.54385	5.96595
28	4.38409	.22616	4.43096	7.17851
29	4.85746	.21999	4.31022	8.98654
30	5.34183	.21118	4.13760	11.14578
31	5.86725	.17868	3.50081	13.88477
32	6.36747	.17759	3.47949	16.95309
33	6.89875	.17589	3.44620	20.72152
34	7.49889	.17143	3.35869	25.68540
35	8.19944	.18281	3.58175	32.46393
36	8.97158	.16672	3.26641	41.36650
37	9.85053	.16963	3.32343	53.61475
38	10.85566	.22507	4.40967	70.72462
39	11.89084	.16514	3.23542	91.98548

9. Cu-Cr 33.62 ppm .3 K - 12 K Zero Field

N	T	ΔC	ΔC/c	$C_{Cu}(H=0)$
3	.38424	.08649	2.57271	.26766
4	.42017	.08723	2.59469	.29323
5	.47046	.08618	2.56333	.32927
6	.52307	.08910	2.65013	.36733
7	.58121	.08668	2.57833	.40987
8	.60500	.08682	2.58253	.42742
9	.66901	.08730	2.59674	.47515
10	.73738	.08506	2.53013	.52699
11	.81422	.08612	2.56145	.58642
12	.88526	.08074	2.40154	.64257
13	.87815	.08357	2.48565	.63689
14	.95806	.08193	2.43708	.70143
15	1.03931	.07978	2.37299	.76887
16	1.13684	.07755	2.30675	.85250
17	1.24291	.07851	2.33523	.94723
18	1.36931	.07435	2.21152	1.06622
19	1.51465	.07638	2.27177	1.21192
20	1.64829	.07289	2.16805	1.35448
21	1.80966	.07769	2.31087	1.53824
22	2.00469	.07451	2.21633	1.77908
23	2.20214	.06684	1.98817	2.04592
24	2.40894	.07120	2.11786	2.35260
25	2.63957	.06297	1.87308	2.73052
26	2.89772	.07033	2.09186	3.20271
27	3.18739	.05004	1.48830	3.80160
28	3.51986	.06659	1.98081	4.58389
29	3.85572	.03974	1.18190	5.49106
30	4.20432	.05206	1.54858	6.56693
31	4.60316	.05103	1.51785	7.97745
32	5.03814	.00600	.17836	9.75836
33	5.51880	.03960	1.17780	12.01529
34	6.07164	.02974	.88470	15.08289
35	6.59891	.00998	.29693	18.52733
36	7.19957	.00848	.25220	23.11277
37	7.82613	.07419	2.20660	28.70920
38	8.50468	-.07346	-2.18500	35.79478
39	9.32623	-.10376	-3.08625	46.01499
40	10.23702	.05230	1.55554	59.80583
41	11.20746	-.26822	-7.97813	77.50199

10. Cu-Cr 33.62 ppm .3 K - 12 K 38 kOe

$C_N = 0.0461694/T^2$ (mJ/K-mole Cu)

N	T	ΔC	ΔC/c	$C_{Cu}(H=0)$
1	.34503	.02579	.76697	.23991
2	.38436	.02644	.78647	.26810
3	.42983	.02948	.87682	.30013
4	.48467	.03656	1.08745	.33952
5	.54217	.04369	1.29965	.38125
6	.60902	.04852	1.44309	.43040
7	.67230	.05563	1.65456	.47762
8	.74189	.06021	1.79082	.53044
9	.81959	.06983	2.07692	.59062
10	.89451	.07518	2.23624	.64997
11	.98514	.08173	2.43095	.72370
12	1.07725	.09113	2.71049	.80104
13	1.19239	.09750	2.90014	.90158
14	1.31071	.10451	3.10867	1.01015
15	1.43048	.11694	3.47829	1.12638
16	1.57609	.12459	3.70572	1.27643
17	1.74278	.13652	4.06073	1.46046
18	1.92410	.14419	4.28891	1.67694
19	2.11043	.15441	4.59267	1.91897
20	2.32317	.15442	4.59318	2.22186
21	2.56844	.15686	4.66573	2.60973
22	2.87281	.16768	4.98760	3.15475
23	3.19324	.14571	4.33404	3.81334
24	3.48524	.15823	4.70646	4.49716
25	3.79193	.16049	4.77377	5.30934
26	4.15579	.11474	3.41286	6.40856
27	4.57160	.13693	4.07287	7.85863
28	5.01603	.08885	2.64289	9.66200
29	5.51791	.11736	3.49080	12.01078
30	6.10176	.11657	3.46735	15.26609
31	6.66961	.08391	2.49576	19.02864
32	7.30130	.07769	2.31097	23.96568
33	7.97495	.05452	1.62177	30.16435
34	8.70159	.14914	4.43618	38.07187
35	9.50389	-.02187	-.65053	48.48857
36	10.41195	.13797	4.10375	62.77258
37	11.38564	-.15665	-4.65946	81.10648

11. Cu-Cr 21.160 ppm .06 K - .6 K Zero Field

N	T	ΔC	ΔC/c	$C_{Cu}(H=0)$
2	.09351	.03019	1.42661	.06476
3	.09407	.03042	1.43784	.06515
4	.10853	.03346	1.58150	.07512
5	.12480	.03401	1.60717	.08635
6	.14130	.03863	1.82555	.09774
9	.09586	.03124	1.47636	.06639
10	.10953	.03491	1.64969	.07581
11	.11920	.03349	1.58264	.08248
12	.13590	.03852	1.82032	.09402
13	.10003	.03205	1.51446	.06926
14	.11894	.03517	1.66201	.08231
15	.13437	.03808	1.79952	.09296
16	.09937	.03102	1.46613	.06380
17	.11081	.03377	1.59574	.07669
19	.10815	.03249	1.53551	.07486
20	.12530	.03416	1.61415	.08670
22	.15159	.04028	1.90372	.10484
23	.13456	.03789	1.79073	.09309
24	.15283	.04105	1.93983	.10569
25	.17341	.04293	2.02898	.11988
26	.19561	.04341	2.05174	.13521
27	.21781	.04598	2.17275	.15061
28	.13447	.03741	1.76777	.09303
29	.13128	.03596	1.69965	.09083
30	.15042	.04036	1.90738	.10403
31	.17153	.04391	2.07493	.11858
32	.19187	.04399	2.07473	.13262
33	.20255	.04493	2.12333	.14002
34	.22349	.04567	2.15818	.15302
35	.20638	.04564	2.15673	.14267
36	.23141	.04802	2.26934	.16005
37	.26155	.04867	2.30011	.18102
38	.29553	.05043	2.38330	.20475
39	.21122	.04599	2.17341	.14603
40	.24027	.04833	2.28410	.16621
41	.27352	.04756	2.24779	.18936
42	.30122	.05099	2.40984	.20874
43	.34073	.05132	2.42511	.23651
44	.38366	.05100	2.41012	.26687
45	.43339	.05128	2.42331	.30229
46	.49111	.05052	2.38756	.34379
47	.55687	.05279	2.49499	.39167
48	.30092	.05056	2.38922	.20853
49	.33940	.05121	2.42013	.23557
50	.31939	.05097	2.40393	.22149
51	.35853	.05132	2.42514	.24908
52	.41011	.05152	2.43499	.28567
53	.46990	.05097	2.40362	.32849

11. (continued)

N	T	ΔC	ΔC/c	$C_{Cu}(H=0)$
54	.53626	.05206	2.46009	.37658
55	.52925	.05318	2.51343	.37147
56	.61827	.05418	2.56037	.43700
57	.71937	.05449	2.57514	.51319
58	.83922	.05569	2.63164	.60632
59	.52312	.05283	2.49681	.36701
60	.60700	.05351	2.52870	.42863
61	.65619	.05499	2.59890	.46533
62	.74561	.05307	2.50809	.53332
63	.85084	.05647	2.66855	.61552
64	.06765	.02258	1.06728	.04693
65	.06604	.02280	1.07744	.04582
66	.06555	.02402	1.13508	.04548
67	.06579	.02445	1.15532	.04565
68	.06669	.02266	1.07087	.04627
69	.07127	.02416	1.14180	.04943
70	.06906	.02402	1.13497	.04790
71	.06823	.02468	1.16635	.04733
72	.06926	.02283	1.07880	.04804
73	.07892	.02899	1.37014	.05470
74	.08809	.02886	1.36396	.06103
75	.10116	.03123	1.47566	.07004
76	.11735	.03374	1.59471	.08121
77	.13810	.03739	1.76710	.09553
78	.07302	.02509	1.18550	.05064
79	.08497	.02907	1.37397	.05888
81	.08144	.02848	1.34612	.05645

12. Cu-Cr 21.160 ppm .3 K - 7 K Zero Field

N	T	ΔC	ΔC/c	$C_{Cu}(H=0)$
4	.45975	.05606	2.64940	.32158
5	.52216	.05826	2.75334	.36668
6	.58361	.05680	2.68448	.41163
7	.63115	.05797	2.73983	.44683
8	.70000	.05736	2.71101	.49854
9	.77996	.05889	2.78294	.55976
10	.86698	.05742	2.71353	.62800
11	.96111	.05588	2.68817	.70393
12	1.07704	.05548	2.66926	.80038
13	1.18996	.05421	2.56182	.89942
14	1.30786	.05315	2.51196	1.00746
15	1.43993	.05489	2.59413	1.13583
16	1.58641	.05268	2.48951	1.28744
17	1.75111	.05466	2.58339	1.47001
18	1.92905	.05498	2.59809	1.68311
19	2.11399	.04983	2.35489	1.92379
20	2.30740	.05269	2.49026	2.19838
21	2.52222	.05638	2.66427	2.53329
22	2.75007	.03704	1.75053	2.92600
23	2.99215	.04834	2.28441	3.38935
24	3.25973	.03384	1.59909	3.96178
25	3.55308	.04825	2.28011	4.66826
26	3.89933	.03334	1.57583	5.61793
27	4.29085	.03934	1.85894	6.85640
28	4.72280	.04411	2.08443	8.44007
29	5.21900	.00551	.26017	10.56983
30	5.78732	.02170	1.02564	13.43713
31	6.40425	.01135	.53646	17.19656

13. Cu-Cr 21.160 ppm .08 K - .9 K 3 kOe

$C_N = 0.00028776/T^2$ (mJ/K-mole Cu)

N	T	ΔC	ΔC/c	$C_{Cu}(H=0)$
2	.08447	.03443	1.62696	.05853
3	.09991	.03597	1.69971	.06918
5	.12779	.04332	2.04735	.08841
6	.08309	.03185	1.50525	.05758
9	.13325	.04325	2.04410	.09218
11	.09756	.03982	1.88200	.06756
12	.11395	.04338	2.05003	.07686
16	.12147	.03814	1.80236	.08405
17	.13567	.04277	2.02145	.09386
18	.08937	.03416	1.61422	.06191
19	.10671	.03681	1.73946	.07387
20	.12375	.03875	1.83131	.08563
21	.13824	.03897	1.84177	.09563
22	.16441	.04248	2.00761	.11368
23	.13093	.03597	1.69991	.09058
24	.15208	.04279	2.02206	.10518
25	.17517	.04661	2.20296	.12110
26	.19861	.04797	2.26706	.13729
27	.23255	.05229	2.47119	.16094
29	.15419	.03825	1.80780	.10663
30	.17696	.04386	2.07297	.12233
31	.19945	.04780	2.25905	.13787
32	.22500	.05127	2.42305	.15560
33	.20551	.04807	2.27155	.14207
34	.23604	.04929	2.32956	.16327
35	.27286	.04900	2.31591	.18890
36	.32020	.05406	2.55471	.22206
37	.19875	.04513	2.13285	.13739
38	.22665	.04473	2.11371	.15674
39	.26168	.05030	2.37714	.18111
40	.30351	.05639	2.66501	.21034
41	.30261	.05509	2.60366	.20971
42	.34965	.05809	2.74544	.24280
43	.40246	.05808	2.74501	.28023
44	.45878	.05841	2.76052	.32049
45	.52725	.05832	2.75608	.37002
46	.59631	.05980	2.82627	.42071
47	.30540	.05456	2.57856	.21166
48	.35994	.05555	2.62524	.25007
49	.41933	.05754	2.71907	.29224
50	.48412	.05818	2.74959	.33874
51	.56109	.06047	2.85780	.39476
52	.53046	.05959	2.81598	.37236
53	.61604	.06280	2.96783	.43534
54	.71416	.06382	3.01595	.50922
55	.81802	.05902	2.78907	.58962
56	.54083	.06155	2.90871	.37992
57	.63106	.06208	2.93387	.44652
58	.72338	.06359	3.00516	.51626
59	.82502	.05924	2.79975	.59513

14. Cu-Cr 21.160 ppm .3 K - 7 K 38 kOe

$C_N = 0.0461694/T^2$ (mJ/K-mole Cu)

N	T	ΔC	ΔC/c	$C_{Cu}(H=0)$
1	.35142	.02234	1.05559	.24443
2	.39350	.02115	.99940	.27424
3	.44531	.02314	1.09357	.31121
4	.50511	.02783	1.31513	.35430
5	.55873	.02883	1.36237	.39336
6	.59857	.03216	1.51993	.42267
7	.66661	.03702	1.74963	.47335
8	.74754	.04176	1.97358	.53477
9	.83006	.04899	2.31518	.59883
10	.90939	.05226	2.46984	.66193
11	1.00703	.05806	2.74404	.74185
12	1.12273	.06331	2.99181	.84021
13	1.25342	.07097	3.35398	.95685
14	1.39894	.07608	3.59529	1.09517
15	1.55676	.08636	4.08134	1.25594
16	1.72988	.09161	4.32941	1.44572
17	1.92936	.09935	4.71896	1.68350
18	2.14232	.10212	4.82605	1.96250
19	2.36901	.10877	5.14057	2.29109
20	2.60522	.10592	5.00588	2.67170
21	2.86177	.11248	5.31549	3.13367
22	3.15419	.09547	4.51175	3.72813
23	3.47042	.10348	4.89045	4.46043
24	3.81602	.11032	5.21373	5.37744
25	4.19639	.08151	3.85189	6.54252
26	4.60392	.09185	4.34065	7.99924
27	5.05912	.05962	2.81773	9.85035
28	5.60690	.07007	3.31143	12.46813
29	6.21860	.06357	3.00412	15.99255

15. Cu-Fe 81.4 ppm .3 K - 25 K Zero Field

Two runs - before and after exposure to 38 kOe

N	T	ΔC	ΔC/c	$C_{Cu}(H=0)$
1	.36332	.03053	.37506	.25205
2	.32850	.02970	.36491	.22753
3	.36647	.03070	.37710	.25427
4	.40827	.03269	.40159	.28387
5	.47971	.03754	.46118	.33493
6	.39564	.03235	.39741	.27491
7	.45307	.03577	.43942	.31582
8	.49759	.03948	.48502	.34782
9	.55255	.04416	.54255	.38771
10	.60670	.04805	.59027	.42747
11	.66722	.05214	.64051	.47250
12	.74583	.05832	.71647	.53203
13	.82931	.06467	.79449	.59668
14	.90551	.06945	.85319	.65712
15	.98565	.07205	.88519	.72228
16	1.07779	.07823	.96110	.79943
18	1.25254	.08927	1.09666	.95322
19	1.38295	.09971	1.22496	1.07662
20	1.52253	.10559	1.29720	1.21739
21	1.66311	.11509	1.41386	1.36815
23	1.77382	.12109	1.48765	1.49359
24	1.93737	.13384	1.64423	1.69075
25	2.11659	.14110	1.73342	1.92454
26	2.29971	.14795	1.81758	2.18416
27	2.51233	.15472	1.90076	2.51420
28	2.71117	.16712	2.05302	2.85297
29	2.97615	.16622	2.04198	3.35373
30	3.27109	.17876	2.19609	3.98372
31	3.59605	.19438	2.38792	4.77475
32	3.92662	.20057	2.46395	5.69351
33	4.36894	.20203	2.48200	7.12019
34	4.86331	.20316	2.49587	9.01079
35	5.37491	.19558	2.40264	11.32483
36	5.92371	.19754	2.42675	14.25182
37	6.51402	.20046	2.46271	17.97691
38	7.13249	.21913	2.69205	22.60700
39	7.80530	.21069	2.58833	28.56595
40	8.48500	.20200	2.48153	35.65363
41	9.24874	.19155	2.35325	45.06654
42	10.10907	.23299	2.86227	57.81621
43	11.06293	.28402	3.48919	74.73790
44	12.06199	.25191	3.09467	96.03647
45	13.18327	.11758	1.44444	125.02366
46	14.51345	-.01457	-.17905	167.56426
47	15.93359	-.19796	-2.43188	224.40743
48	17.52544	.34379	4.22351	304.31381
49	19.24550	1.43428	17.62011	412.05379
50	21.08000	.01425	.17503	555.48715

15. (continued)

N	T	ΔC	ΔC/c	$C_{Cu}(H=0)$
51	23.27507	1.08345	13.31016	769.90809
1	.34149	.02974	.36531	.23667
3	.41065	.03358	.41255	.28556
5	.49504	.03935	.48341	.34597
7	.60190	.04692	.57646	.42392
9	.72131	.05549	.68166	.51333
11	.86910	.06615	.81266	.62807
13	1.01796	.07482	.91922	.74905
15	1.21851	.08593	1.05560	.92239
17	1.46456	.10271	1.26177	1.15788
19	1.78173	.12203	1.49909	1.50279
23	2.67646	.17000	2.08839	2.79163
21	2.17110	.14024	1.72284	1.99955
25	3.31755	.19144	2.35185	4.09038
27	4.04255	.21139	2.59696	6.04481
29	4.84030	.23429	2.87823	8.91542
31	5.68160	.20641	2.53578	12.90057
32	6.04216	.18324	2.25106	14.94903
33	6.59479	.19921	2.44730	18.53782
34	7.16240	.20688	2.54146	22.85099
35	7.77748	.24656	3.02901	28.29945
36	8.46254	.19908	2.44567	35.40099
37	9.20197	.13066	1.60511	44.44161
38	10.11015	.27351	3.36003	57.83354
39	11.12914	.33944	4.17007	76.03004
40	12.15057	.33537	4.12002	98.12079
41	13.30352	.27057	3.32390	128.48726
42	14.61915	.37902	4.65628	171.36492
43	16.03179	.24818	3.04885	228.82395
44	17.59211	.61429	7.54661	308.06083
45	19.42940	.85816	10.54245	425.01087
46	21.30632	.58013	7.12688	575.50167
47	23.46589	.83322	10.23612	790.13093

16. Cu-Fe 81.4 ppm .3 K - 2.5 K 20 kOe

$C_N = 0.0127893/T^2$ (mJ/K-mole Cu)

N	T	ΔC	ΔC/c	$C_{Cu}(H=0)$
3	.36644	.02800	.34399	.25425
4	.39791	.02824	.34688	.27652
5	.43263	.02978	.36591	.30121
6	.46737	.03485	.42810	.32607
7	.50762	.03850	.47293	.35506
8	.55249	.04538	.55753	.38766
9	.59104	.04686	.57573	.41592
10	.64741	.05050	.62043	.45768
11	.70721	.05428	.66678	.50264
12	.77195	.06117	.75150	.55210
13	.84553	.06663	.81851	.60943
14	.91550	.07332	.90070	.66515
15	.99413	.07649	.93962	.72928
16	1.08223	.08032	.98678	.80321
17	1.19058	.08835	1.08532	.89744
18	1.32547	.09957	1.22328	1.02114
19	1.48257	.10956	1.34599	1.17620
20	1.63764	.11897	1.46153	1.34016
21	1.81924	.13268	1.62994	1.54688
22	1.99279	.14208	1.74547	1.76100
23	2.17999	.15572	1.91308	2.01196
24	2.38013	.16008	1.96659	2.30526

17. Cu-Fe 81.4 ppm .3 K - 2.5 K 30 kOe

$C_N = 0.028776/T^2$ (mJ/K-mole Cu)

N	T	ΔC	ΔC/c	$C_{Cu}(H=0)$
1	.30971	.02929	.35988	.21435
2	.32676	.02975	.36551	.22631
3	.35077	.03136	.38529	.24320
4	.37944	.02920	.35875	.26344
5	.41376	.02960	.36363	.28777
6	.45510	.03172	.38968	.31727
7	.50513	.03582	.44008	.35326
8	.55766	.04041	.49642	.39143
9	.60063	.04382	.53831	.42299
10	.65617	.04708	.57833	.46423
11	.71406	.05145	.63204	.50783
12	.78302	.05617	.69001	.56065
13	.85544	.06182	.75947	.61725
14	.92459	.06683	.82103	.67248
15	1.00787	.07239	.88936	.74066
16	1.09719	.07765	.95394	.81600
17	1.20498	.08188	1.00585	.91027
18	1.34217	.09514	1.16876	1.03709
19	1.49850	.10598	1.30198	1.19253
20	1.66076	.11612	1.42654	1.36556
21	1.84907	.13017	1.59908	1.58248
22	2.03562	.14233	1.74855	1.81652
23	2.22037	.14777	1.81538	2.06899
24	2.42645	.15886	1.95156	2.37704

18. Cu-Fe 81.4 ppm .3 K - 25 K 38 kOe

$C_N = 0.0461694/T^2$ (mJ/K-mole Cu)

N	T	ΔC	ΔC/c	$C_{Cu}(H=0)$
3	.35735	.03025	.37167	.24784
4	.37984	.02883	.35421	.26372
5	.40930	.02923	.35911	.28461
6	.44312	.03030	.37220	.30870
7	.48359	.03328	.40883	.33772
8	.53336	.03659	.44948	.37373
9	.57582	.03996	.49096	.40473
10	.62926	.04395	.53987	.44418
11	.69266	.04744	.58283	.49163
12	.77286	.05374	.66019	.55280
13	.86803	.06047	.74285	.62722
14	.96028	.06573	.80748	.70146
15	1.04605	.07152	.87859	.77258
16	1.14645	.07624	.93661	.85858
17	1.26480	.08629	1.06009	.96445
18	1.39549	.09622	1.18201	1.08894
19	1.53211	.10369	1.27378	1.22738
20	1.69786	.11807	1.45047	1.40685
21	1.83648	.12754	1.56685	1.56739
22	1.99954	.13730	1.68678	1.76967
23	2.18947	.14499	1.78122	2.02526
24	2.41802	.15765	1.93674	2.36386
25	2.67151	.16593	2.03839	2.78296
26	2.96169	.17344	2.13076	3.32488
27	3.31253	.18925	2.32489	4.07875
28	3.67746	.19672	2.41671	4.98995
29	4.03458	.20997	2.57950	6.02015
30	4.41848	.20830	2.55895	7.29500
31	4.82458	.21713	2.66738	8.85068
32	5.26531	.20316	2.49584	10.79692
33	5.75706	.20803	2.55561	13.31130
34	6.23678	.20246	2.48723	16.14826
35	6.77829	.21105	2.59280	19.86033
36	7.35937	.23873	2.93275	24.50522
37	7.99157	.24518	3.01203	30.39715
38	8.68542	.24811	3.04804	37.96625
39	9.52405	.33971	4.17340	48.88435
40	10.47756	.31264	3.84078	63.99065
41	11.39917	.25116	3.08551	81.46905
42	12.37361	.34113	4.19074	103.51938
43	13.56350	.12533	1.53968	136.22522
44	14.86104	.12819	1.57483	180.31174
45	16.31889	.30168	3.70620	242.11714
46	17.91303	.29523	3.62694	326.56712
47	19.81107	.91412	11.23002	452.85739
48	21.95167	1.45899	17.92365	635.68597

19. Cu-Fe 195 ppm .3 K - 25 K Zero Field

N	T	ΔC	ΔC/c	$C_{Cu}(H=0)$
1	.35372	.07443	.38171	.24528
2	.39180	.07839	.40201	.27219
3	.44001	.08562	.43908	.30648
4	.49029	.09545	.48951	.34255
5	.54690	.10554	.54121	.38359
7	.38871	.07739	.39686	.27000
8	.42447	.08361	.42875	.29540
9	.46660	.09043	.46372	.32551
10	.51120	.09950	.51027	.35765
11	.55505	.10764	.55200	.38953
12	.59653	.11466	.58801	.41996
13	.64808	.12346	.63312	.45818
14	.72008	.13526	.69367	.51240
15	.80208	.15064	.77253	.57543
16	.87570	.16152	.82833	.63331
17	.95164	.17423	.89350	.69442
18	1.02983	.18664	.95714	.75896
19	1.11831	.19827	1.01674	.83417
20	1.22529	.21618	1.10863	.92850
21	1.33292	.23503	1.20530	1.02824
22	1.44574	.25615	1.31358	1.13888
23	1.56594	.26644	1.36637	1.26298
24	1.73111	.29002	1.48730	1.44446
25	1.90846	.31023	1.59092	1.65481
26	2.09676	.33058	1.69527	1.89771
27	2.32338	.34955	1.79258	2.21934
28	2.55764	.37594	1.92788	2.58874
29	2.81581	.39629	2.03226	3.04375
30	3.08184	.41137	2.10961	3.57035
31	3.36156	.43186	2.21468	4.19335
32	3.65078	.45301	2.32310	4.91865
33	3.99717	.46289	2.37380	5.90543
34	4.38004	.48906	2.50802	7.15909
35	4.75764	.49206	2.52336	8.57891
36	5.16928	.49623	2.54477	10.34912
37	5.68710	.47856	2.45417	12.93017
38	6.18454	.49945	2.56127	15.81971
39	6.74404	.47767	2.44958	19.60835
40	7.31541	.51211	2.62619	24.12874
41	7.96461	.54857	2.81320	30.12706
42	8.74904	.60392	3.09704	38.72288
43	9.63529	.47883	2.45554	50.49899
44	10.57910	.58589	3.00457	65.77033
45	11.56559	.47312	2.42624	84.96043
46	12.62904	.50609	2.59531	109.97328
47	13.84484	.29574	1.51663	144.99487
48	15.06694	.44160	2.26462	188.20780
49	16.39895	.46105	2.36435	245.92482
50	17.89905	.26076	1.33721	325.74499
51	19.50356	-.81688	-4.18914	430.32019

20. Cu-Fe 195 ppm .3 K - 2.5 K 20 kOe

$C_N = 0.0127893/T^2$ (mJ/K-mole Cu)

N	T	ΔC	ΔC/c	$C_{Cu}(H=0)$
1	.33933	.06607	.33883	.23514
2	.35752	.07120	.36510	.24795
3	.38117	.07306	.37467	.26466
4	.40717	.07660	.39284	.28309
5	.43509	.08111	.41594	.30297
6	.46650	.08586	.44032	.32544
7	.50738	.09560	.49024	.35489
8	.55748	.10529	.53993	.39131
9	.61584	.11307	.57987	.43422
10	.67935	.12907	.66188	.48161
11	.74995	.14286	.73263	.53519
12	.82881	.15797	.81012	.59629
13	.92387	.17499	.89740	.67189
14	1.01000	.18846	.96646	.74243
15	1.10751	.20294	1.04070	.82486
16	1.21950	.22130	1.13487	.92329
17	1.35383	.24230	1.24255	1.04831
18	1.49803	.26338	1.35065	1.19205
19	1.64930	.28581	1.46569	1.35294
20	1.82287	.31146	1.59726	1.55119
21	2.01657	.33540	1.72000	1.79170
22	2.21869	.35642	1.82778	2.06659
23	2.43441	.37777	1.93728	2.38952

21. Cu-Fe 195 ppm .3 K - 2.5 K 30 kOe

$C_N = 0.028776/T^2$ (mJ/K-mole Cu)

N	T	ΔC	ΔC/c	$C_{Cu}(H=0)$
1	.33018	.06571	.33696	.22872
2	.34617	.06694	.34326	.23996
3	.36473	.06778	.34758	.25305
4	.38628	.06873	.35246	.26828
5	.41229	.07270	.37282	.28673
6	.44039	.07748	.39731	.30675
7	.47213	.08281	.42468	.32949
8	.51229	.09065	.46489	.35844
9	.56340	.09964	.51099	.39563
10	.61876	.10974	.56275	.43639
11	.67728	.12056	.61827	.48005
12	.74512	.13250	.67947	.53149
13	.82849	.14921	.76518	.59604
14	.91837	.16180	.82973	.66746
15	.99830	.17440	.89435	.73273
16	1.09009	.18793	.96374	.80992
17	1.20668	.20584	1.05557	.91179
18	1.33420	.22790	1.16874	1.02946
19	1.46287	.24690	1.26618	1.15617
20	1.60228	.26796	1.37417	1.30181
21	1.77058	.29383	1.50681	1.48982
22	1.96214	.32170	1.64972	1.72193
23	2.19471	.34759	1.78252	2.03263
24	2.44274	.37708	1.93376	2.40265
25	2.69191	.40361	2.06979	2.81882

22. Cu-Fe 195 ppm .3 K - 2.5 K 38 kOe

$C_N = 0.0461694/T^2$ (mJ/K-mole Cu)

N	T	ΔC	ΔC/c	$C_{Cu}(H=0)$
1	.33167	.06318	.32402	.22976
2	.34410	.06793	.34834	.23850
3	.35947	.06684	.34276	.24933
4	.37858	.06868	.35221	.26283
5	.40837	.07082	.36320	.28394
6	.44348	.07567	.38807	.30896
7	.48739	.08303	.42579	.34046
8	.54618	.09297	.47679	.38306

23. Cu-Fe 640 ppm .06 K - 1 K Zero Field

by J. C. F. Brock

N	T	ΔC	ΔC/c	$C_{Cu}(H=0)$
1	.06679	.11916	.18619	.04596
11	.06682	.11414	.17834	.04598
2	.07216	.12819	.20029	.04966
12	.07217	.12672	.19801	.04967
3	.07768	.13636	.21306	.05346
4	.08305	.14017	.21902	.05716
5	.08819	.14773	.23083	.06070
15	.08821	.14572	.22769	.06072
6	.09609	.16009	.25013	.06615
7	.10387	.17036	.26619	.07151
8	.11144	.17930	.28016	.07673
9	.11936	.18922	.29566	.08219
10	.12912	.20169	.31513	.08892
12	.15156	.22640	.35374	.10441
13	.16572	.23927	.37385	.11420
14	.18136	.25239	.39437	.12502
15	.19798	.26259	.41030	.13652
16	.21703	.27306	.42665	.14973
17	.23842	.28521	.44564	.16459
18	.27118	.30172	.47143	.18741
19	.30176	.31588	.49356	.20879
20	.33634	.33330	.52079	.23304
21	.37291	.35241	.55064	.25882
22	.07903	.13645	.21320	.05440
23	.08628	.14626	.22853	.05939
24	.09294	.15505	.24227	.06397
25	.12549	.19711	.30798	.08641
26	.13561	.20763	.32443	.09340
28	.15860	.23271	.36360	.10928
29	.17083	.23764	.37131	.11773
30	.18544	.25304	.39537	.12784
31	.19920	.26136	.40838	.13737
32	.21429	.27002	.42190	.14783
33	.23210	.28169	.44014	.16020
34	.25002	.28950	.45234	.17266
35	.27019	.30229	.47234	.18672
36	.29464	.31264	.48850	.20380
37	.32374	.32643	.51005	.22419
38	.36344	.34557	.53996	.25213
39	.41376	.37056	.57900	.28778
40	.46868	.39948	.62419	.32701
41	.53221	.43398	.67809	.37289
42	.60635	.47489	.74201	.42720
43	.70057	.52496	.82026	.49761
44	.79641	.57370	.89640	.57102
45	.93457	.63734	.99585	.68054
46	1.08648	.69563	1.08692	.80684
47	.33275	.32904	.51412	.23052

23. (continued)

N	T	ΔC	ΔC/c	$C_{Cu}(H=0)$
48	.36651	.34636	.54119	.25430
49	.40129	.36557	.57120	.27892
50	.43911	.38457	.60089	.30584
52	.52514	.43123	.67380	.36775
53	.57944	.46092	.72018	.40739
54	.63929	.49056	.76650	.45164
55	.71206	.52748	.82419	.50630
56	.78871	.56804	.88757	.56505
57	.86418	.60529	.94577	.62416
58	.94910	.64659	1.01030	.69235
59	1.04198	.69390	1.08421	.76915

24. Cu-Fe 640 ppm .3 K - 25 K Zero Field

N	T	ΔC	ΔC/c	$C_{Cu}(H=0)$
1	.34844	.33775	.52773	.24156
2	.40072	.36243	.56629	.27851
3	.34097	.32706	.51103	.23630
4	.39316	.35911	.56110	.27315
5	.43750	.38135	.59586	.30469
6	.49275	.41111	.64236	.34432
7	.55469	.44500	.69530	.38927
8	.60253	.47106	.73603	.42439
9	.66182	.50157	.78370	.46846
10	.72229	.53370	.83391	.51407
11	.78369	.56530	.88329	.56116
12	.84552	.59800	.93438	.60942
13	.91836	.63296	.98900	.66745
14	.99902	.67187	1.04979	.73332
15	1.10316	.71857	1.12276	.82112
16	1.21872	.76656	1.19775	.92258
17	1.33992	.81847	1.27885	1.03494
18	1.48881	.87898	1.37341	1.18258
19	1.61162	.92741	1.44908	1.31188
20	1.75583	.98002	1.53128	1.47278
21	1.91893	1.03202	1.61253	1.66777
22	2.09655	1.08644	1.69756	1.89744
23	2.31002	1.14050	1.78204	2.19943
24	2.53611	1.19667	1.86979	2.55312
25	2.72923	1.23115	1.92368	2.88527
26	3.00883	1.27779	1.99655	3.41964
27	3.32564	1.34096	2.09526	4.10916
28	3.88809	1.41313	2.20802	5.58019
29	4.30862	1.45232	2.26926	6.91155
30	4.77227	1.49324	2.33319	8.63780
31	5.30179	1.52119	2.37685	10.97061
32	5.88948	1.50907	2.35793	14.05481
33	6.39291	1.55762	2.43378	17.16015
34	6.94826	1.58022	2.46909	21.14605
35	7.58263	1.62669	2.54170	26.48260
36	8.27790	1.69914	2.65491	33.37343
37	9.03051	1.61578	2.52466	42.20651
38	9.87367	1.65211	2.58142	54.09343
39	10.77472	1.70466	2.66354	69.29746
40	11.75409	1.50622	2.35347	89.04777
41	12.84711	1.65294	2.58271	115.71981
42	14.12475	1.22554	1.91491	154.14080
43	15.53176	1.44281	2.25440	207.01492
44	17.08614	1.14805	1.79383	280.43749
45	18.92689	2.34868	3.66981	390.29789
46	21.12296	.22191	.34673	559.24511
47	23.53355	-.21740	-.33969	797.34384

25. Cu-Fe 640 ppm .3 K - 1 K 1 kOe

$C_N = 0.00003197/T^2$ (mJ/K-mole Cu)

N	T	ΔC	ΔC/c	$C_{Cu}(H=0)$
1	.33749	.34907	.54542	.23386
2	.33680	.34671	.54173	.23337
3	.38092	.37063	.57912	.26448
4	.42481	.39273	.61364	.29564
5	.46811	.41478	.64810	.32660
6	.51348	.44004	.68756	.35931
7	.54937	.45812	.71581	.38539
8	.59904	.48391	.75612	.42181
9	.65303	.51112	.79863	.46188
10	.71688	.54391	.84987	.50997
11	.79339	.58270	.91046	.56868
12	.87674	.62301	.97345	.63413
13	.97628	.67069	1.04795	.71457

26. Cu-Fe 640 ppm .3 K - 8 K 3 kOe

$C_N = 0.00028776/T^2$ (mJ/K-mole Cu)

N	T	ΔC	ΔC/c	$C_{Cu}(H=0)$
1	.36318	.36847	.57574	.25195
2	.40792	.39689	.62015	.28362
3	.44587	.42082	.65753	.31067
4	.35990	.36675	.57304	.24964
5	.39796	.38955	.60867	.27656
6	.43857	.41550	.64922	.30545
7	.48035	.44139	.68968	.33539
8	.51922	.46636	.72869	.36346
9	.56558	.49408	.77200	.39723
10	.62246	.52699	.82343	.43913
11	.68743	.56127	.87698	.48769
12	.76257	.60003	.93755	.54488
13	.85109	.64760	1.01187	.61381
14	.95546	.69668	1.08857	.69753
15	1.05451	.73840	1.15376	.77970
16	1.17161	.78872	1.23238	.88065
17	1.29704	.84206	1.31571	.99431
18	1.52732	.93158	1.45560	1.22238
19	1.42299	.88672	1.38550	1.11614
20	1.59871	.94939	1.48342	1.29797
21	1.76915	1.01543	1.58660	1.48818
22	1.98124	1.07910	1.68610	1.74621
23	2.21180	1.13723	1.77692	2.05679
24	2.47682	1.20573	1.88396	2.45683
25	2.75179	1.26005	1.96883	2.92597
26	2.98839	1.30372	2.03707	3.37832
27	3.30341	1.35274	2.11366	4.05770
28	3.64314	1.41422	2.20971	4.89837
29	3.99854	1.45828	2.27856	5.90961
30	4.40886	1.49530	2.33641	7.26083
31	4.86730	1.52619	2.38467	9.02736
32	5.37365	1.54252	2.41019	11.31862
33	5.91630	1.54788	2.41857	14.20902
34	6.42287	1.55306	2.42665	17.35958
35	7.02225	1.59875	2.49805	21.72432
36	7.64271	1.68944	2.63974	27.03357

27. Cu-Fe 640 ppm .3 K - 25 K 10 kOe

$C_N = 0.0031973/T^2$ (mJ/K-mole Cu)

N	T	ΔC	ΔC/c	$C_{Cu}(H=0)$
1	.32654	.28819	.45029	.22616
2	.37979	.32804	.51256	.26369
3	.42817	.36352	.56800	.29803
4	.47572	.39932	.62393	.33207
5	.52932	.44082	.68878	.37079
6	.59519	.48734	.76148	.41898
7	.68801	.54991	.85923	.48813
11	.73228	.57975	.90586	.52168
12	.81622	.63296	.98901	.58644
13	.91219	.69041	1.07876	.66248
14	1.02769	.75361	1.17752	.75717
15	1.15494	.81743	1.27723	.86601
16	1.26996	.87113	1.36114	.96919
17	1.40180	.93224	1.45663	1.09516
18	1.54705	.99020	1.54719	1.24303
19	1.70685	1.05540	1.64907	1.41697
20	1.86753	1.10586	1.72790	1.60475
21	2.02424	1.15674	1.80741	1.80167
22	2.20531	1.20064	1.87599	2.04760
23	2.36385	1.24326	1.94259	2.28038
24	2.58365	1.29284	2.02006	2.63224
25	2.82603	1.33987	2.09354	3.06286
26	3.08572	1.37832	2.15363	3.57849
27	3.37015	1.42971	2.23392	4.21367
28	4.03056	1.50990	2.35922	6.00777
29	3.69485	1.46722	2.29253	5.03684
30	4.03702	1.50931	2.35830	6.02769
31	4.44051	1.54554	2.41491	7.37375
32	4.88162	1.56703	2.44849	9.08716
33	5.31992	1.59353	2.48990	11.05770
34	5.81172	1.55307	2.42668	13.61468
35	6.33451	1.62601	2.54064	16.77636
36	7.01523	1.63861	2.56033	21.66896
37	7.77014	1.69520	2.64876	28.22949
38	8.59181	1.65759	2.58998	36.87278
39	9.45305	1.64522	2.57066	47.87630
40	10.34486	1.66740	2.60532	61.71633
41	11.34748	1.79350	2.80234	80.40643
42	12.38914	1.75379	2.74030	103.90358
43	13.62521	1.64367	2.56824	138.11319
44	15.11976	1.91699	2.99529	190.27630
45	16.82868	1.87357	2.92745	267.11201
46	18.79778	2.14062	3.34472	381.72766
47	21.00295	2.16545	3.38352	548.79492
48	23.18052	3.04238	4.75372	759.95651

28. Cu-Fe 640 ppm .3 K - 1 K 18 kOe

$C_N = 0.010359/T^2$ (mJ/K-mole Cu)

N	T	ΔC	ΔC/c	$C_{Cu}(H=0)$
1	.31520	.24669	.38546	.21820
2	.34471	.26481	.41376	.23893
3	.39933	.30175	.47149	.27752
4	.45064	.33727	.52699	.31408
5	.49612	.36944	.57725	.34675
6	.54392	.40417	.63151	.38141
8	.34013	.26092	.40770	.23571
9	.37609	.28618	.44716	.26107
10	.41385	.31136	.48650	.28784
11	.45341	.33916	.52993	.31606
12	.49422	.36789	.57483	.34538
13	.54315	.40373	.63083	.38085
14	.59926	.44336	.69275	.42198
15	.65544	.48041	.75064	.46368
16	.72392	.52678	.82309	.51532
17	.80453	.57985	.90601	.57734

29. Cu-Fe 640 ppm .3 K - 3 K 24 kOe

$C_N = 0.018417/T^2$ (mJ/K-mole Cu)

N	T	ΔC	ΔC/c	$C_{Cu}(H=0)$
1	.32967	.23797	.37183	.22836
2	.35625	.25459	.39780	.24706
3	.38944	.27424	.42850	.27051
4	.42143	.29602	.46253	.29324
5	.45843	.31910	.49860	.31966
6	.50449	.35128	.54887	.35280
7	.54611	.37973	.59333	.38301
8	.33896	.24077	.37621	.23489
9	.36770	.26224	.40975	.25514
10	.40364	.28361	.44315	.28059
11	.44017	.30806	.48134	.30660
12	.58875	.40870	.63860	.41423
13	.64254	.44246	.69134	.45405
14	.69975	.47917	.74870	.49699
15	.76298	.51937	.81152	.54519
16	.84487	.57217	.89402	.60891
17	.92579	.62181	.97158	.67344
18	1.01404	.67285	1.05132	.74579
19	1.10593	.72405	1.13133	.82350
20	1.21872	.78109	1.22045	.92258
21	1.35815	.85567	1.33698	1.05248
22	1.51785	.93266	1.45728	1.21253
23	1.69842	1.01701	1.58908	1.40749
24	1.91707	1.10928	1.73325	1.66545
25	2.16864	1.20115	1.87680	1.99613

30. Cu-Fe 640 ppm .3 K - 2 K 30 kOe

$C_N = 0.028776/T^2$ (mJ/K-mole Cu)

N	T	ΔC	ΔC/c	$C_{Cu}(H=0)$
1	.32712	.18444	.28819	.22657
2	.34718	.19455	.30399	.24067
3	.37294	.20758	.32434	.25884
4	.40082	.22270	.34796	.27858
5	.43072	.23899	.37343	.29985
6	.46225	.25637	.40057	.32240
7	.49275	.27532	.43018	.34432
8	.52801	.29533	.46146	.36984
9	.56741	.31864	.49788	.39857
10	.60924	.34356	.53681	.42934
11	.66405	.37419	.58467	.47012
12	.70687	.39799	.62186	.50238
13	.75634	.42664	.66663	.54009
14	.82114	.46285	.72320	.59029
15	.88712	.49934	.78021	.64240
16	.96420	.54000	.84375	.70467
17	1.05347	.58736	.91776	.77883
18	1.15339	.63508	.99231	.86465
19	1.26199	.68982	1.07785	.96187
20	1.38259	.75112	1.17363	1.07627
21	1.50853	.79988	1.24981	1.20288
22	1.65289	.87126	1.36134	1.35688
23	1.80205	.93847	1.46636	1.52658
24	1.96924	1.00450	1.56954	1.73093
25	2.16008	1.06829	1.66921	1.98423

31. Cu-Fe 640 ppm .3 K - 2 K 33 kOe

$C_N = 0.034819/T^2$ (mJ/K-mole Cu)

N	T	ΔC	ΔC/c	C_{Cu}(H=0)
1	.30834	.15829	.24732	.21340
2	.33185	.18311	.28611	.22989
3	.36006	.19602	.30628	.24975
4	.39350	.21320	.33312	.27339
5	.43189	.23325	.36446	.30068
6	.47237	.25552	.39925	.32966
7	.51983	.28300	.44219	.36391
8	.57739	.31446	.49134	.40588
9	.66204	.36193	.56551	.46862
10	.74762	.40932	.63956	.53341
11	.82914	.45450	.71015	.59655
12	.92719	.50815	.79398	.67457
13	1.01677	.55348	.86481	.74806
14	1.11581	.60273	.94176	.83201
15	1.21279	.64794	1.01241	.91726
16	1.31565	.70131	1.09579	1.01183
17	1.42127	.75223	1.17536	1.11443
19	1.66637	.86914	1.35804	1.37176
20	1.80554	.92506	1.44540	1.53069
21	1.95103	.98165	1.53384	1.70790
22	2.11385	1.09690	1.71391	1.92082
23	2.29361	1.09327	1.70824	2.17515

32. Cu-Fe 640 ppm .3 K - 25 K 36 kOe

$C_N = 0.041438/T^2$ (mJ/K-mole Cu)

N	T	ΔC	ΔC/c	C_{Cu}(H=0)
1	.31560	.16539	.25842	.21848
2	.35129	.22450	.35079	.24357
3	.39142	.24773	.38707	.27192
4	.43334	.27109	.42358	.30172
5	.48414	.30110	.47047	.33812
6	.54463	.33857	.52902	.38193
7	.59666	.36994	.57803	.42006
8	.65729	.40544	.63350	.46506
9	.71695	.43925	.68632	.51002
10	.78241	.47808	.74699	.56018
11	.85564	.52071	.81361	.61740
12	.92617	.56001	.87501	.67375
13	1.01057	.60500	.94531	.74290
14	1.09652	.64833	1.01302	.81542
15	1.19277	.69999	1.09374	.89939
16	1.30188	.75815	1.18460	.99884
17	1.43638	.82579	1.29029	1.12950
18	1.58050	.89450	1.39766	1.27846
19	1.74880	.97534	1.52397	1.46469
20	1.91632	1.04942	1.63972	1.66453
21	2.08196	1.10931	1.73329	1.87785
22	2.30821	1.19346	1.86478	2.19675
23	2.48636	1.25603	1.96254	2.47215
24	2.72907	1.33412	2.08456	2.88498
25	2.99498	1.40526	2.19573	3.39161
26	3.27365	1.46999	2.29685	3.98954
27	3.56960	1.53708	2.40169	4.70635
28	3.88540	1.59481	2.49189	5.57234
29	4.21280	1.63363	2.55255	6.58947
30	4.58284	1.68278	2.62934	7.89798
31	4.97593	1.70956	2.67119	9.48818
32	5.39954	1.73345	2.70851	11.44593
33	5.88090	1.72147	2.68979	14.00577
34	6.40484	1.77270	2.76984	17.23937
35	7.09205	1.82212	2.84706	22.28023
36	7.82295	1.87084	2.92318	28.73602
37	8.54507	1.83646	2.86947	36.33555
38	9.31537	1.83121	2.86126	45.96854
39	10.18610	1.88419	2.94405	59.07073
40	11.19150	1.91772	2.99643	77.26183
41	12.19379	1.96411	3.06892	99.15014
42	13.28172	1.84876	2.88869	127.85388
43	14.60378	1.69675	2.65117	170.80794
44	16.14972	1.67775	2.62148	234.21612
45	17.84580	1.90746	2.98040	322.62529
46	19.85685	1.45179	2.26841	456.28655
47	21.98920	1.33755	2.08992	639.31749
48	23.88557	.58751	.91799	835.18179

33. Cu-Fe 640 ppm .3 K - 2 K 38 kOe

$C_N = 0.0461694/T^2$ (mJ/K-mole Cu)

N	T	ΔC	ΔC/c	$C_{Cu}(H=0)$
1	.30443	.13677	.21370	.21065
2	.32110	.17653	.27583	.22234
3	.34124	.18231	.28487	.23649
4	.36501	.19256	.30088	.25324
5	.40272	.20630	.32235	.27993
6	.43786	.22515	.35180	.30495
7	.47754	.24606	.38446	.33337
8	.52811	.27531	.43017	.36991
9	.59007	.30876	.48244	.41520
10	.65224	.34063	.53223	.46129
11	.71416	.37325	.58320	.50790
12	.78529	.41146	.64290	.56240
13	.86271	.45236	.70681	.62300
14	.92078	.48190	.75297	.66940
15	1.00006	.52239	.81623	.73418
16	1.08645	.56251	.87893	.80682
17	1.19088	.61453	.96020	.89770
18	1.30051	.66758	1.04310	.99756
19	1.41983	.72383	1.13098	1.11300
20	1.56861	.78773	1.23083	1.26580
21	1.70559	.85543	1.33661	1.41555
22	1.85295	.91621	1.43158	1.58714
23	1.99272	.97397	1.52183	1.76091
24	2.14441	1.02658	1.60403	1.96259

34. Cu-Fe 2560 ppm .3 K - 25 K Zero Field

N	T	ΔC	ΔC/c	$C_{Cu}(H=0)$
1	.48325	1.28208	.50081	.33748
2	.53003	1.41308	.55199	.37131
3	.59176	1.57955	.61701	.41645
4	.65350	1.74655	.68225	.46223
5	.72219	1.93670	.75652	.51400
6	.80192	2.15845	.84315	.57531
7	.88477	2.38881	.93313	.64053
8	.96325	2.60094	1.01599	.70389
9	1.04330	2.81710	1.10043	.77026
10	1.14751	3.09344	1.20838	.85951
11	1.27780	3.43569	1.34207	.97643
12	1.41249	3.79339	1.48179	1.10572
13	1.54447	4.12274	1.61045	1.24032
14	1.68858	4.46586	1.74448	1.39646
15	1.86539	4.85972	1.89833	1.60215
16	2.06237	5.26149	2.05527	1.85176
17	2.28671	5.60907	2.19104	2.16500
18	2.55007	5.84284	2.28236	2.57618
19	2.83487	5.95155	2.32482	3.07945
20	3.15668	5.96334	2.32943	3.72984
21	3.52228	5.95417	2.32585	4.58577
22	3.88422	5.92228	2.31339	5.56889
23	4.26225	5.86429	2.29074	6.75426
24	4.66999	5.80330	2.26691	8.23231
25	5.07016	5.74597	2.24452	9.90110
26	5.52007	5.65238	2.20796	12.05222
27	5.92747	5.56171	2.17254	14.27360
28	6.46137	5.49476	2.14639	17.61832
29	7.01969	5.44299	2.12617	21.70410
30	7.65614	5.40661	2.11196	27.15790
31	8.32285	5.32774	2.08115	33.85904
32	9.05537	5.33576	2.08428	42.52510
33	9.93974	5.33983	2.08587	55.12176
34	10.88230	5.34907	2.08948	71.29357
35	11.81358	5.33514	2.08404	90.36771
36	12.85416	5.01376	1.95850	115.90913
37	13.92113	4.49240	1.75484	147.44563
38	15.23656	4.58735	1.79193	194.91144
39	16.95886	4.23074	1.65263	273.78780
40	18.78536	4.25874	1.66357	380.91047
41	20.69696	3.67364	1.43501	522.79947
42	22.80264	4.61785	1.80385	720.68889

35. Cu-Fe 2560 ppm .3 K - 25 K 38 kOe

$C_N = 0.0461694/T^2$ (mJ/K-mole Cu)

N	T	ΔC	ΔC/c	$C_{Cu}(H=0)$
1	.35426	.79779	.31164	.24566
2	.38440	.84863	.33150	.26694
3	.42145	.90599	.35390	.29325
4	.45865	.98744	.38572	.31982
5	.50456	1.08138	.42242	.35285
6	.55986	1.20012	.46880	.39304
7	.62079	1.32940	.51930	.43789
8	.68210	1.45171	.56707	.48367
9	.75561	1.61083	.62923	.53953
10	.82353	1.74671	.68231	.59216
11	.90904	1.91179	.74679	.65995
12	1.00521	2.10169	.82097	.73845
13	1.10216	2.27478	.88858	.82027
14	1.20911	2.47267	.96589	.91396
15	1.33786	2.70220	1.05555	1.03296
16	1.44891	2.89504	1.13087	1.14208
17	1.58197	3.11016	1.21490	1.28003
18	1.71348	3.30855	1.29240	1.42446
19	1.84986	3.51910	1.37465	1.58342
20	2.00997	3.73381	1.45852	1.78314
21	2.17817	3.94067	1.53933	2.00941
23	2.33849	4.11631	1.60793	2.24200
24	2.54873	4.35314	1.70045	2.57396
25	2.80248	4.60130	1.79738	3.01895
26	3.08864	4.83405	1.88830	3.58463
27	3.38267	5.07612	1.98286	4.24341
28	3.71308	5.30463	2.07212	5.08636
29	4.09654	5.51182	2.15305	6.21376
30	4.49928	5.71686	2.23315	7.58691
31	4.93158	5.89399	2.30234	9.29804
32	5.42266	6.04379	2.36086	11.56048
33	5.90560	6.13146	2.39510	14.14737
34	6.43822	6.23741	2.43649	17.46238
35	7.00560	6.36234	2.48529	21.59321
36	7.58777	6.46907	2.52698	26.52936
37	8.22799	6.48536	2.53334	32.84013
38	8.98780	6.58962	2.57407	41.66322
39	9.89808	6.63964	2.59361	54.47175
40	10.93158	6.63630	2.59230	72.22158
41	11.94695	6.55165	2.55924	93.37926
42	13.05121	6.23994	2.43748	121.30248
43	14.34157	5.71395	2.23201	161.52224
44	15.83956	5.92224	2.31337	220.24087
45	17.42018	5.22807	2.04221	298.46264
46	19.26105	5.77643	2.25642	413.13775
47	21.56548	5.09798	1.99140	599.11311
48	23.78026	2.79898	1.09335	823.81398

F. RESULTS AND DISCUSSION

1. Kondo State Heat Capacity in Cu-Cr

The heat capacity of the Kondo state was determined by plotting $\Delta C/c$ (J/mole-impurity) versus log T. This representation is convenient because it allows graphical integration to obtain the entropy associated with the peak while compressing the very broad transition. Moreover, theoretical calculations indicated the approximate symmetry of $\Delta C/c$ as a function of log T. The zero field data for all three Cu-Cr samples are presented in Fig. 10 with the theoretical curve of Bloomfield and Hamann[24] (curve b of Ref. 24, $D = 10^5$ K and $\gamma = -0.105$ calculated for spin 1/2). The Bloomfield-Hamann curve has been scaled vertically to agree with the peak height of the experimental data and then shifted to give a best fit to the data. The Kondo temperature determined by the fit is $T_K = 2.11$ K in excellent agreement with the recent estimate[4] $T_K = 2.2$ K based on analysis of the resistivity measurements.[66]

Also shown in Fig. 10 is the extrapolation of $\Delta C/c$ as a function proportional to T at low T. This behavior, predicted by the CZK model and inferred for spin fluctuation theory, is observed in our measurements on very dilute Cu-Fe and also for Au-V.[67] For the above reasons and additional evidence to be presented later, we will assume the linear behavior is the correct dependence at very low T and represent the heat capacity in the Cu-Cr system above 0.1 T_K by the numerical results of the scaled BH curve and below 0.03 T_K by the extrapolation of $\Delta C/c$ linear in temperature. The interpolation of $\Delta C/c$ in the region

$0.03\ T_K < T < 0.1\ T_K$ is based on the Cu-Cr data. The error bars shown in Fig. 10 represent the effect of a 0.1% error in the total heat capacity on the Kondo heat capacity of the 51 ppm sample. Interaction effects start to appear in the 51 ppm sample near 0.1 K, and the magnetization building up on the impurity site induces a hyperfine interaction on the copper nuclei as described in section E. 2. Except for this effect ΔC is proportional to concentration at all T to ± 5%. The magnitude of the hyperfine term is in excellent agreement with the hyperfine terms measured for Cu-Fe samples[36] showing interaction effects near the same reduced temperature ($T/T_K \sim 0.05$).

It is apparent that interaction effects are very easy to detect with low temperature heat capacities because of the nuclear hyperfine contribution. The 21 ppm sample is seen to be free from interaction effects down to our lowest operating temperature. Analysis of our Cu-Fe data to be presented later shows that the temperature at which interaction effects produce a detectable influence on the heat capacity is approximately proportional to concentration in the temperature region near the Kondo peak. This implies interaction effects in the 21 ppm sample will not appear until $T \lesssim 0.04$ K.

Our data agree within the scatter of the measurements reported by Daybell, Pratt, and Steyert[37] on a single Cu-Cr sample up to 0.3 K. Above this temperature the data disagree with their extrapolation and 1.05 R ln 4 is obtained for the entropy under the anomaly instead of 0.79 R ln 4. (The authors of Ref. 37 do not indicate whether their concentration was determined from their resistivity -- concentration relation in

Ref. 60. If this were the case, it would not remove the present discrepancy but contribute an additional 15% difference.)

The BH curve is based on the NHB theory which is known to adequately describe experimental results for $T > T_K$. The theory is also known to be incorrect at low temperatures where it violates the Mattis singlet ground state theorem.[68, 69] The NHB calculations for the resistivity[18] agree well with experiment only to $T \sim T_K$ and we must regard the fact that they fit the heat capacity to $T \sim .1\ T_K$ as fortuitous. The peak height of the experimental data is twice the height of BH curve if the curve is normalized to give the R ln 2 value for the entropy expected for spin 1/2. (The ratio R ln 4/R ln 2 = 2). Since the fit to theory is very good at high T and there is little difference in entropy between all low T extrapolations indicated by theory and experiment, the entropy value 1.05 R ln 4 is felt to be accurate to ± 10% with half of this error resulting from the uncertainty in the concentration.

It is very gratifying to see that the spin 1/2 results can be scaled to give good agreement with experiment since theoretical work indicates that the compensation of larger spins is not properly described by current models which permit only s-wave scattering. Schrieffer[17] has suggested generalization of the models to take account of the d-like character of the scattering potential J. In his simple model d-wave scattering of conduction electrons occurs only between conduction electrons and localized moment electrons with the same magnetic quantum number. There are as many independent d-wave channels as there are localized moment electrons (each having a different magnetic quantum number). Consequently, the resistivity should be composed of three independent channels

for spin 3/2 -- each contributing additively and giving a total resistivity which saturates at three times the unitarity limit for spin 1/2. Heat capacities or entropies are not expected to be additive like transport properties, but the higher spin functions should still be similar to their spin 1/2 counterpart (cf., Schottky peaks for higher spins).

The data for all three Cu-Cr samples in 38 kOe are shown in Fig. 11 with the theoretical Schottky curve for an ideal paramagnet with $S = 3/2$. The experimental peak height is ~80% of that for the full Schottky peak and intermediate field data (see section F. 4) indicate that substantially higher fields will be necessary to completely destroy the Kondo state. At lower temperatures strong correlations still appear to exist and the dotted curve in Fig. 11 indicates the difference between the experimental data and 80% of the theoretical Schottky. This excess heat capacity peaks at the same temperature as the zero field Kondo heat capacity (also shown in Fig. 11) but is definitely more sharply peaked.

The accuracy and precision of the heat capacity points in Fig. 11 begins to deteriorate at low temperatures because of the very large contribution from the nuclear heat capacity of copper. The data for the three samples show a spread of ~0.5% of the total heat capacity below 0.4 K -- comparable to the precision with which the magnetic field was set.

2. Kondo State Heat Capacity in Cu-Fe

The data for the 81.4 and 195 ppm Cu-Fe samples were used for determination of the Kondo heat capacity for this system. The data are shown in Fig. 12. The situation is very difficult experimentally because

the rapidly increasing lattice heat capacity does not allow an accurate determination of ΔC in the vicinity of the peak. Some information can be obtained in this region by applying magnetic fields above 30 kOe to suppress low temperature interaction effects in very concentrated alloys and these measurements (see section F.3 and Fig. 17) show that ΔC is comparable with its peak value up to 20 K. (These data are not displayed in Fig. 12 because of questions about the temperature dependence of residual contributions from interactions at high temperatures.)

In any case the total entropy measured for the 2560 ppm sample is (1.0 ± 0.05) R ln 4 for either zero field or 38 kOe based on a BH extrapolation of either of these sets of data to higher temperature. In Fig. 12 the characteristic curve (c) for the Kondo state in Cu-Cr is shown fitted to the data. The fit is poor and curves (a) and (b) represent attempts to get a better fit by scaling curve (c) by factors of 1.22 and 1.12 respectively. The Kondo temperatures of curves (a), (b), and (c) are 47.3 K, 42.2 K, and 38.9 K. These values should be compared with the estimate[4] $T_K = 34$ K based on the resistivity.[70] Even though curve (a) fits the data adequately at low temperatures, it gives an unreasonably high entropy and indicates a T_K that is not in good agreement with the estimate from the resistivity. We feel forced to conclude that the Kondo heat capacity curve for Cu-Fe does not appear to be identical in shape to the Kondo curve for Cu-Cr. Perhaps this should have been anticipated because the "universal curve" for the resistivity shows ~10% deviations from a universal behavior below T_K. Curve (d) in Fig. 12 is the BH curve with $T_K = 28$ K and the peak value of Cu-Cr. Deviations from this

curve appear slightly above $T = 0.1\ T_K$ and are more pronounced than in the case of Cu-Cr. A combination of curve (d) above 4 K and curve (a) below 4 K gives a good fit to the data and an entropy of 1.01 R ln 4. This curve is also in much better agreement with the high field measurements on the 2560 ppm sample (see Fig. 17).

The type of behavior described by the deviations of the Cu-Cr and Cu-Fe data from the BH curve is predicted by th CZK model and the Nagaoka calculation for the Kondo state neglecting spin-flip scattering. Both of these calculations predict

$$\Delta C \propto (1/|J|)(T/T_K),\ T << T_K \qquad (16)$$

The important point here is that $J \cong -0.8$ ev in Cu-Fe compared with $J \simeq -0.6$ ev in Cu-Cr, therefore deviations from the BH curve are predicted to be more severe in the case of Cu-Fe. In Fig. 13 $\Delta C/c$ is plotted vs. T on a log-log scale in order to emphasize the difference in the low T behavior predicted by the BH curves (solid lines) and the Nagaoka-CZK calculations represented schematically by dashed lines for various choices of J.

If Eq. (16) is assumed to be valid, T_K in the NHB theory can be estimated for Cu-Fe from T_K for Cu-Cr. Now $\Delta C/c \simeq 1.0\ T$ for Cu-Fe, $T < 0.03\ T_K$ and $\Delta C/c \geq 17.6\ T$ for Cu-Cr, where the value 17.6 may be a low estimate because our data do not extend to low enough T to allow an accurate estimate for the coefficient of the linear term. In any case $T_K\,(\mathrm{CuFe}) \gtrsim (17.6/1.0)(0.6/0.8)(2.11\ \mathrm{K}) \sim 28$ K.

It is important to note the difference between the physical interpretation of the full NHB theory and the Nagaoka calculation. The Nagaoka calculation is certainly wrong at high temperatures because it neglects the spin-flip scattering contribution of the localized moment. On the other hand, at very low temperatures spin-flip scattering is impossible because the localized moment is completely compensated (assuming the singlet ground state theorem[70] is accepted). The complete NHB theory violates the ground state theorem[71] and predicts an overcompensation of the localized moment at $T = 0$ for spin 1/2. This situation implies that the spin-flip contributions which give the anomalous low T behavior in the complete NHB theory would disappear as $T \rightarrow 0$ in a correct treatment.

The compensation of the localized moment occurs continuously as $T \rightarrow 0$ and is never complete at $T > 0$, it must be expected that an exactly linear behavior for the heat capacity will never be attained.

It is possible to artificially suppress spin flip scattering at low temperatures by applying a magnetic field $\mu H \gg kT$. Figure 14 shows $\Delta C/cT$ for the Cu-Fe samples with 81.4, 195, 640, and 2560 at. ppm Fe in a magnetic field of 38 kOe. In the temperature region $0.4\ K < T < 4\ K$, where the excess heat capacity is substantial, the data are identical to $\pm 5\%$. Interaction effects have been pushed up to $T \gtrsim 4\ K$. The data should be compared with the solid curve representing the zero field heat capacities on the interaction free samples (81.4 and 195 ppm). $\Delta C/cT$ has been decreased by less than 15% at all temperatures and reasonably uniformly. This variation with field looks remarkably similar to the decrease of the resistivity in magnetic fields of comparable magnitude.

This latter effect has already been shown to be adequately correlated with the increase in magnetization on the impurity site[71, 60] or, equivalently, the reduction in the resonant scattering that produces cancellation of the localized magnetic moment.

Figure 15 shows $\Delta C/cT$ for the 640 ppm Cu-Fe sample in fields of 1, 3, 10, 18, 24, 30, and 38 kOe. At low temperatures and low fields the heat capacity increases with increasing field. Since the field dependence of the heat capacity is related to the temperature dependence of the susceptibility by

$$\partial C_p(H, T)/\partial H = T\left[\partial^2 M(H, T)/\partial T^2\right]_H ,$$

these measurements correspond to least qualitatively to the anomalous $T^{-1/2}$ susceptibility.[72] The zero field heat capacity for the 81.4 and 195 ppm samples is represented by the dashed curve in Fig. 15. In 20 kOe the heat capacity for these samples is identical within the scatter to the zero field data. In 30 and 38 kOe the heat capacity decreases slightly in good agreement with the measurements on the 640 ppm sample. It seems that fields of ~30 kOe are required to suppress interaction effects at these temperatures and the low field increase in $\Delta C/c$ with applied field and the $T^{-1/2}$ susceptibility are associated with Fe-Fe interactions rather than the Kondo effect.

Golibersuch and Heeger[38] (GH) have analyzed their NMR data for Cu-Fe in a manner consistent with the susceptibility analysis reported in Ref. 72. Basically they see an NMR linewidth that increases rapidly as a function of field for fields less than 3 kOe, more slowly at fields up

to 30 kOe, and linearly at an even slower rate above 30 kOe. They subtract off the rapid low field dependence and call it the interaction contribution. The linear high field contribution is certainly associated with the RKKY oscillations induced by the increasing magnetization on the impurity and they discard this also and suggest that the intermediate region represents the destruction of the quasi-bound state -- a destruction essentially complete at 40 kOe.

There is a serious objection to this reasoning. If the condensed state were destroyed at ~40 kOe, then a small excess field should saturate the moment and a field independent linewidth (such as observed in Cu-Mn) would be found. Moreover our results indicate that interaction effects are not suppressed until fields of ~30 kOe are applied and that this field does little damage to the Kondo state. The interpretation is obvious. Apparently the entire anomalous linewidth (which is in agreement with the Mössbauer hyperfine field) may be associated with Fe-Fe interactions and only the RKKY linewidth can be used to represent the destruction of the Kondo state in a magnetic field. The approximate size of the field necessary to destroy the Kondo state can be estimated from the fact that 38 kOe does considerable damage to the condensed state in Cu-Cr. Multiplying 38 kOe by the ratio of the Kondo temperatures gives a value ~600 kOe.

At first sight, it would seem that the anomalous NMR contribution interpreted by GH to represent the thermal destruction of the "quasi-particle amplitude" originates from interaction effects also. On closer investigation, however, it appears that this is not the case and our measurements appear to confirm parts of their interpretation.

The basis of their argument is an interpretation of the published Mössbauer and bulk susceptibility data in which they conclude that the Mössbauer data and the high temperature susceptibility are in agreement and represent the local-d spin susceptibility. The low temperature susceptibility measurements of Daybell and Steyert saturate (if a small field is applied) at a value twice as large as that predicted by the high temperature measurements of Hurd.[73] Since this anomalous increase occurs in the temperature range where the Kondo state is forming, it is reasonable to associate it with the formation of an extended spin polarization having a susceptibility. This part of the GH interpretation seems to certainly be incorrect. The excess susceptibility reported by Daybell and Steyert appears to be associated with interactions, and if their Cu-Cr results are any indication, the application of a magnetic field such that $H/T_K \sim 1$ kOe/K should result in the saturation value

$$\chi\ (\text{Cu-Fe}) = \frac{\mu^2_{eff}}{3k\theta} \text{ where } \theta = 34 \text{ K}$$

in agreement with the value anticipated from Hurd's high temperature work.

In Fig. 16 our entropy values for Cu-Cr (see Fig. 21 for a graph of the zero field entropies) are plotted on a linear scale for $\langle S_Z \rangle / H$. The points for a given temperature have been plotted by assuming

$$\chi \propto \langle S_Z \rangle / H \propto \frac{\mu^2_{eff}}{3k(T+\theta)} \tag{17}$$

after Golibersuch and Heeger.[38] The value $\theta = T_K = 2.11$ K has been used to be consistent with Cu-Fe where $\theta = T_K = 34$ K. This value of θ is in agreement with the data of Daybell and Steyert[37] in 4.6 kOe or a linear

extrapolation of their higher field data to zero field. The agreement of Fig. 16 with Figs. 13 and 14 in GH is striking. The slope of the field dependence of the NMR linewidth and the entropies are in agreement within the scatter of the NMR points. The Cu-Fe entropies would give essentially the same curve as long as the Bloomfield-Hamann extrapolation to high temperature is made with $T_K = \theta = (32 \pm 5)$ K.

The "anomalous" rise in the curve in Fig. 16 for high values of $\langle S_Z \rangle / H$ is sensitive to the choice of θ, and in view of the uncertainty in the value of θ in the absence of interactions, it is worth considering whether an appropriate choice of θ will give a straight line in Fig. 16. A "best choice" for θ for this purpose is $\theta = 0.65$ K. The data do not give a very good straight line but it might be argued that this is due to uncertainties in the extrapolation of the heat capacity curve, etc. Once a straight line through the data is defined, a heat capacity representative of this line can be calculated and used to make a more sensitive test of the adequacy of the fit. The solution for $\theta = 0.65$ K is given by

$$C \ (\text{J/K-mole Cr}) = \frac{10.0 \ T}{(T+0.65)^2}$$

and is not a good representation of our data.

The significance of the linear extrapolation of S(T) giving a value ~0.5 R ln 4 is not understood by the author although it may be related to the division of the spin polarization into local RKKY type effects and the nonlocal "quasiparticle" formation near T_K (see Golibersuch and Heeger[38] and references contained therein).

One further point should be mentioned in connection with the use of the susceptibility to interpret Kondo state experiments. Calculations of magnetic susceptibility in the NHB theory predict

$$\chi = \frac{\mu^2_{eff}}{3k(T+4.5\ T_K)} \quad , \quad T > T_K \tag{18}$$

that is, $\theta = 4.5\ T_K$ instead of $\theta = T_K$ as observed experimentally. The source of this discrepancy is not known.

3. Interactions

Nagaoka[74] has pointed out that deviations from the single impurity limit are expected to occur when the concentration of magnetic impurities reaches a critical concentration

$$c^* \simeq \frac{k\,T_K}{\epsilon_F} . \qquad (19)$$

This condition is obtained by comparing the electron mean free path with the coherence length of the quasibound state, $\xi = \hbar v_F/k\,T_K$, where v_F is the Fermi velocity. Nagaoka's general conclusions have been assumed to be qualitatively correct, and the argument can be described by noting that there are only a finite number of electron states that can be used to compensate the local moment.[20] Since only electron states within $\sim kT_K$ of the Fermi surface are available for compensation, this implies a range of the order $\xi = \hbar v_F/kT_K$ for the coherent state they form and a limit proportional to T_K/T_F to the moments that can be compensated. This restriction sets Eq. 19 as a lower limit to the allowed impurity concentration in the dilute impurity problem. Star and Boerstoel[20] have offered experimental evidence for the existence of this coherence length and concentration limit by observing changes in the resistivity slope, $d\rho/dT$, in three different systems: Au-V, Pd-Cr, and Cu-Fe.

Since T_K is not a "sharply" defined transition temperature, it must be expected that neither the coherence length nor the critical concentration will be sharp either. In Fig. 17 deviations from the dilute impurity limit appear near 10 K for 2560 ppm Cu-Fe and near 1 K for 640 ppm Cu-Fe. The curves (a) and (d) represent the curves drawn through the heat capacity data for the 81.4 and 195 ppm samples. A field of 38 kOe is effective

in pushing the Fe-Fe interaction effects up to high temperature. The data for the 2560 ppm sample in 38 kOe offer support for our choice of (d) as the best description of the high temperature data for the dilute impurity limit, and the data for both zero field and 38 kOe support 1.0 R ln 4 for the entropy - assuming the validity of the BH curve at high temperatures. Our measurements agree well with those of Frank et al.[30], up to 6 K. At temperatures above this the excess heat capacity becomes small and they see a rapidly decreasing value of ΔC which goes negative. Our higher precision measurements indicate their data in this region are in error and their reported value for the entropy, S = 0.5 R ln 4 is considerably low.

Even though the Kondo condensation occurs over a very wide range of temperature and heat capacity deviations from the dilute impurity limit occur at different temperatures for different concentrations, Eq. (19) should always be valid for $T \ll T_K$ (where $\ll$ means at least two decades in this case). The critical concentrations for Cu-Fe and Cu-Cr in this limit are estimated to be ~ 130 ppm and ~ 8.4 ppm respectively.

At very low temperatures (< .1 K) the size of the magnetic moment on impurity sites with $c > c^*$ can be characterized from the size of the nuclear Schottky contribution induced by the RKKY oscillations. This term is comparable for the 51 ppm Cu-Cr sample and the 640 ppm Cu-Fe sample which both show deviations from the dilute impurity limit near $T/T_K \sim .03$ (note that 640 ppm/51 ppm $\simeq$ 34 K/ 2.2 K). The size of the nuclear hyperfine term is expected to be roughly proportional to $c - c^*$, thus tending to a concentration proportional behavior for $c \gg c^*$.

The interaction region is characterized by a heat capacity linear in T in the low T limit and roughly independent of concentration. The RKKY Hamiltonian has been used by Marshall[29] and others to explain the interaction region observed in several dilute magnetic alloy systems. Souletie and Tournier[75] have recently reexamined the molecular field model formulated by Marshall and we will follow their presentation. The authors of Ref. 75 point out that because the long range part of the RKKY oscillations decrease as the cube of the distance, it is possible to rewrite the molecular field equation in a reduced form

$$H_i^M = A \sum_{j \neq i} \mu_j \frac{\cos(2k_F r_{ij} + \phi)}{r_{ij}^3} \tag{20}$$

$$H_i^M/c = A \sum_{j \neq i} \mu_j \frac{\cos(2k_F r_{ij} + \phi)}{c\, r_{ij}^3} \tag{21}$$

where the molecular field H_i^M has been written in reduced form H_i^M/c in Eq. (21). The point is that an alloy of concentration c can be represented by one of concentration c' merely by changing the distance,

$$c\, r^3 = c'\, r'^3 = c''\, r''^3 .$$

The cos function in Eq. (21) will always be characterized by a mean value and higher order moments as long as the distance between impurities is large compared with the wavelength of the oscillating term. Thus the solutions H^M/c of Eq. (21) are possible solutions for any other low concentration.

The energy of the magnetic impurities can be expressed

$$E = -1/2\, Nc \int p(H^M, T)\, \mu\, H^M\, B_s \left[\frac{\mu H^M}{kT}\right] dH^M \tag{22}$$

where $p(H^M,T)$ is the molecular field distribution function and B_s is the Brillouin function. Equation (22) can be rewritten as

$$E = -1/2\, Nc^2 \int c\, p(H^M,T)\, \mu(H^M/c)\, B_s \frac{\mu(H^M/c)}{kT}\, d(H^M/c). \quad (23)$$

After integration over all values of the molecular field we obtain

$$\Delta C/c = \frac{\partial (E/c)}{\partial T} = \Gamma\,(T/c) \qquad (24)$$

where Γ is a universal concentration independent function of T/c (if $\Delta C = \gamma T$, then Eq. (24) implies γ is independent of concentration).

In Fig. 18 our data for the four Cu-Fe samples are plotted with smooth curves approximating the data of Hill and Pickett.[28] $\Delta C/c$ for the more concentrated samples (above 1900 at. ppm) is roughly described by a universal function of the reduced temperature T/c, but significant deviations still occur and are most apparent near the peak in Fig. 18.

A glance back to Fig. 17 will serve to clarify the reason for this behavior. The 38 kOe data for the 640 and 2560 at. ppm samples show the Kondo state is well formed even in these samples showing strong interaction effects. The important point is that the Kondo heat capacity will become approximately concentration independent at some concentration c^+ because there are no more electron states available for spin compensation ($c^+ \sim 2000$ at. ppm Fe and is not the same as c^* where interaction effects first start to appear in the limit of very low T). Thus there are two contributions to the heat capacity at high concentrations: (a) The Kondo heat capacity $\Delta C/c^+$ is a universal function of T. (b) Interaction effects make a contribution $\sim \Delta C/c$ which is a universal function of T/c. Both (a) and (b) make contributions which are approximately linear in T at low T and independent of concentration giving a total value of $\Delta C/T$

which is also roughly independent of concentration at low T. Measurements on Ag-Mn (see Ref. 75) show much smaller deviations from a universal behavior because T_K and c^+ are very much smaller than in Cu-Fe.

The spin-spin interactions can be thought of as the sum of a distribution of Schottky type interactions centered around zero molecular field. The application of a magnetic field pushes these weak coupled effects up to $kT \approx \mu H$ but leaves the strongly correlated Kondo contribution relatively undisturbed as long as $\mu H \ll kT_K$. Technically, these two contributions should not be treated together; however, accurate decomposition into the two components is difficult and we will represent the total interaction of a localized moment with its environment by an effective distribution function $P(H^M)$ and Eq. (23) with $P(H^M)$ substituted for the spin-spin distribution function $p(H^M)$.

Since $\Delta C \propto T$ at low T, $\Delta C/Tc$ is proportional to the distribution function $P(H^M)$ as $T \rightarrow 0$.[29] If the weak temperature dependence of $P(H^M)$ is neglected, we can make the association $P(H^M) \longleftrightarrow \Delta C/Tc$ and $|H^M| \longleftrightarrow kT/g\mu_B$. Such an association surely breaks down at high T, but it at least allows a qualitative sketch of $P(H^M)$. In Fig. 19 $P(H^M)$ is sketched for 640, 2560, and 5600 at. ppm Fe in Cu. The solid curve shown for comparison is the dilute impurity limit.

In Fig. 20 the total effective distribution function $\overline{P(H^t)}$ for the 640 and 2560 ppm samples in 38 kOe is compared with the zero field result where $\overline{P(H^t)} = P(H^M)$. $\overline{H}^t$ has been defined by assuming $\overline{H}^t = kT/g\mu_B$ so that $\overline{H}^t = |H^M|$ in zero external field.

One fact immediately apparent from Fig. 20 is that the major contribution to the total effective distribution function for zero field

near $\bar{H}^t = |H^M| \rightarrow 0$ comes from the Kondo state in the 2560 ppm sample.

Equation (21) implies that $cp(H^M)$ is a universal concentration independent function of H^M/c. Consequently, $p(H^M = 0)$ will be proportional to $1/c$ and $p(H^M)$ will have a breadth proportional to c. Because of the interference of the Kondo state, c in the molecular field equations should be replaced by $(c-c^*)$. Such a correction makes little difference for $c \gg c^*$, but explains the large narrow spin-spin interaction contributions for $H^M \rightarrow 0$ in the 640 ppm sample as well as the nonlinear concentration dependence of the RKKY hyperfine contribution observed in this work for Cu-Cr and Ref. 36 for Cu-Fe.

The discussion above should serve to demonstrate the necessity of avoiding the measurement of interaction effects in a temperature region where the Kondo condensation will make a large contribution to the excess heat capacity. Systems with very low Kondo temperatures are the most suitable.

If the problems discussed above were not enough, mention should also be made of additional complications associated with the interpretation of measurements made in a magnetic field. The magnetic field will have some effect on the partially compensated localized moments, and the fraction of bare moment exposed will be a function of both magnetic field and concentration.

We have defined $\bar{H}^t$ in terms of temperature without attempting to relate this quantity to H^M and H for non-zero field. Some authors have assumed $\bar{H}^t = \vec{H}^M + \vec{H}$ consistent with a one-dimensional model. We note that such an assumption implies that the application of a magnetic field will increase the number of local moments exposed to zero total effective field

for some value of H. This assumption seems to be unphysical and is not in agreement with our data which imply that the excess heat capacity at T = 0 always decreases with increasing H (see Fig. 15). An assumption consistent with the data is $\overline{H}^t = |H^M| + |H|$ for all spins - the spins re-ordering their spatial orientation distribution to take advantage of the lower ground state energy made possible by the application of the magnetic field. The picture alluded to above is not the usual regular lattice Ising approximation and a word of clarification is in order.

Instead of a unique orientation axis Z for all spins, we are suggesting an ensemble of orientation axis Z_i for each spin where the Z_i will be "randomly" oriented in zero field. The spin on site i is subjected to an effective field H_i^M in the Z_i direction from its interaction with all near neighbors. The application of a magnetic field along the Y axis will result in a redistribution of the Z_i axes distributed preferentially around the Y axis.

In any case, the field dependence of the Kondo state will surely alter the functional dependence of $\overline{P(H^t)}$ on H^M and make an accurate description of the situation exceedingly complicated. (This statement may be less true for the more concentrated alloys studied by Hill and Pickett - increasing field and increasing Fe concentration are both effective in destroying the spin-compensated state and the effect of a magnetic field on a state already substantially suppressed may well be negligible.)

4. Magnetic Degradation of the Kondo State In Cu-Cr

Since Cu-Cr has a much lower T_K than Cu-Fe, it is expected that magnetic fields up to 38 kOe would at least partially break up the correlations

between the local moment and the itinerant electrons. Moreover, by making use of the NMR results for other systems and our own work on interaction effects, the destruction of the correlated state is expected to proceed linearly with field at high fields until the chromium moment approaches free spin behavior. In Fig. 21 the heat capacity data for the 51 at ppm sample is shown for 10, 20, 30 and 38 kOe. The data show the gradual transformation from the correlated Kondo state represented by the dashed curve toward the free spin Schottky peak (see Fig. 11 for a comparison of the theoretical Schottky with the 38 kOe results). The peak position for a given field identifies the Cr spin state as $S = 3/2 \pm 10\%$ in agreement with susceptibility measurements[76] (the g value for Cr in Cu has been measured and is less than 1% greater than 2.0 at all temperatures).

In Fig. 22 the entropy is plotted on a log T scale for the 51 ppm sample in 0, 10, 20, 30 and 38 kOe.

Decomposition of the Schottky and Kondo contribution has not been attempted except for the 38 kOe results (Fig. 11).

G. CONCLUSION

The experimental results presented in this work appear to resolve the two particularly puzzling features of the recent experimental data which have been associated with the formation of the quasibound state in dilute alloys, namely, the low entropy and $T^{-1/2}$ susceptibility.

Previous reports[30,37] that heat capacity results indicate considerably less than the R ln 4 entropy expected for spin 3/2 systems appear to be in error. The difficulty has been associated with the extrapolations made to describe ΔC at very high temperatures. Our data give excellent agreement with the Bloomfield-Hamann theoretical curve for the heat capacity of Cu-Cr above 0.1 T_K. At lower temperatures the theory is known to be incorrect and our data for Cu-Fe indicate the heat capacity for $T < .03\ T_K$ is approximately linear in T in the absence of Fe-Fe interactions. Our estimate for the entropy of Cu-Cr is (1.05±.10) R ln 4. For Cu-Fe we estimate (1.01-1.12) R ln 4 based on the assumption that the behavior of Cu-Fe for $T > T_K$ is similar to Cu-Cr as indicated by the BH calculations.

Measurements on Cu-Fe samples in magnetic fields indicate that the divergent susceptibility $\chi \propto T^{-1/2}$ and the strongly field dependent susceptibility for low fields are associated with Fe-Fe interactions. Interaction effects can be suppressed with the application of a large magnetic field apparently without significant damage to the Kondo state correlations. Below T ~ 3K the 38 kOe heat capacity of Cu-Fe samples showing interactions effects is essentially identical to the zero field heat capacity in the dilute impurity limit. Anomalous contributions to the NMR and Mossbauer measurements for H < 30 kOe are also indicated to be of interaction origin

allowing a very simple interpretation for the magnetic destruction of the Kondo state. On the other hand, our measurements appear to substantially confirm the interpretation of the NMR data representing the thermal destruction of the spin-compensated state.

Table I. Selected theoretical results.

	Group 1	Group 2		Group 3
		Ground State Models		
	Nagaoka Hamann-Bloomfield (NHB) Refs. 18, 23, 24	A Kondo-Appelbaum Ref. 22	B Celli-Zuckermann Klein (CZK) Refs. 20, 21	Spin fluctuation theory Refs. 1, 2
Resistivity $T \ll T_K$	Unitarity limit $\rho_0 \left\{1 - \left[\frac{\pi^2 S(S+1)}{4 \ln^2 (T/T_K)}\right]\right\}$	Unitarity limit $\rho_0 \left\{1 - \alpha\left[(T/T_K)\ln(T/T_K)\right]^2\right\}$	Unitarity limit $\rho_0 \left[1 - \alpha(T/T_K)^2\right]$	Unitarity limit $\rho_o \left[1 - \alpha(T/T_K)^2\right]$
Specific heat $T \sim T_K$	Numerical results broad peak in ΔC	Anomaly implied	Anomaly implied	------
Specific heat $T \ll T_K$	$\frac{\pi^2 S(S+1)}{\ln^4 (T/T_K)} \approx \alpha T^{0.57}$	$\frac{T}{T_K} \ln \left(\frac{T}{T_K}\right)$	$\frac{8 \pi k}{9JN(0)} \cdot \frac{T}{T_K}$	-----
Magnetic susceptibility $T \ll T_K$	Negative	$2JN(0) \cdot \frac{\mu^2}{kT_K}$	$\frac{5.4\mu_b^2}{kT_K}\left[1 - \frac{\pi^2}{6}\left(\frac{T}{T_K}\right)^2\right]$	$\frac{\alpha(g\mu_b)^2}{\pi k T_K}\left[1 - \frac{\pi^2}{3}\beta\left(\frac{T}{T_K}\right)^2\right]$

α, β are not determined in most results.
T_K is a characteristic temperature that appears in each theory — T_K in one theory is normally not directly comparable to T_K in another.
$\tau_0 = 1/T_K$ has been assumed in writing down the spin fluctuation results.
See Refs. 4, 5 for a complete list of references.

Table II. Germanium thermometer characteristics

Thermometer	R at 77K Ω	R at 4.2K Ω	R at 0.3K Ω	R at.060K Ω	R(4.2)/R(77.)	R(0.3)/R(4.2)	R(0.06)/R(0.3)	Utility
Solitron No. 644	3.4	36.00	379.	>100,000	10.55	10.55	-----	not usable below 0.1K
Solitron No. 1477	6.62	39.8	114.6	~ 340.	6.01	2.88	~3.	going metallic - not usable below .1K
Cryocal No. 985	5.38	16.03	17.5	~ 17.5	2.98	1.09	~1.0	metallic - not usable
Cryocal No. 986	6.88	43.0	150.0	~1000.	6.25	3.5	~6.7	usable down to .030K
Cryocal No. 1751	8.02	45.48	227.8	1093.5	5.67	5.00	4.81	usable down to .030K (est.)

Table III. Composition of Cu-Fe samples, Fe concentrations are listed in atomic ppm.

Cu-Fe sample		Concentration from wet analysis	Concentration inferred from resistivity	Value used[a]
No. 1	Top	2620	2417 ± 10%	2560
	Bottom	2500		
No. 2	Top	615	706 ± 10%	640
	Bottom	660		
No. 3	Top	198	195 ± 2%	195
	Bottom	191		
No. 4	Top	80.8	83.9 ± 2%	81.4
	Bottom	81.9		
No. 5[b]	Top	8.9	----	8.9
	Bottom	----		
Accuracy		± 2% or .5 ppm		

[a]Concentration values used were based on the wet analysis.

[b]Sample No. 5 is the Cominco "pure" copper used in the preparation of samples No. 1-4.

Table IV. Composition of Cu-Cr samples, Cr concentrations are listed in atomic ppm.

Cu-Cr sample		Concentration from wet analysis	Concentration from neutron activation analysis	Concentration inferred from resistivity ratio	Nominal concentration	Value used[a]
No. 1	Top	51.3	35.4	51.04	50.47	51.04
	Bottom	51.3	26.1			
No. 2	Top	35.5	19.7	33.62	30.407	33.62
	Bottom	33.9	17.3			
No. 3	Top	23.2	9.8	21.16	20.004	21.16
	Bottom	20.8	12.1			
Accuracy		± 5% or 1 ppm				

[a]Value used was based on the higher precision values inferred from the resistivity ratio.

REFERENCES

1. M. J. Levine, T. V. Ramakrishnan, R. A. Weiner, Phys. Rev. Letters 20, 1370 (1968).
2. N. Rivier, M. J. Zuckermann, Phys. Rev. Letters 21, 904 (1968).
3. The experimental review of M. D. Daybell and W. A. Steyert, Rev. Mod. Phys. 40, 380 (1968) takes the view that several systems normally considered treatable only with spin fluctuation theories are really just Kondo effect systems.
4. The extensive experimental review by A. J. Heeger in Solid State Physics, Seitz, Turnbull, and Ehrenreich, Ed. (Academic Press, New York, 1969), Vol. 23, p. 283, includes a discussion of lifetimes and spin fluctuation effects on localized moment systems.
5. J. Kondo, Solid State Physics, Vol. 23, p. 183 (see ref. 4)
6. C. Zener, Phys. Rev. 81, 440 (1951).
7. E. W. Hart, Phys. Rev. 106, 467 (1957).
8. J. Friedel, Advan. Phys. (Phil. Mag. Suppl.) 3, 466 (1954); Nuovo Cimento Suppl. I, 287 (1958).
9. M. A. Ruderman, C. Kittel, Phys. Rev. 96, 99 (1954).
10. T. Kasuya, Progr. Theoret. Phys. (Kyoto) 16, 45 (1956).
11. K. Yosida, Phys. Rev. 106, 893 (1957).
12. P. W. Anderson, Phys. Rev. 124, 41 (1961).
13. J. R. Schrieffer, P. A. Wolff, Phys. Rev. 149, 491 (1966). M. Bailyn, Advan. Phys. (Phil. Mag. Suppl.) 15, 179 (1966).
14. M. P. Sarachik, E. Corenzwit, L. D. Longinotti, Phys. Rev. 135 A 1041 (1964).

15. J. Kondo, Prog. Theoret. Phys. (Kyoto) 32, 37 (1964).

16. D. R. Hamann, Phys. Rev. 154, 596 (1967).

17. J. R. Schrieffer, J. Appl. Phys. 38, 1143 (1967).

18. D. R. Hamann, Phys. Rev. 158, 570 (1967).

19. W. M. Star, G. J. Nieuwenhuys, Phys. Letters 30A, 22 (1969).

20. V. Celli, M. J. Zuckermann, Phys. Letters 25A, 305 (1967).

21. A. P. Klein, Phys. Letters 26A, 57 (1967).

22. J. Appelbaum, J. Kondo, Phys. Rev. Letters 19, 906 (1967).

23. Y. Nagaoka, Phys. Rev. 138, A 1112 (1965).

24. P. E. Bloomfield, D. R. Hamann, Phys. Rev. 164, 856 (1967).

25. H. Suhl, Phys. Rev. Letters 17, 1141 (1966).

26. J. De Nobel, F. J. DuChatenier, Physica. 25, 969 (1959).

27. J. E. Zimmerman, F. E. Hoare, J. Phys. Chem. Solids 17, 52 (1960).

28. R. W. Hill and G. R. Pickett, Proceedings of the Tenth International Conference on Low Temperature Physics, Moscow, 1966, Viniti, 1967.

29. W. Marshall, Phys. Rev. 118, 1519 (1960).

30. J. P. Franck, F. D. Manchester, D. L. Martin, Proc. Roy. Soc. (London) A263, 494 (1961).

31. N. M. Senozen, (Ph. D. Thesis) University of California, Berkeley, (1965), UCRL-11901.

32. Barry Isolation Mount, No. 915-90.

33. N. E. Phillips (unpublished)

34. Emerson and Cuming, Inc. Gardena, Calif.

35. We are indebted to Dr. T. L. Thorp for this suggestion.

36. J. C. F. Brock, J. C. Ho, G. P. Schwartz, N. E. Phillips, Solid State Communications 8, 1139 (1970).

37. M. D. Daybell, W. P. Pratt, Jr., W. A. Steyert, Phys. Rev. Letters 22, 401 (1969).

38. D. C. Golibersuch, A. J. Heeger, Phys. Rev. 182, 584 (1969).

39. M. Suomi, A. C. Anderson, B. Holmstrom, Physica 38, 67 (1968).

40. Stycast 2850 GT is now recommended for this purpose.

41. J. C. Ho, (Ph. D. Thesis) University of California, Berkeley, (1965), UCRL-16180.

42. H. R. O'Neal (Ph. D. Thesis) University of California, Berkeley, (1963), UCRL-10426.

43. Bulk silver was cast from Cominco Inc. 99.9999% pure splatter. 1/16" silver wire was obtained from Engelhard Industries, Inc.

44. The term carbon thermometers refers to Speer resistors, Allen-Bradley, resistors, and Aquadag films.

45. Cryocal, Inc., Riviera Beach, Florida.

46. Keithley Model 147 nanovolt null detector.

47. Dr. T. L. Thorp has taken the Cryocal No. 986 down to 0.020K where the resistance is approximately 60,000 Ω.

48. A. C. Anderson, W. Reese, J. C. Wheatley, Rev. Sci. Instr. 34, 1386, (1963).

49. A. C. Anderson, J. I. Connolly, O. E. Vilches, J. C. Wheatley, Phys. Rev. 147, 86 (1966).

50. D. L. Martin, private communication.

51. R. W. Hill and G. Pickett, private communications and Pickett's Ph. D. Thesis, Oxford.

52. M. Hansen, Constitution of Binary Alloys (2nd ed.), McGraw-Hill, New York, 1958.

American Society for Metals, Metals Handbook, Cleveland, O., 1948.

53. XN-50 Alumina crucibles, Grade RR, 50 c.c. supplied by Morganite, Inc.

54. Dr. G. M. Gordon, UCLRL, Berkeley.

55. Wet chemistry on Cu-Fe was done by Mr. T. Morrison, Chemistry Dept., U.C., Berkeley.

Wet chemistry on Cu-Cr was done by Mr. Robert Giauque, UCLRL, Berkeley.

High-flux neutron activation analysis was done by Mr. Harold Nass, Union Carbide Corp., Tuxedo, New York.

56. X-ray spectroscopy was done on both the Cu-Fe and the Cu-Cr samples to obtain preliminary concentration values.

57. B. Knook, (Ph. D. Thesis), Leiden (1962).

58. See, for instance, A. N. Gerritsen, Physica 23, 1087 (1957) or Ref. 28.

59. V. W. Kierspe, Z. Metallkunde 58 (12) 895-902 (1967).

60. M. D. Daybell, W. A. Steyert, Phys. Rev. Letters 20, 195 (1968).

61. D. L. Martin, Rev. Sci. Instr. 38, 1738 (1967).

62. D. L. Martin, Phys. Rev. 170, 650 (1968).

63. See, for instance, J. R. and R. A. Hull, J. Chem. Phys. 9, 465 (1941).

64. T. Sugawara, J. Phys. Soc. (Japan) 14, 643 (1959).

65. B. Dreyfus, J. C. Michel, D. Thoulouze, J. Appl. Phys. 39, 1320 (1968).

66. Ref. 4, p. 378.

67. B. M. Boerstoel, W. M. Star, Phys. Letters 29A, 97 (1969).

68. D. C. Mattis, Phys. Rev. Letters 19, 1478 (1967).

69. H. Miwa, Prog. Theoret. Phys. (Kyoto) 34, 1040 (1965).

70. J. W. Loram, T. E. Hall, P. J. Ford, Phys. Rev. (to be published in August, 1970 issue).

71. P. Monod, Phys. Rev. Letters 19, 1113 (1967).

72. M. D. Daybell, W. A. Steyert, Phys. Rev. 167, 536 (1968).

73. C. M. Hurd, Phys. Rev. Letters 18, 1127 (1967).

74. Y. Nagaoka, J. Phys. Chem. Solids 27, 1139 (1966).

75. J. Souletie, R. Tournier, J. of Low Temp. Phys. 1, 95 (1969).

76. P. Monod, S. Schultz, Phys. Rev. 173, 645 (1968).

FIGURE CAPTIONS

Fig. 1. Anderson model (after P. W. Anderson, Phys. Rev. 124, 41 (1961)).

Fig. 1a Unperturbed energy levels in the absence of s-d admixture.

Fig. 1b Density of state distributions in a magnetic case. The "humps" at $\epsilon_d + U \langle n_- \rangle$ and $\epsilon_d + U \langle n_+ \rangle$ are the virtual d "levels" of width 2Γ, for up and down spins, respectively. The numbers of electrons $\langle n_+ \rangle$ and $\langle n_- \rangle$ occupying them are to be computed from the area of the unshaded portion, below the Fermi surface.

Fig. 1c Density of state distributions in a non-magnetic case, $\langle n_+ \rangle \simeq \langle n_- \rangle \simeq 1/2$.

Fig. 2. Shaded zone represents the magnetic state (from P. W. Anderson, Phys. Rev. 124, 41 (1961).

Fig. 3. The lower part of the He^3 cryostat.

Fig. 4. Detail of the sample holder for the He^3 cryostat.

Fig. 5. Persistent mode switch and solenoid.

Fig. 6. Field profile of the superconducting solenoid.

Fig. 7. The silver calorimeter and the adiabatic cryostat.

Fig. 8. The demagnetization cooling salt and magnetic thermometer showing Ge thermometers mounted for calibration.

Fig. 9. Δ plot of deviations from the original fit to Cominco copper containing 8.9 at. ppm Fe. The data shown for the Cominco sample have been corrected to 0 and 2 at. ppm Fe. The data shown for the Asarco sample are uncorrected.

Fig.10. The heat capacities of dilute solutions of Cr in Cu. Measurements in different cryostats on the same sample are distinguished by different symbols. The error bars represent the effect of 0.1%

error in the total heat capacity for the 51 at. ppm sample.

Fig. 11. The heat capacities of Cr in Cu in a magnetic field of 38 kOe. The solid curve represents the Schottky peak for spin 3/2 and g = 2.0. The dot-dash curve shows the behavior in zero magnetic field. The dotted curve indicates the Cu-Cr heat capacity in 38 kOe after 80% of the theoretical Schottky has been subtracted from the experimental data (taken to be represented by the dashed curve).

Fig. 12. The heat capacities of dilute solutions of Fe in Cu. The error bars represent the effect of a 0.1% error in total heat capacity for the 195 at. ppm sample.

Fig. 13. The Bloomfield-Hamann calculation for the excess heat capacity (solid curves) compared with the behavior predicted by the Nagaoka - CZK calculations (dashed curves) on a log-log scale.

Fig. 14. The heat capacities of all Fe in Cu samples in a magnetic field of 38 kOe. Curves (a) and (d) correspond to the curves so labeled in Fig. 12. The error bar represent the effect of a 0.1% error in the total heat capacity for the 195 at. ppm sample.

Fig. 15. The heat capacities of 640 at. ppm Fe in Cu in magnetic fields.

Fig. 16. The zero field entropy of dilute Cr in Cu plotted versus $X \propto \langle S_z \rangle / H$ in arbitrary units. The entropy scale has been inverted to facilitate comparisons with Figs. 13 and 14 of Ref. 38.

Fig. 17. The heat capacities of 640 and 2560 ppm Fe in Cu in zero field and 38 kOe. The curves (a) and (d) correspond to the curves so labeled in Fig. 12.

Fig. 18. The "reduced" heat capacity of Fe in Cu versus "reduced" temperature. The figure shows the transition of $\Delta C/c$ from a universal function of T at low concentrations to a universal function of T/c at high concentrations. The dashed curve represents the behavior of Hill and Pickett's 1900 at. ppm Cu-Fe sample. The solid curves represent their 2900, 3300, 5600, and 9700 at. ppm Cu-Fe samples.

Fig. 19. Schematic molecular field distribution functions for the 640 and 2560 at. ppm Cu-Fe samples and Hill and Pickett's 5600 at. ppm sample in zero external field. The dilute impurity limit is shown for comparison.

Fig. 20. Schematic distribution functions for the total effective field appropriate for the 640 and 2560 at. ppm Cu-Fe samples in 38 kOe. The distribution functions for zero external field are shown for comparison. The weakly coupled interaction effects apparent in the zero field curves have been pushed up to higher values of $\overline{H}^t$.

Fig. 21. The heat capacities of 51 at. ppm Cu-Cr in magnetic fields of 10, 20, 30 and 38 kOe.

Fig. 22. Entropies for dilute Cr in Cu in magnetic fields of 0, 10, 20, 30 and 38 kOe. The error bars represent the effect of 0.1% error in the heat capacity on the entropy for the 51 at. ppm sample.

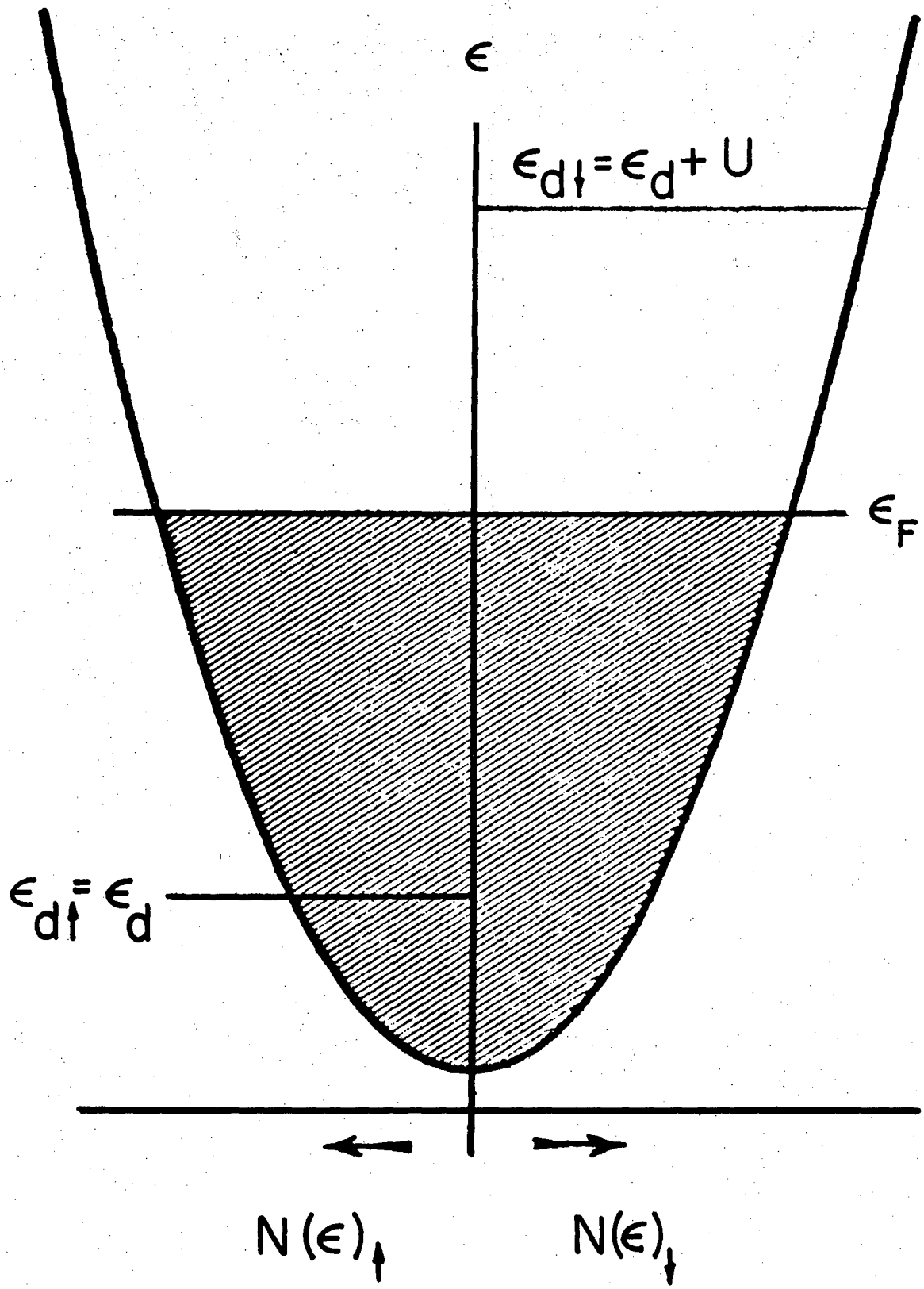

XBL 709-6603

Fig. 1a

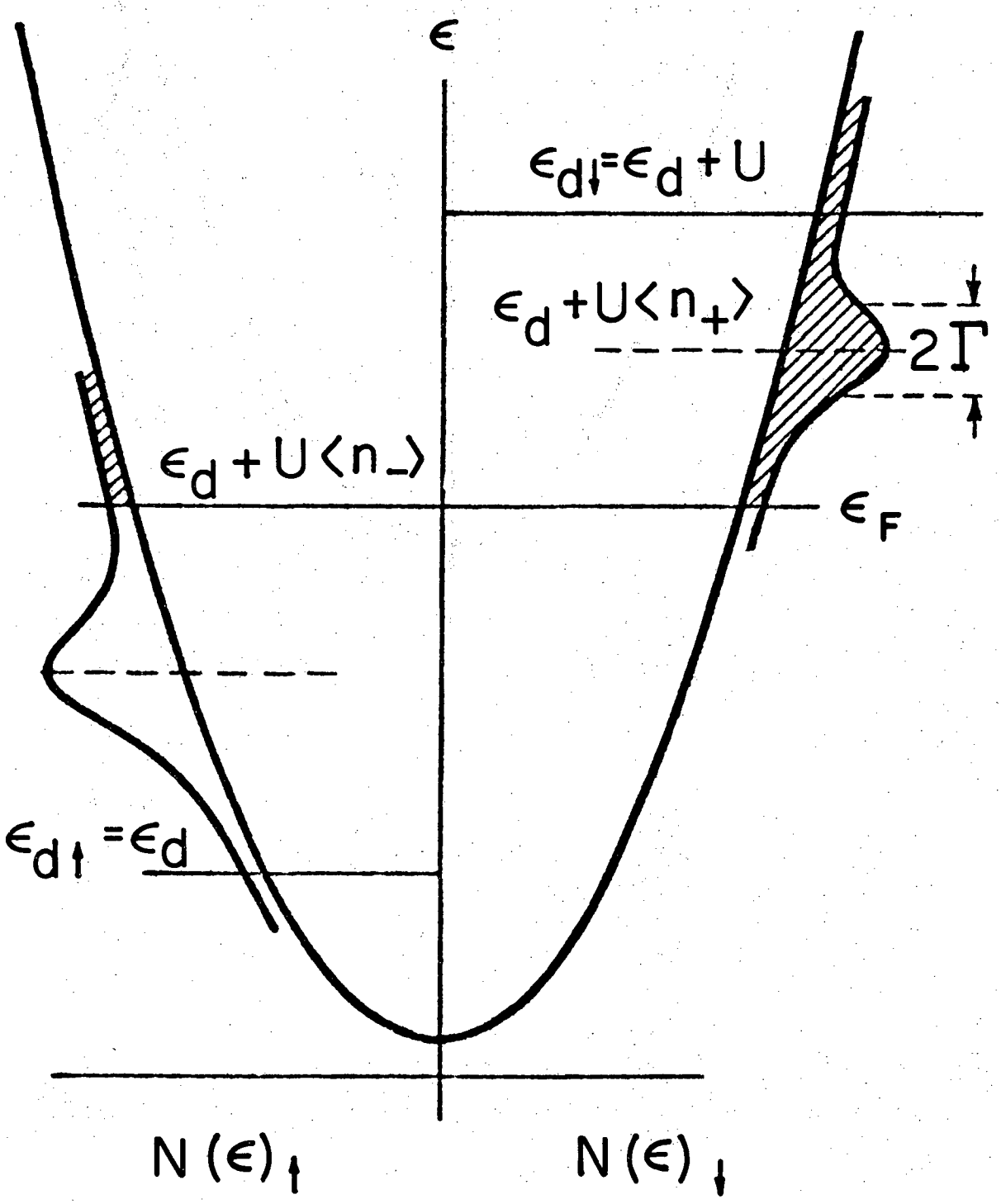

XBL 709-6604

Fig. 1b

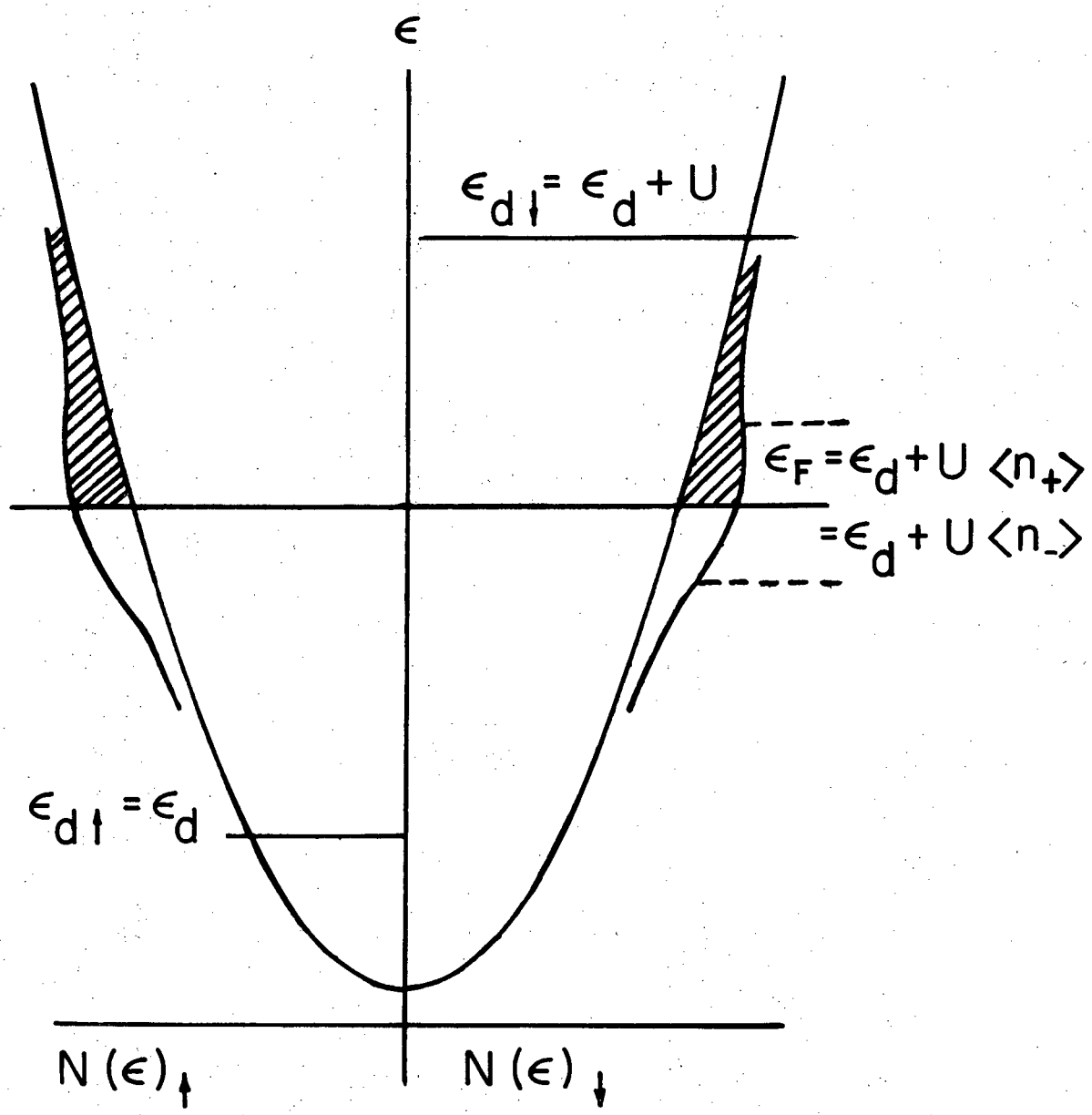

XBL 709-6602

Fig. 1c

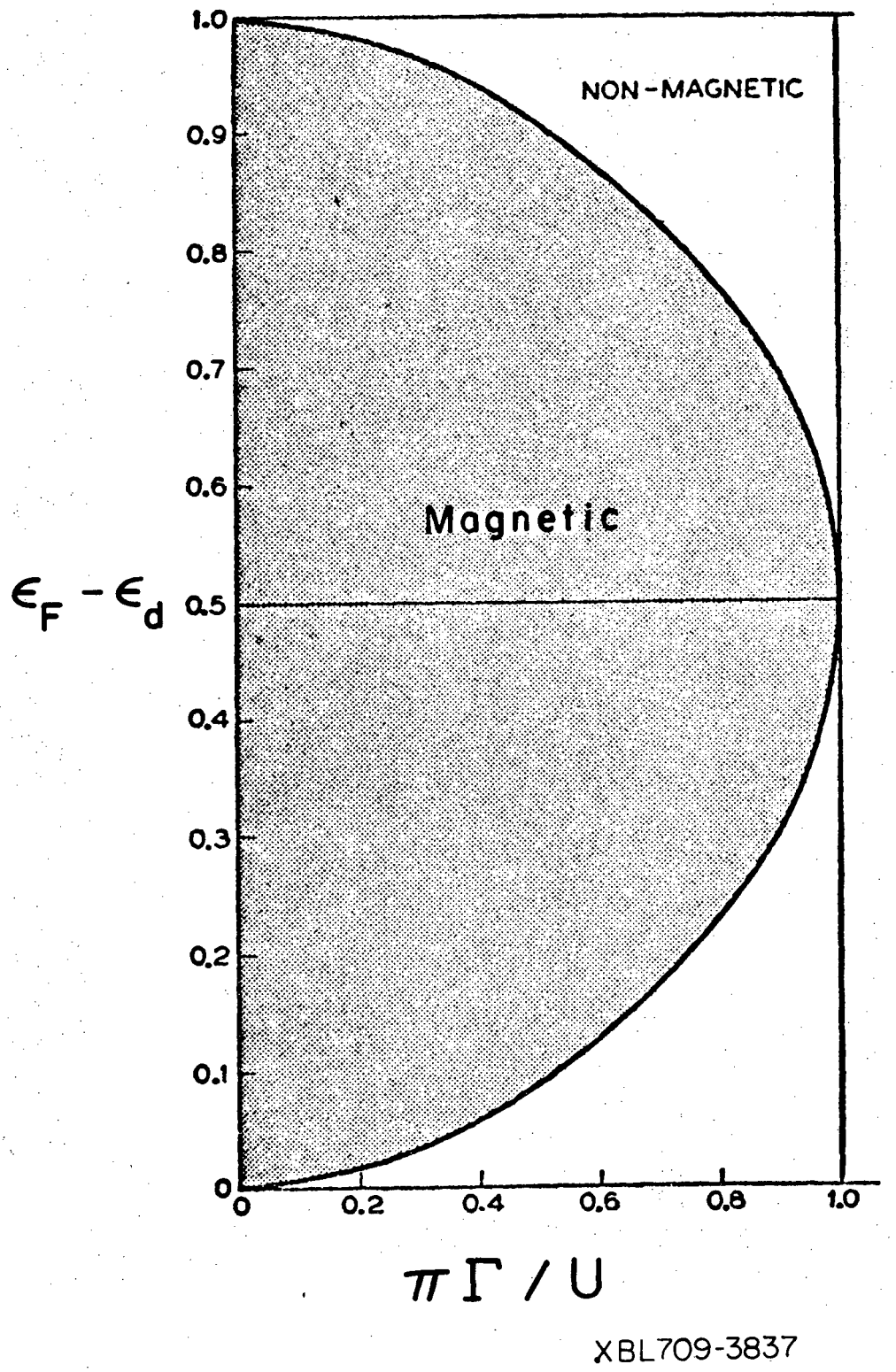
NON-MAGNETIC
Magnetic
$\epsilon_F - \epsilon_d$
1.0
0.9
0.8
0.7
0.6
0.5
0.4
0.3
0.2
0.1
0
0
0.2
0.4
0.6
0.8
1.0
$\pi\Gamma / U$
XBL709-3837

Fig. 2

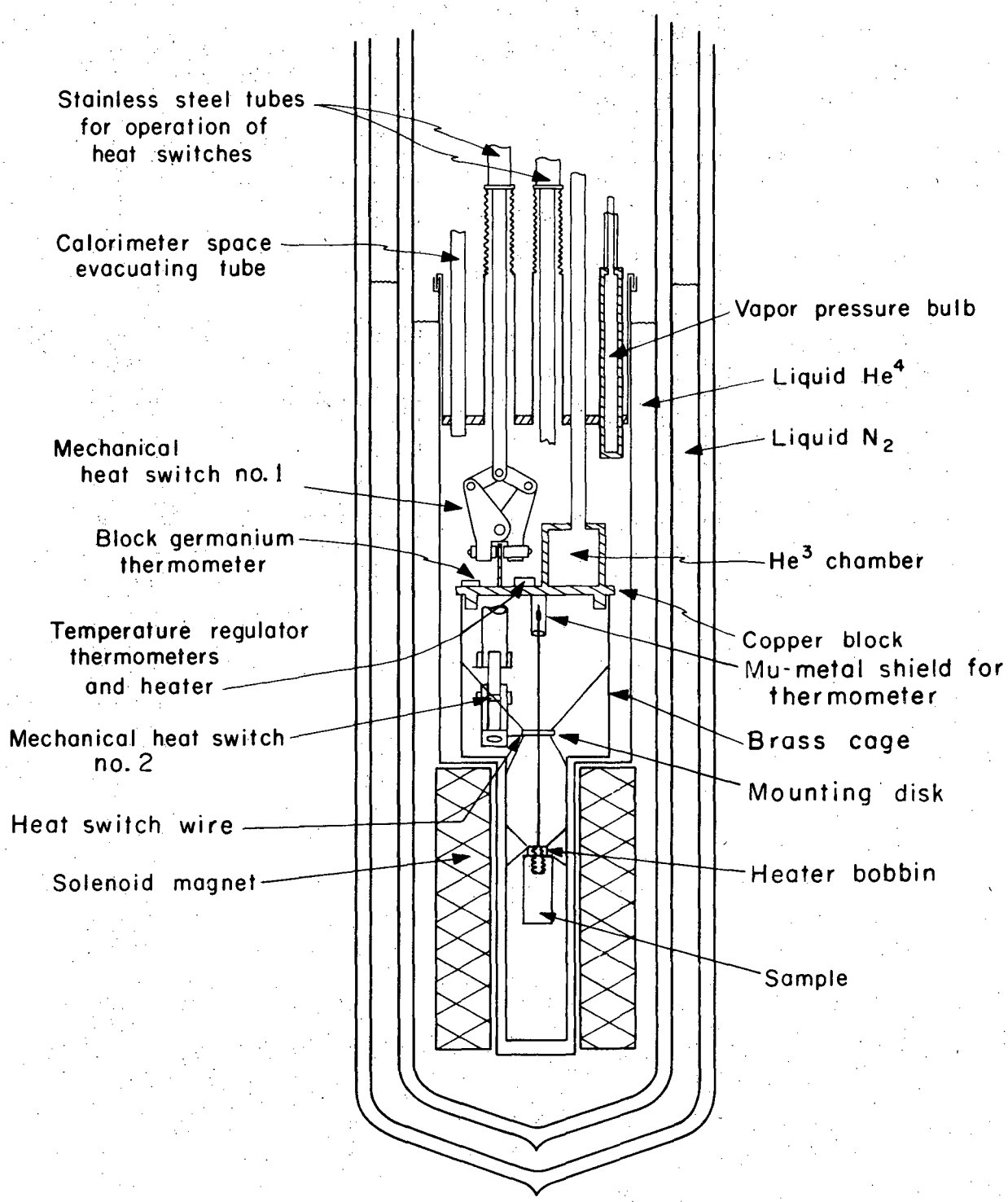

XBL 708-6424

Fig. 3

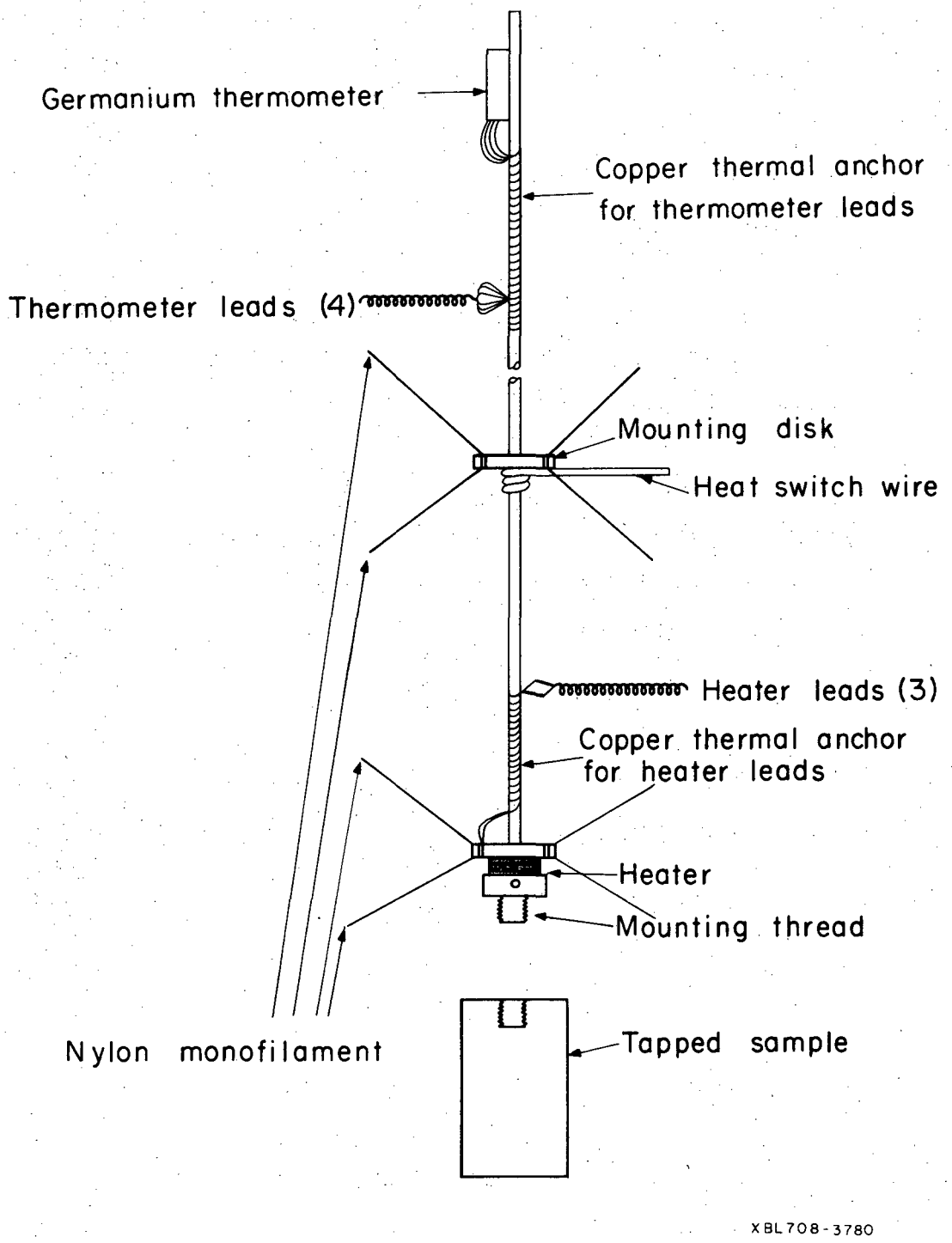
Germanium thermometer
Copper thermal anchor for thermometer leads
Thermometer leads (4)
Mounting disk
Heat switch wire
Heater leads (3)
Copper thermal anchor for heater leads
Heater
Mounting thread
Nylon monofilament
Tapped sample
XBL708-3780

Fig. 4

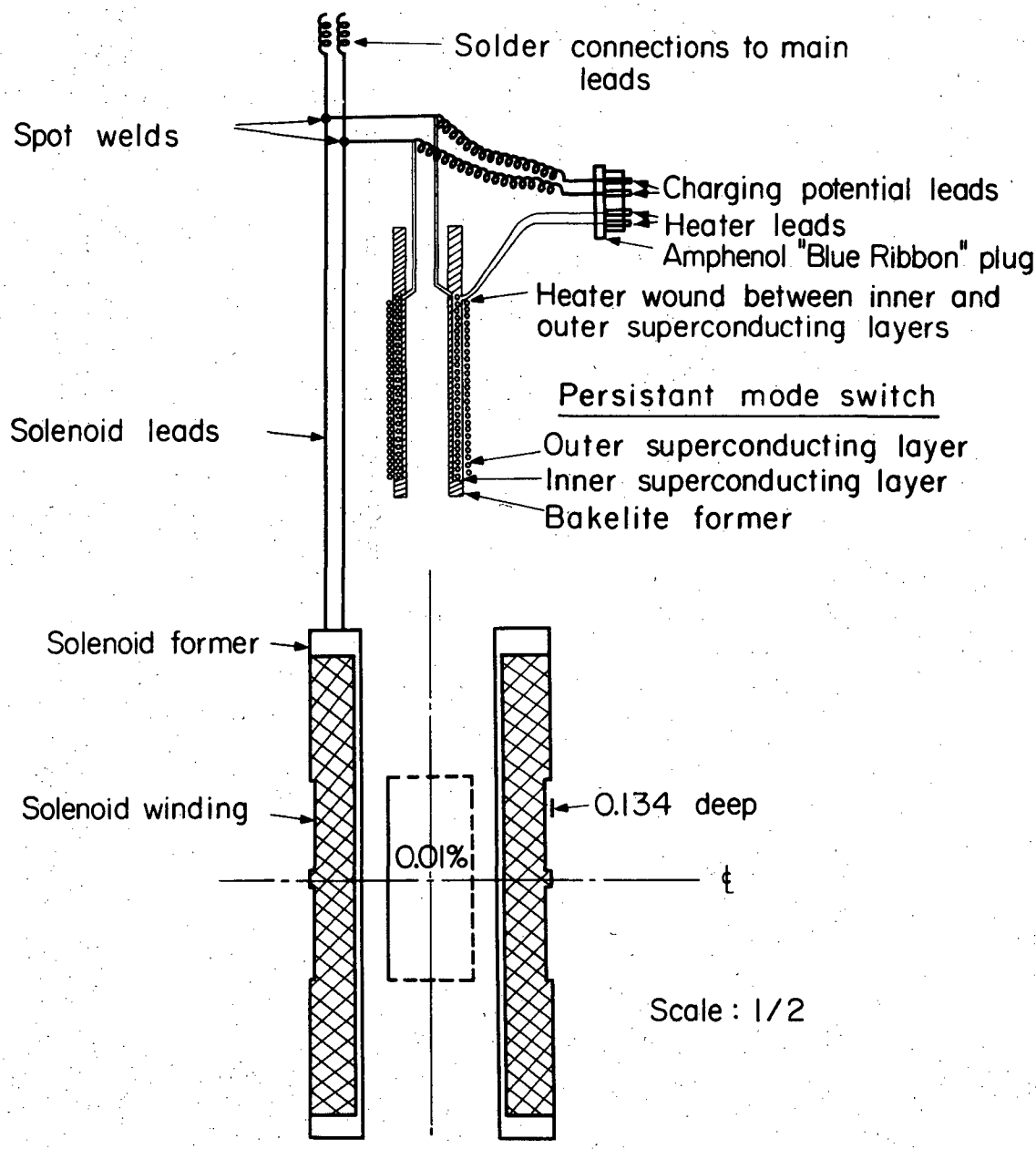

XBL708-3779

Fig. 5

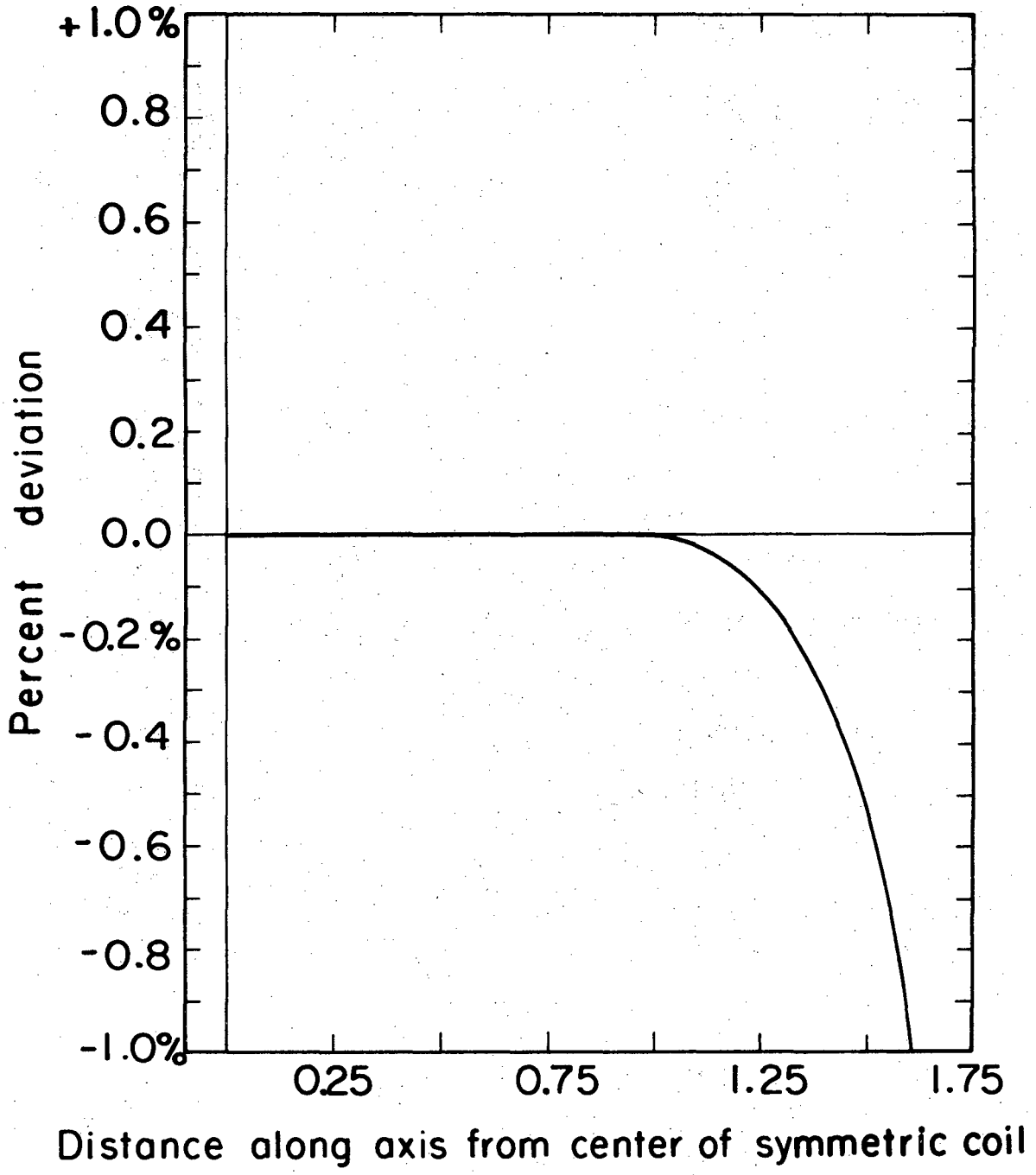

XBL708-3778

Fig. 6

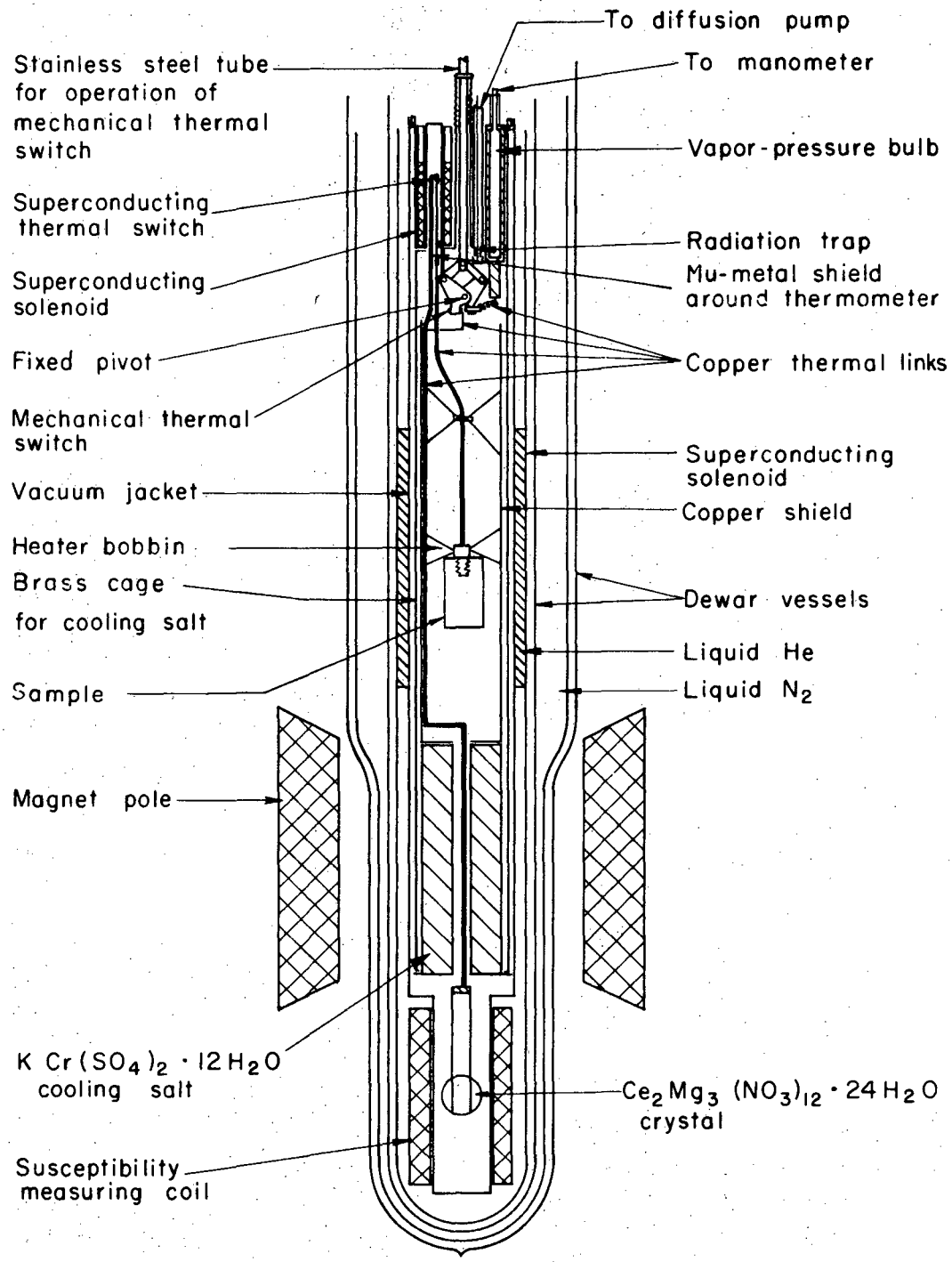

XBL 708-6425

Fig. 7

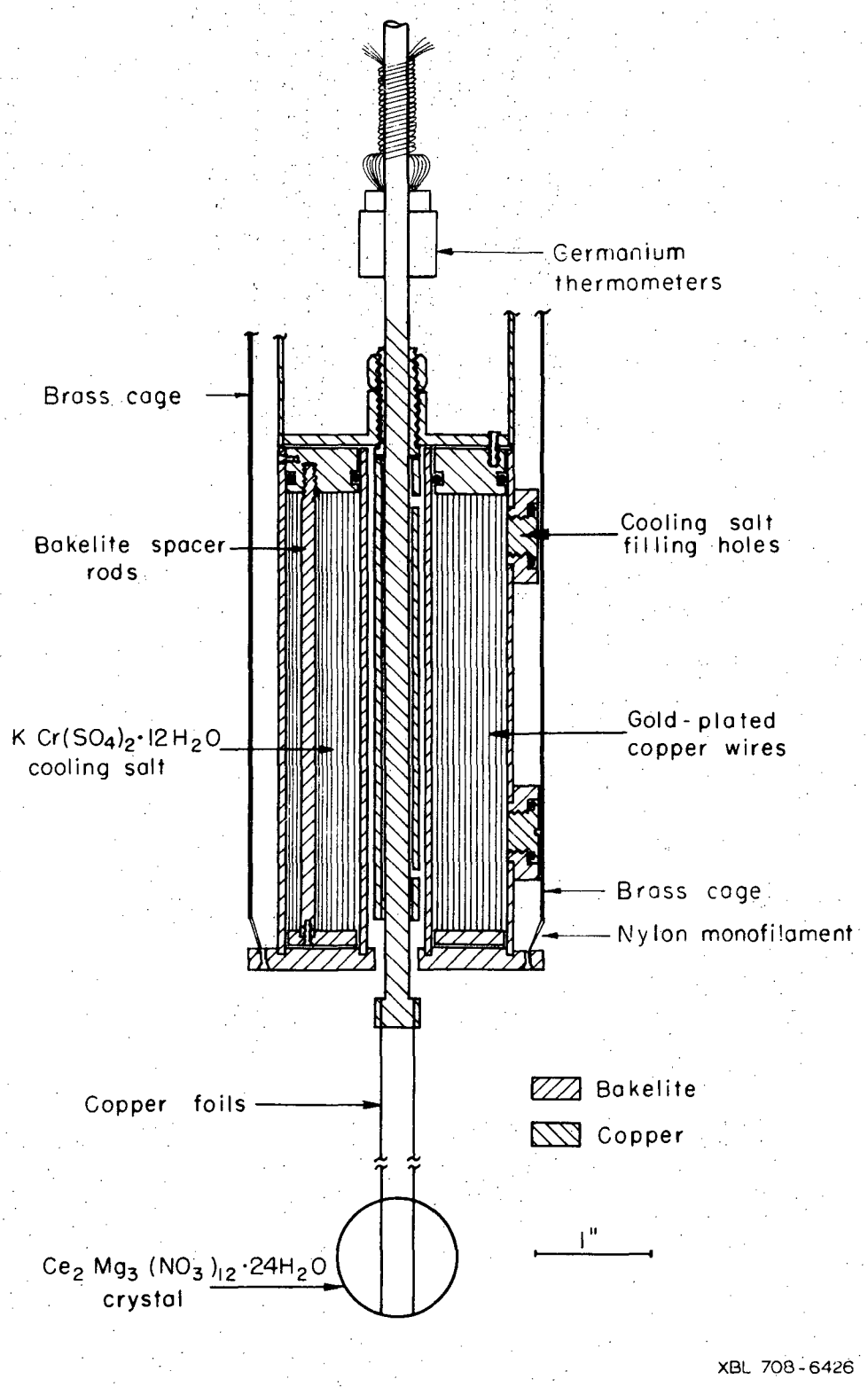
Germanium thermometers
Brass cage
Bakelite spacer rods
Cooling salt filling holes
K Cr(SO4)2·12H2O cooling salt
Gold-plated copper wires
Brass cage
Nylon monofilament
Copper foils
Bakelite
Copper
1"
Ce2 Mg3 (NO3)12·24H2O crystal
XBL 708-6426

Fig. 8

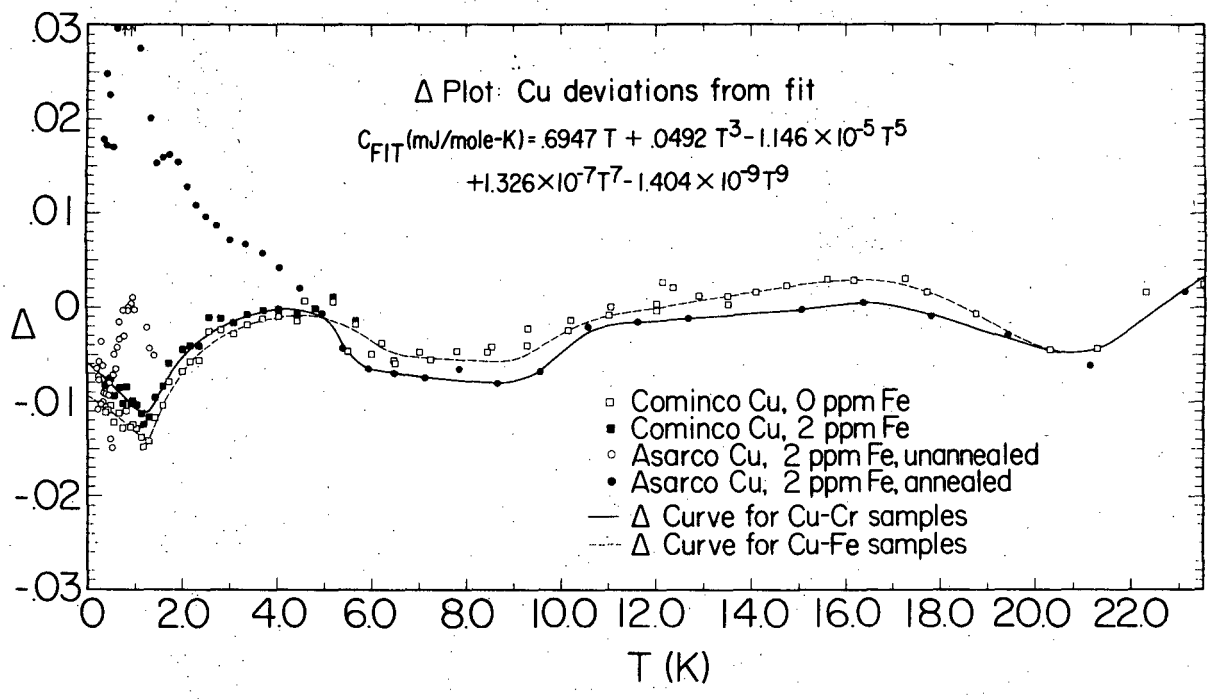

XBL 709-6625

Fig. 9

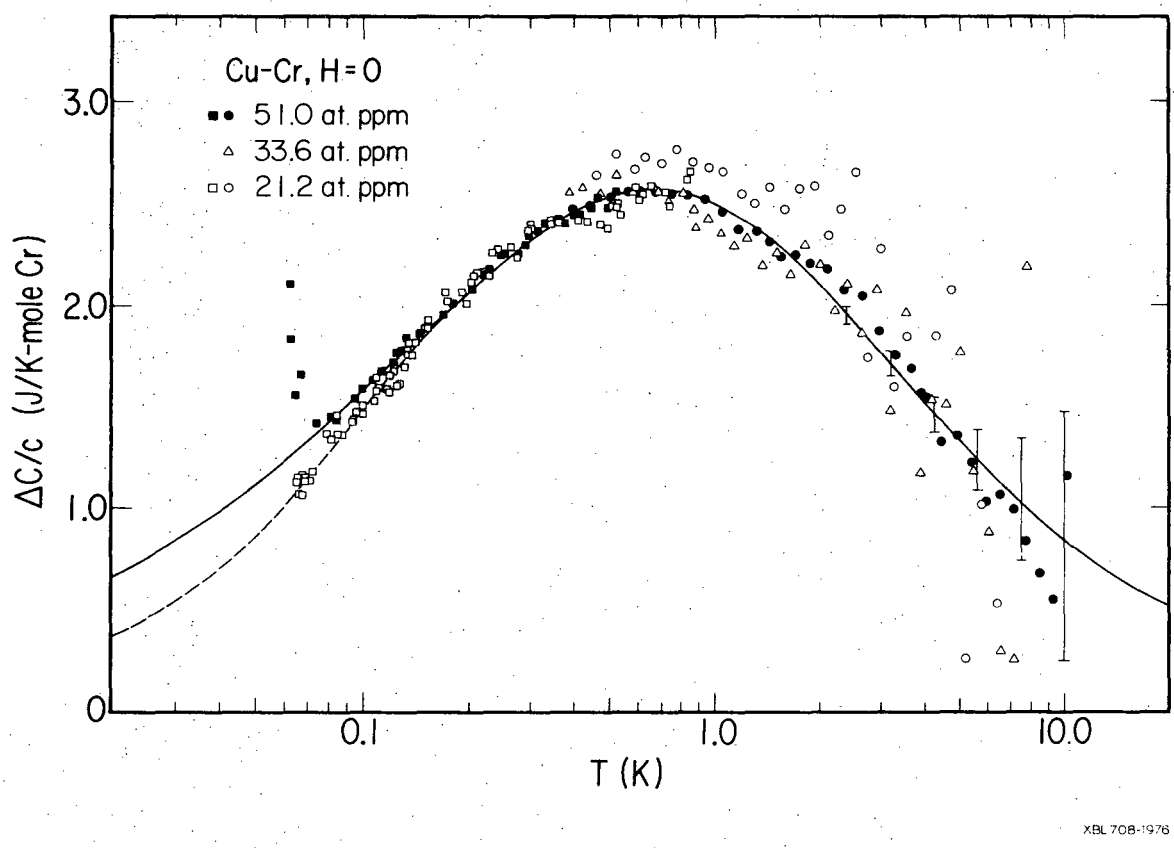
Cu-Cr, H=0
51.0 at. ppm
33.6 at. ppm
21.2 at. ppm
3.0
2.0
1.0
0
ΔC/c (J/K-mole Cr)
0.1
1.0
10.0
T (K)
XBL 708-1976

Fig. 10

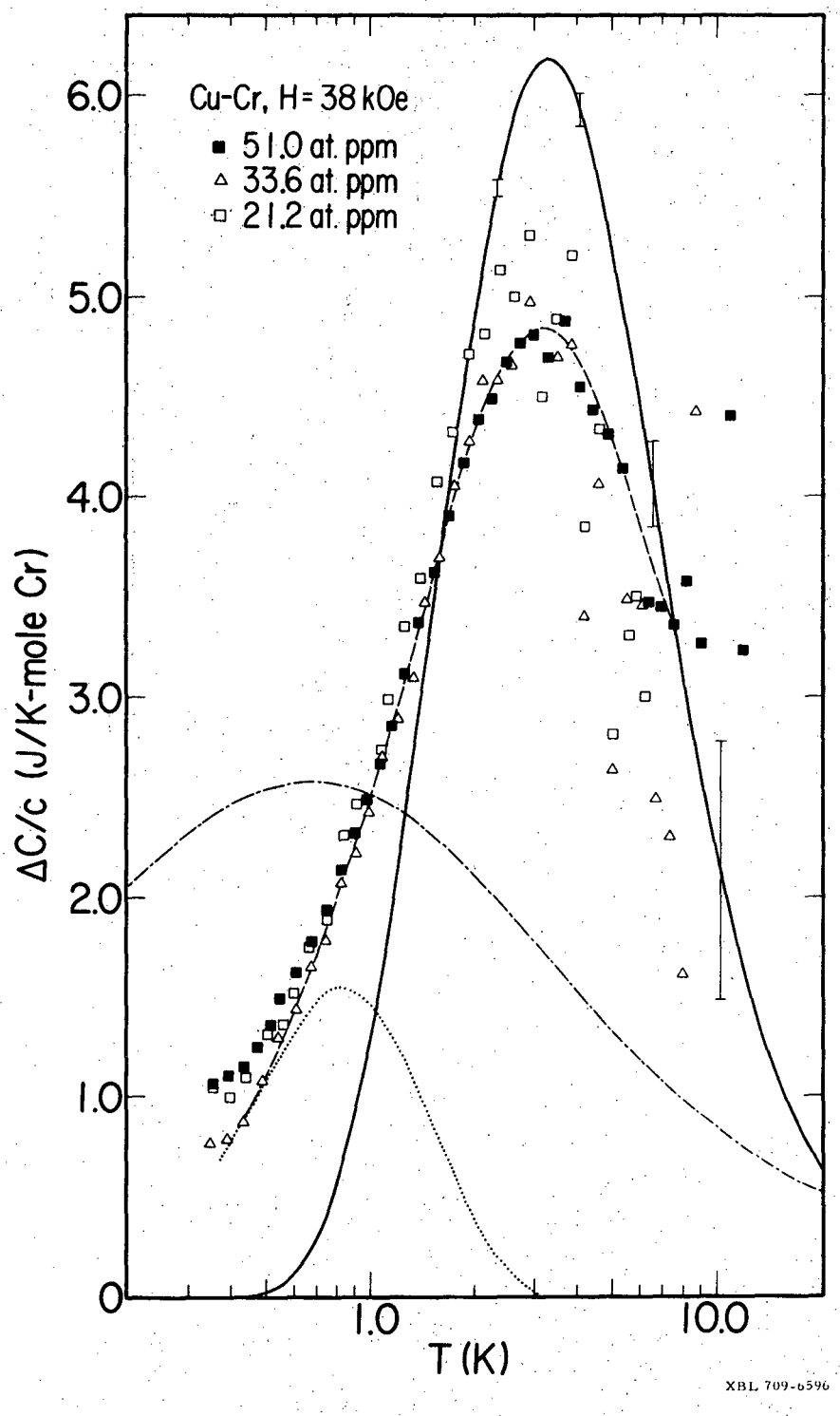
Cu-Cr, H = 38 kOe
51.0 at. ppm
33.6 at. ppm
21.2 at. ppm
6.0
5.0
4.0
3.0
2.0
1.0
0
ΔC/c (J/K-mole Cr)
1.0
10.0
T (K)
XBL 709-6596

Fig. 11

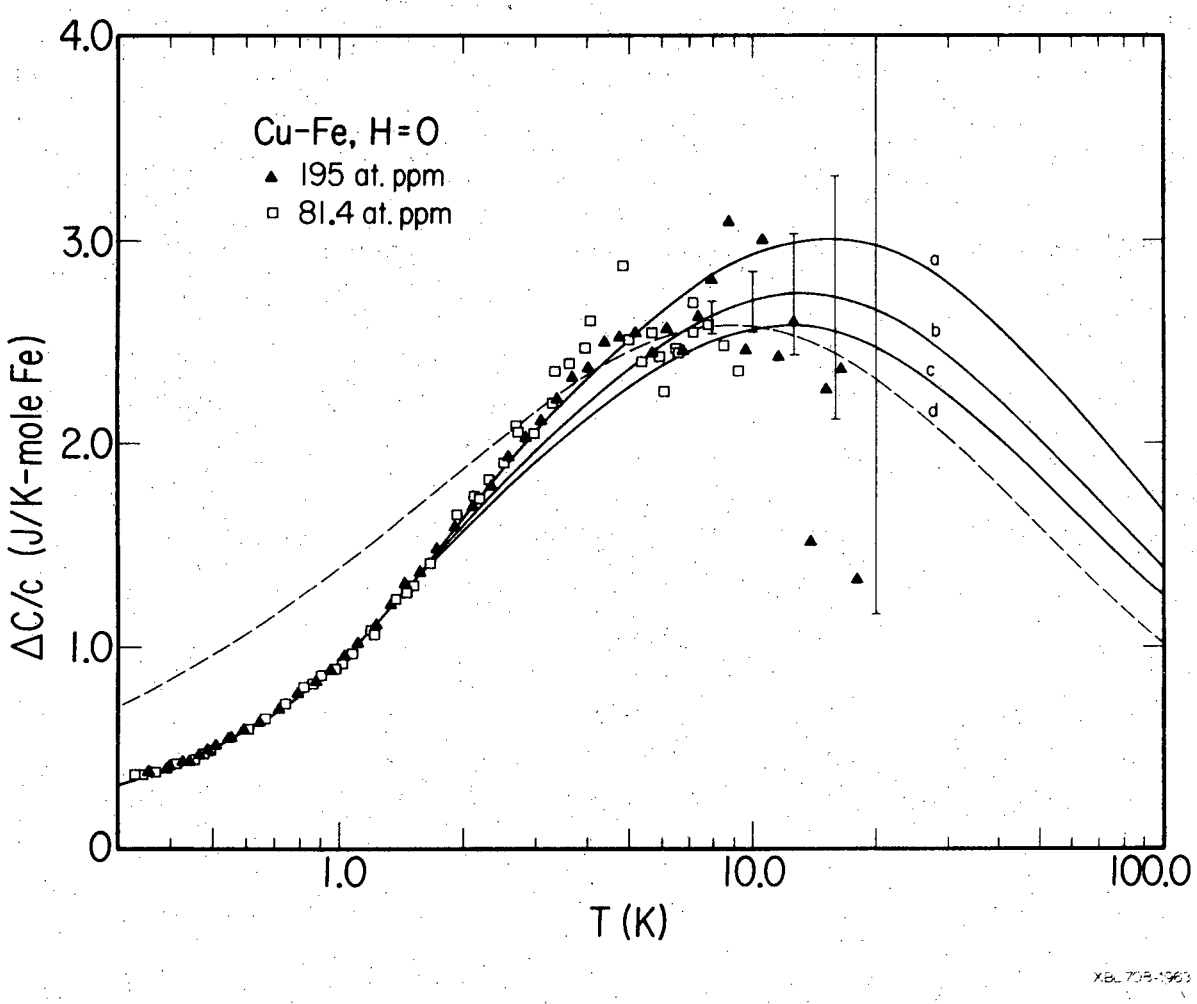
Cu-Fe, H=0
195 at. ppm
81.4 at. ppm
4.0
3.0
2.0
1.0
0
ΔC/c (J/K-mole Fe)
1.0
10.0
100.0
T (K)
a
b
c
d
XBL 708-1963

Fig. 12

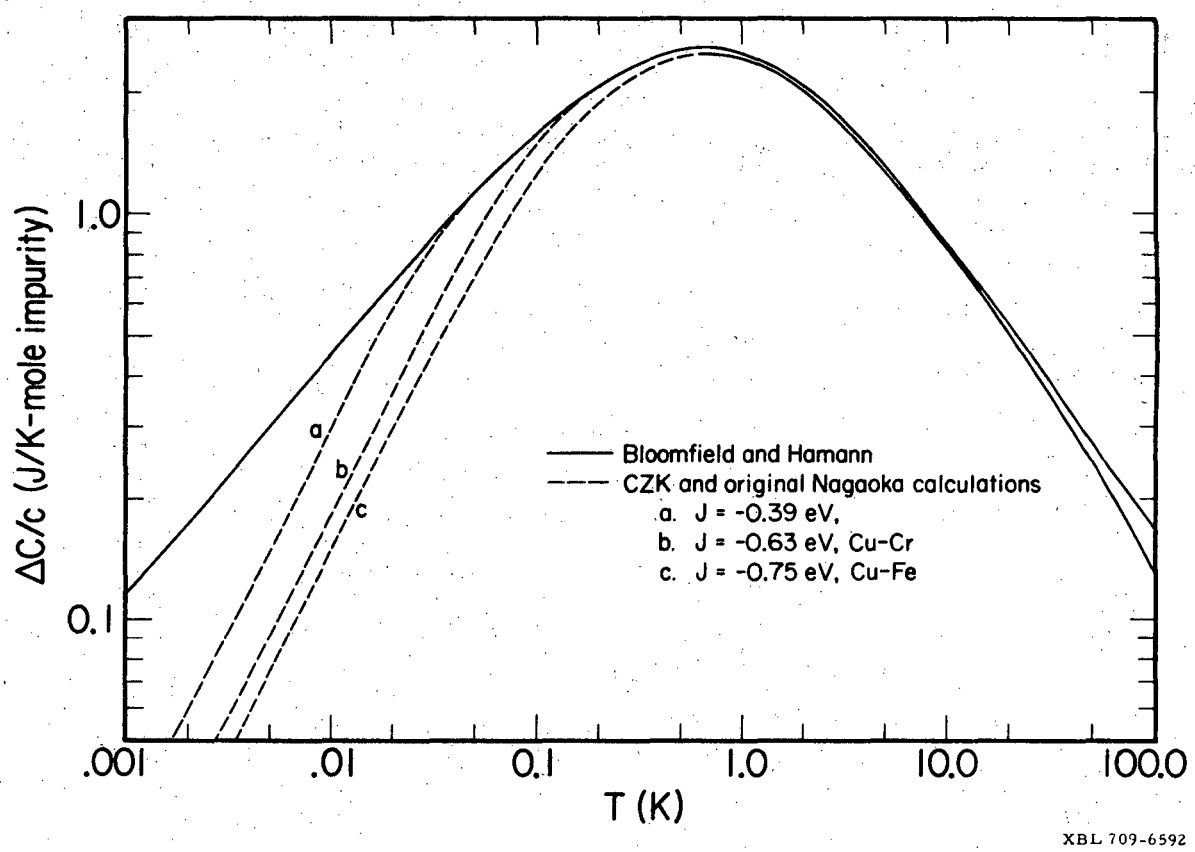
ΔC/c (J/K-mole impurity)
1.0
0.1
.001
.01
0.1
1.0
10.0
100.0
T (K)
a
b
c
Bloomfield and Hamann
CZK and original Nagaoka calculations
a. J = -0.39 eV,
b. J = -0.63 eV, Cu-Cr
c. J = -0.75 eV, Cu-Fe
XBL 709-6592

Fig. 13

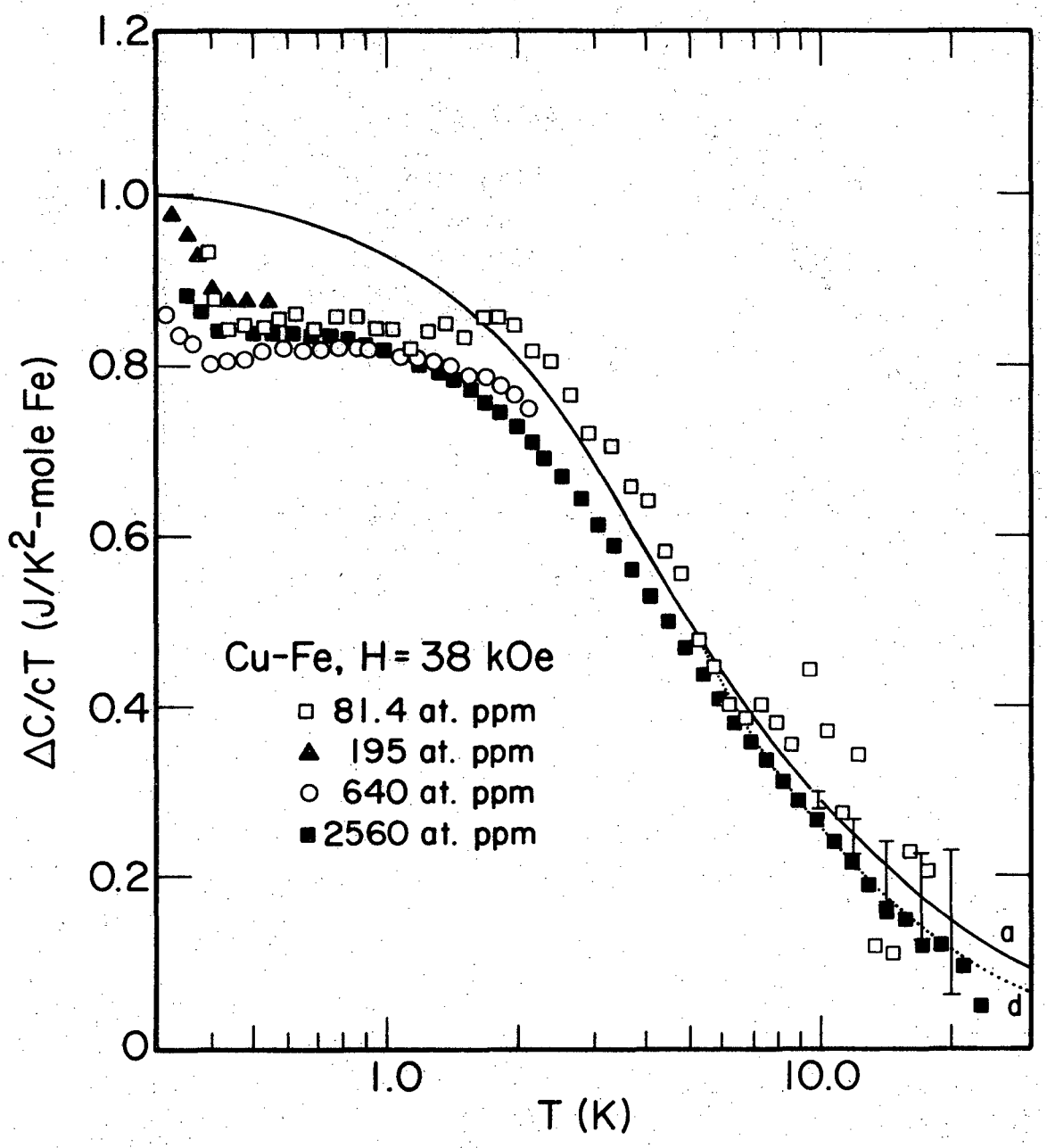

XBL 708-1975

Fig. 14

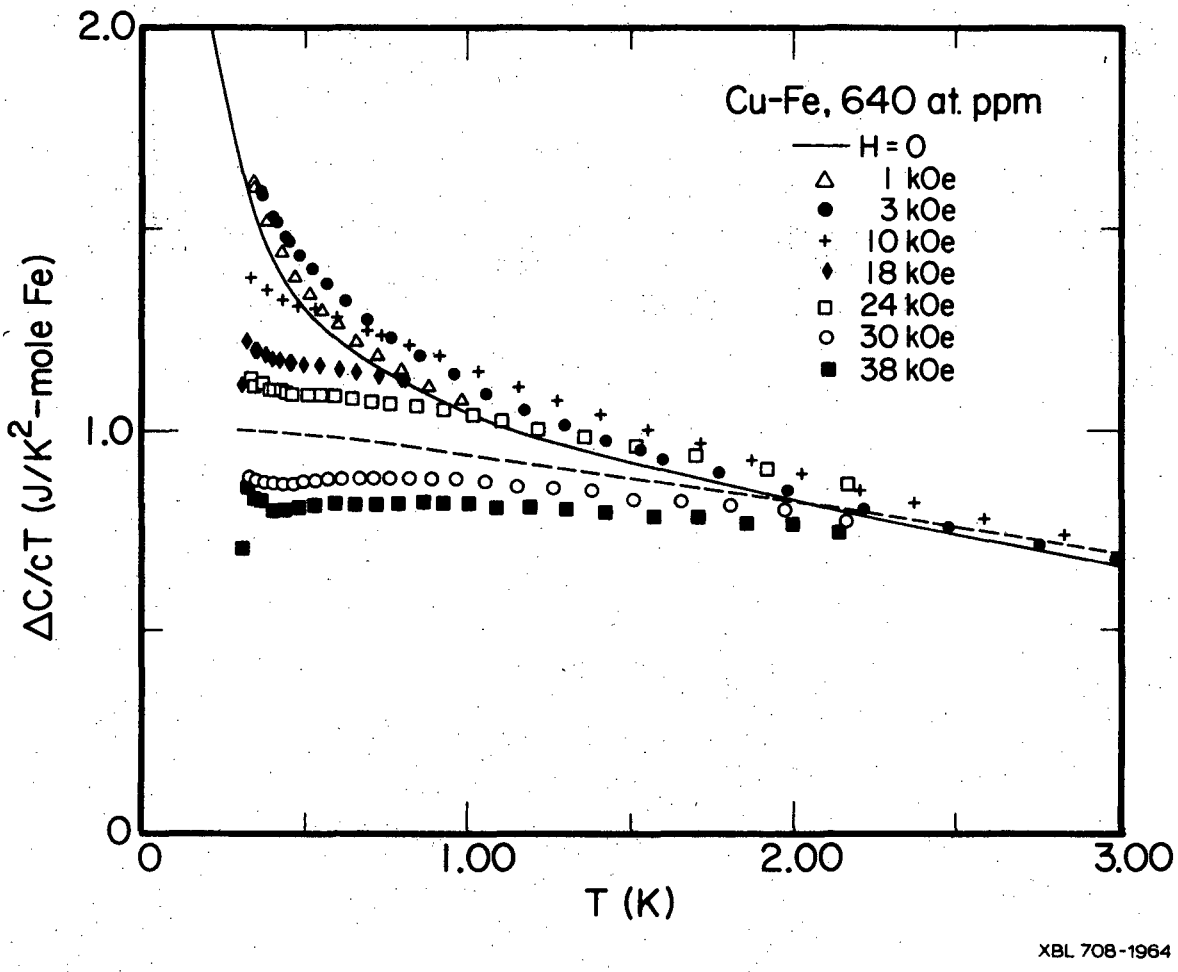
Cu-Fe, 640 at. ppm
H = 0
1 kOe
3 kOe
10 kOe
18 kOe
24 kOe
30 kOe
38 kOe
2.0
1.0
0
ΔC/cT (J/K²-mole Fe)
0
1.00
2.00
3.00
T (K)
XBL 708-1964

Fig. 15

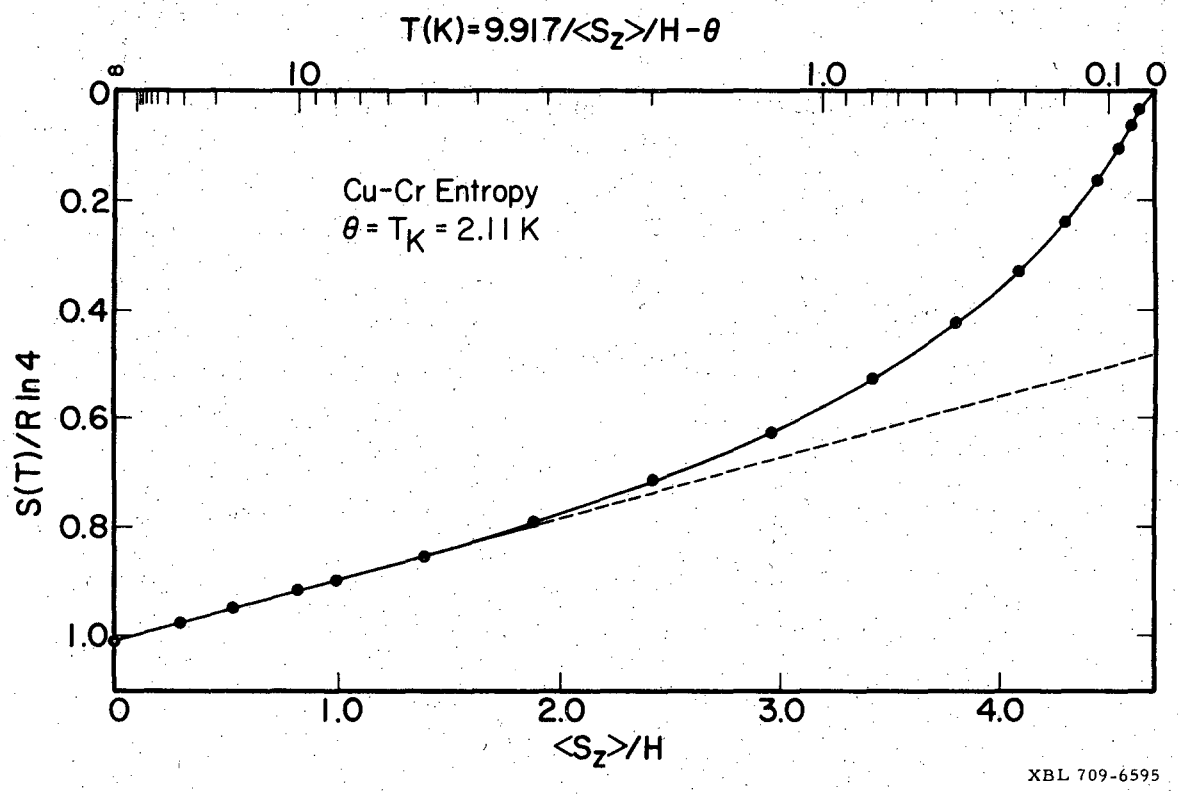
T(K)=9.917/<Sz>/H-θ
∞
10
1.0
0.1
0
Cu-Cr Entropy
θ = TK = 2.11 K
S(T)/R ln 4
0
0.2
0.4
0.6
0.8
1.0
0
1.0
2.0
3.0
4.0
<Sz>/H
XBL 709-6595

Fig. 16

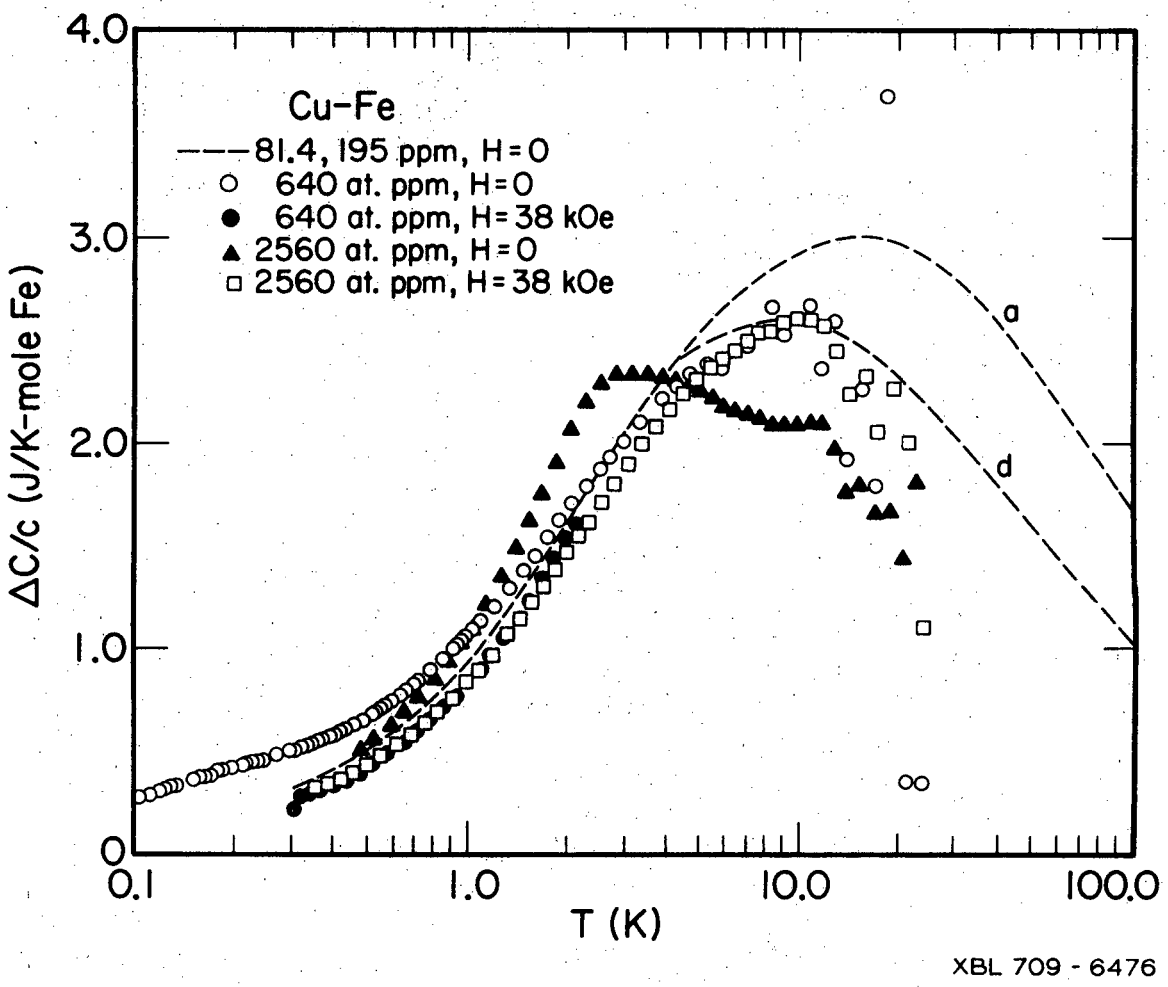
Cu-Fe
81.4, 195 ppm, H=0
640 at. ppm, H=0
640 at. ppm, H=38 kOe
2560 at. ppm, H=0
2560 at. ppm, H=38 kOe
a
d
ΔC/c (J/K-mole Fe)
T (K)
4.0
3.0
2.0
1.0
0
0.1
1.0
10.0
100.0
XBL 709 - 6476

Fig. 17

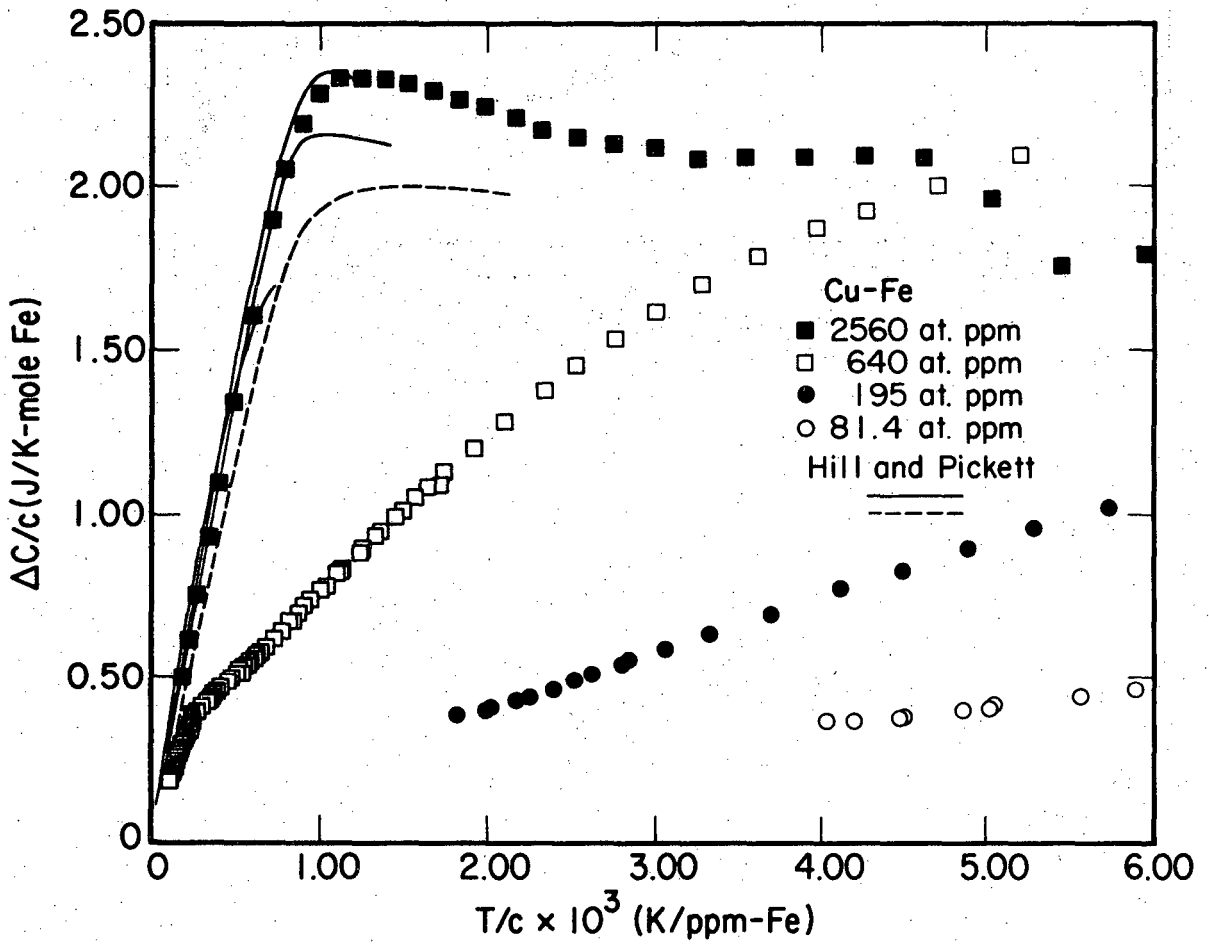

XBL 709-6594

Fig. 18

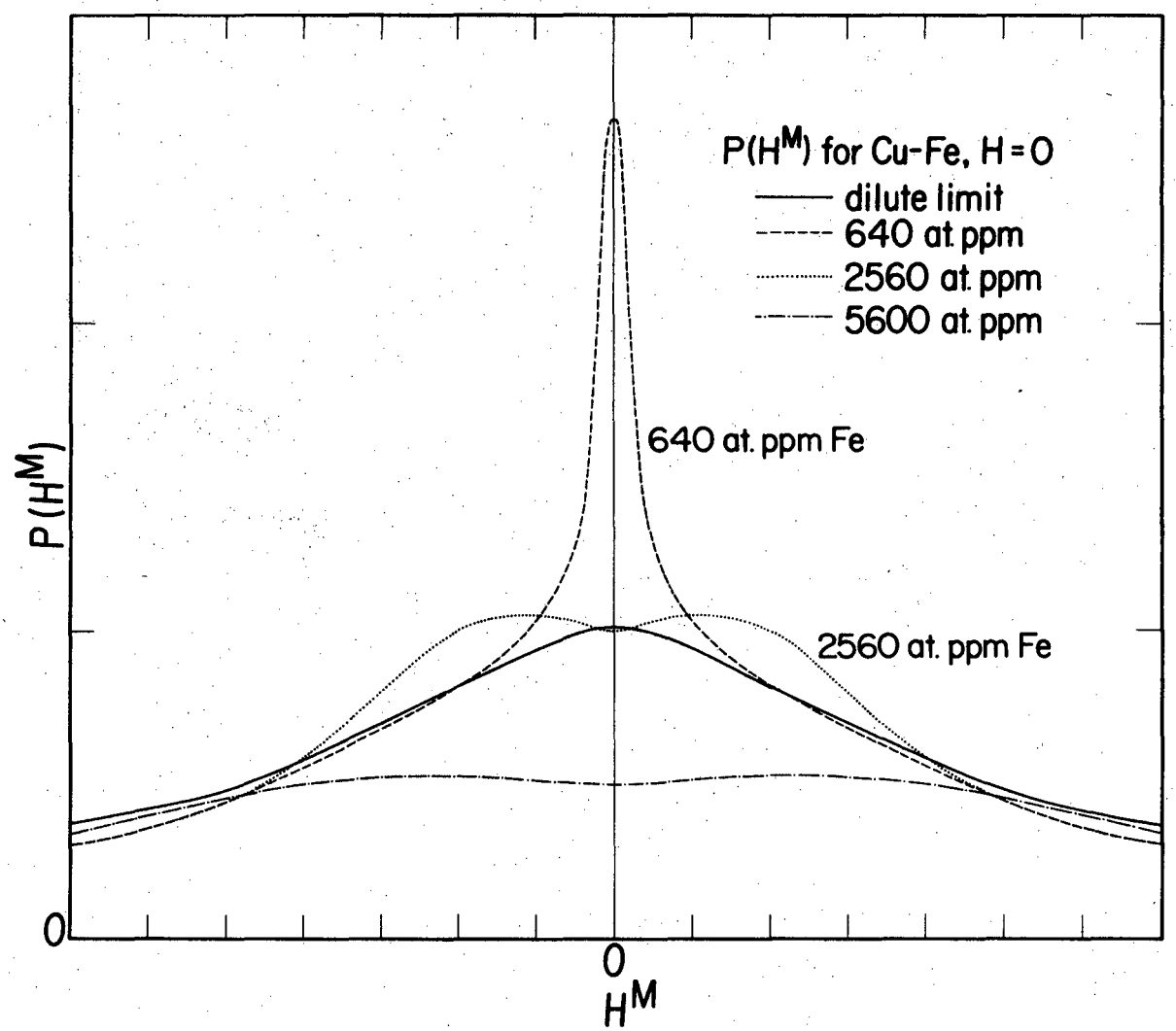

XBL 709-6634

Fig. 19

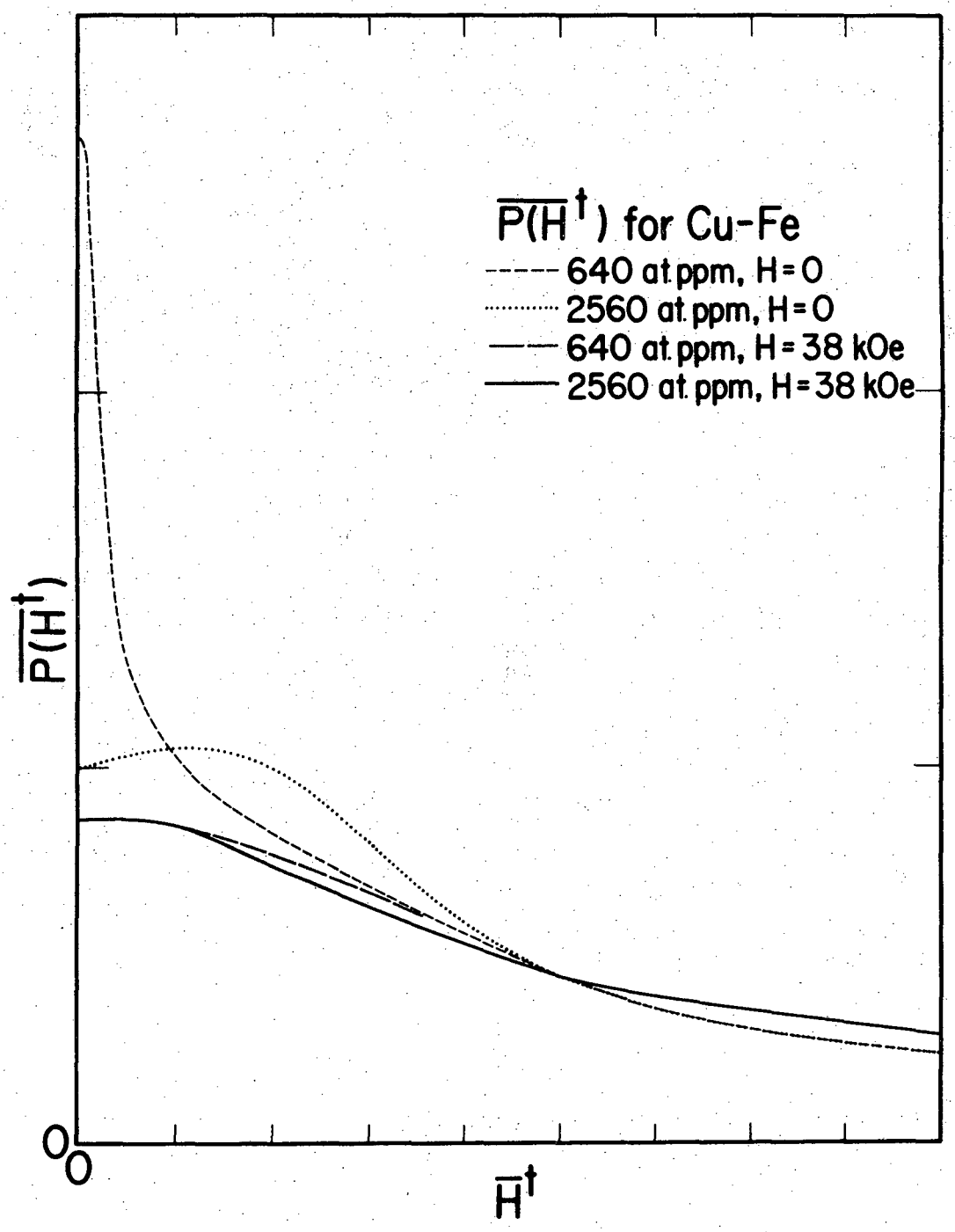

XBL 709-6633

Fig. 20

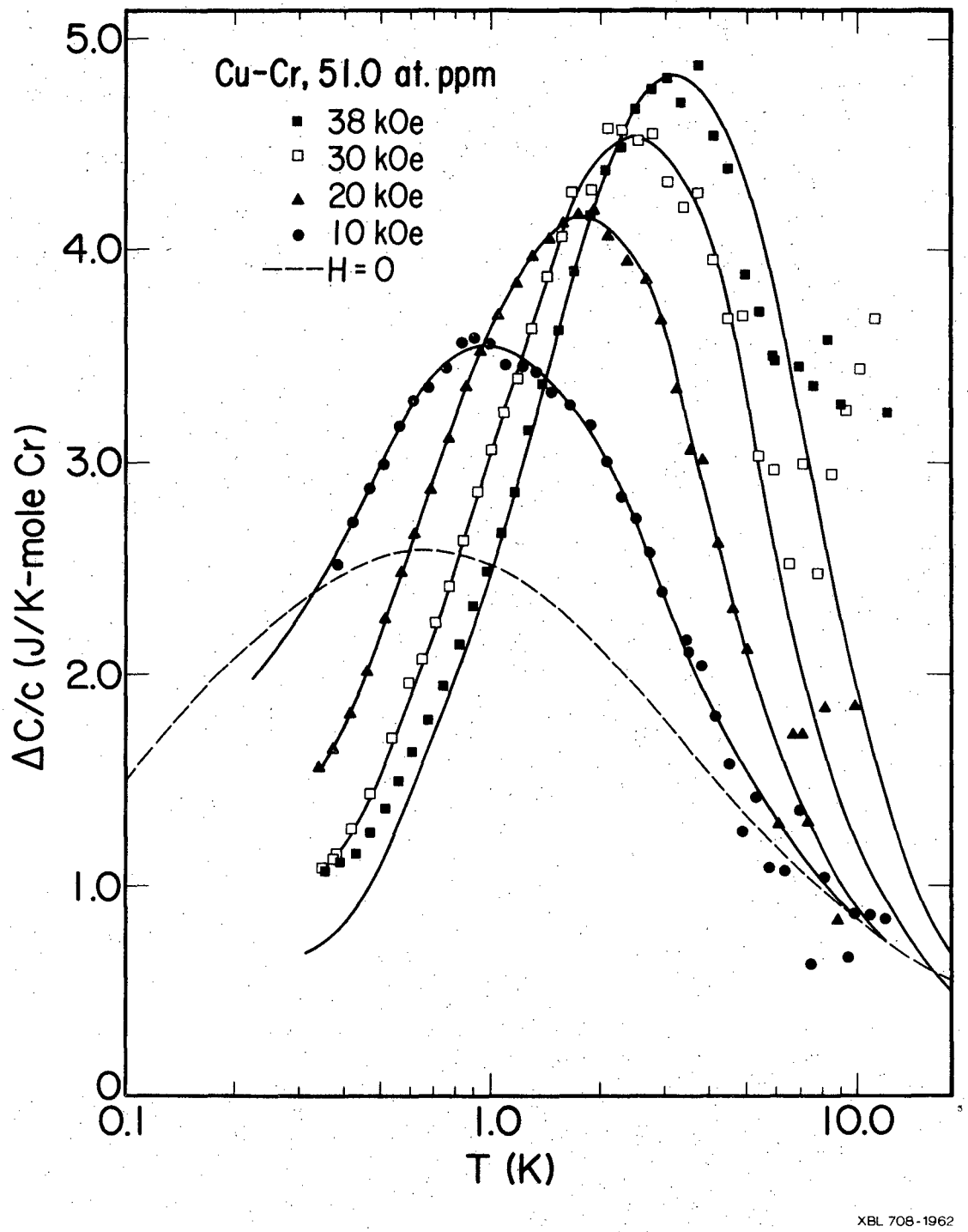
Cu-Cr, 51.0 at. ppm
38 kOe
30 kOe
20 kOe
10 kOe
H = 0
5.0
4.0
3.0
2.0
1.0
0
ΔC/c (J/K-mole Cr)
0.1
1.0
10.0
T (K)
XBL 708-1962

Fig. 21

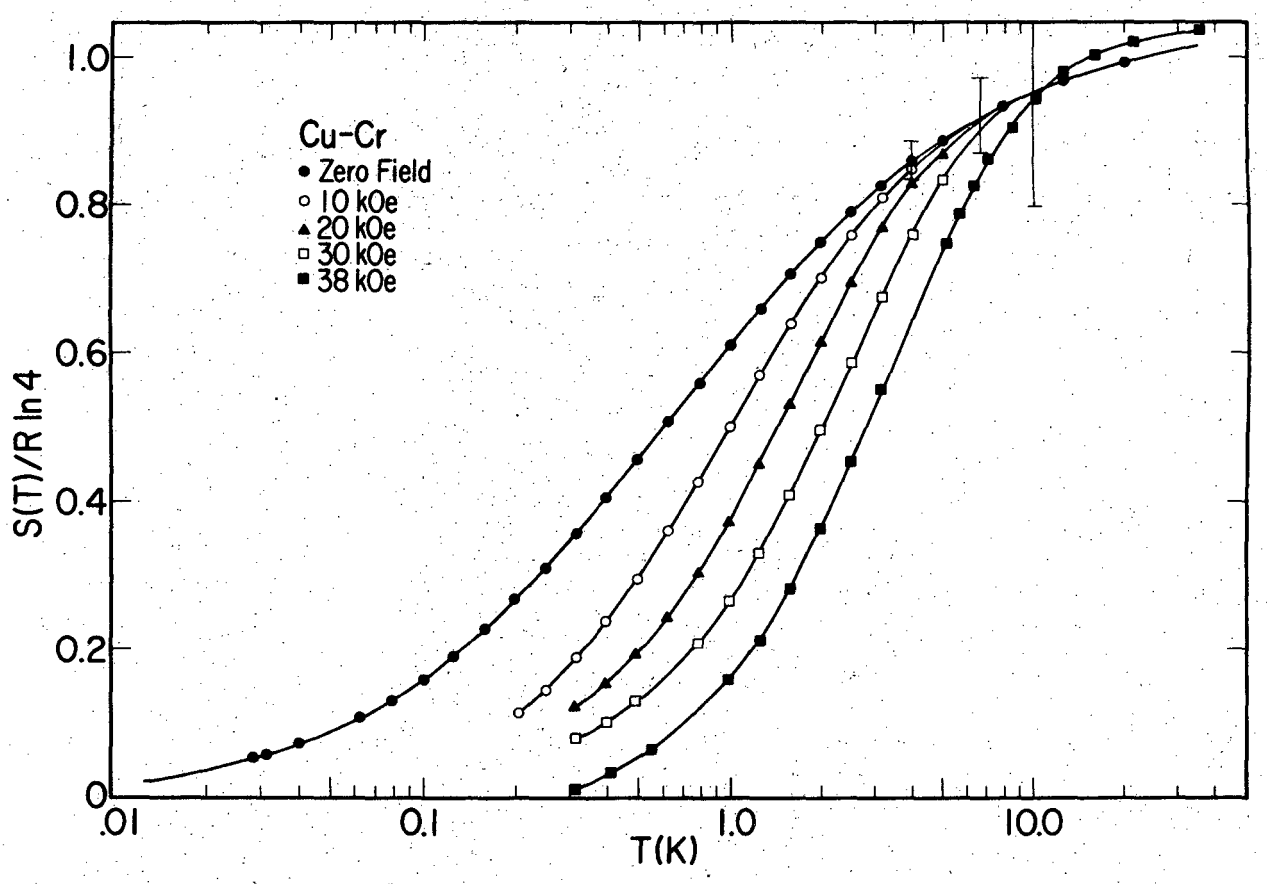

XBL 709-6573

Fig. 22

II. SEARCH FOR SUPERCONDUCTIVITY

A. INTRODUCTION

Recent advances in the theory of metals raise the possibility of reliably predicting the critical temperatures of superconductors from normal-state data. In particular, Allen and Cohen[1] have used a pseudopotential method to treat the electron-phonon interaction for a number of metals, and shown that Mg and Li might be superconducting at experimentally accessible temperatures. A verification of their calculations by the discovery of superconducting transitions in these metals would be of sufficient interest to justify a search for superconductivity even though it is not possible to cover the whole of the temperature regions corresponding to the recognized uncertainty in the calculations. We have accordingly tested magnesium and lithium for superconductivity down to 4 mK. The results were negative, but they do serve to set limits for the parameters related to the critical temperature, and the experimental techniques may also be of some interest.

McMillan[2] has obtained accurate numerical solutions for the critical temperature of a superconductor using the Nambu-Gor'kov-Eliashberg formulation of the BCS theory and a particular phonon spectrum. The results were fitted to an expression of the form

$$\frac{T_c}{\omega_0} = \exp\left[\frac{-(1+\lambda)}{\lambda - \mu^* - (\langle\omega\rangle/\omega_0)\lambda\mu^*}\right], \qquad (1)$$

the analytical solution obtained in a two-square-well approximation. T_c is the critical temperature, ω_0 is the maximum phonon frequency, and μ^* is the coulomb pseudo-potential of Morel and Anderson.[3] The electron-phonon coupling constant is

$$\lambda \equiv 2 \int_0^{\omega_0} \alpha^2(\omega)\, F(\omega)\, \frac{d\omega}{\omega} \quad . \tag{2}$$

and $\langle \omega \rangle$ is an average phonon frequency defined by

$$\langle \omega \rangle \equiv (2/\lambda) \int_0^{\omega_0} \alpha^2(\omega)\, F(\omega)\, d\omega \; . \tag{3}$$

The phonon density of states is $F(\omega)$ and $\alpha^2(\omega)$ is an average of the square of the electron-phonon matrix elements. The numerical solutions of the gap equation were based on the phonon spectrum of Nb, and after fitting to an equation of the same form as Eq. (1), McMillan obtained the result,

$$\frac{T_c}{\Theta} = 0.690 \exp \left[\frac{-1.04(1 + \lambda)}{\lambda - \mu^*(1 + 0.62\lambda)} \right] , \tag{4}$$

where Θ is the Debye temperature. The formula is not expected to be sensitive to the details of the phonon spectrum for $\lambda < 1$ (the case of interest here) and served as the basis for the predictions of T_c by Allen and Cohen.

Allen and Cohen have calculated λ for the hexagonal divalent metals beryllium, magnesium, zinc, and cadmium, using the known (except for cadmium) phonon density of states and deriving the electron phonon

matrix elements from empirical pseudo-potentials that accurately fit the extensive Fermi-surface data. Since the phonon interaction increases the electronic heat capacity by the factor $(1 + \lambda)$, an empirical value of λ can be obtained by comparing the experimental heat capacity with band-structure calculations of the electronic density of states. McMillan has also derived empirical values of λ from his formula and known values of T_c (taking $\mu^* = 0.1$). The theoretical and empirical values of λ are compared in Table I, reproduced from Table V of Reference 1. The good agreement between the various values of λ gives support to the underlying assumptions.

McMillan has suggested that $\mu^* = 0.1$ is a good approximation for simple metals, but in the case of magnesium λ is small enough for the predicted T_c to be relatively sensitive to errors in μ^*. Allen and Cohen used the random phase approximation to calculate μ^* for beryllium, magnesium, zinc, and cadmium. The values so obtained were too small, but, on the assumption that the calculations gave relative values correctly, they used the value of μ^* for zinc (known from the isotope effect) to obtain $\mu^* = 0.16$ for magnesium. McMillan's equation with $\mu^* = 0.16$ and $\lambda = 0.31$ gives $T_c = 0.02$ K for magnesium. However, T_c depends exponentially on λ and μ^*, and the uncertainties in these parameters estimated by Allen and Cohen are such that T_c might be higher or lower by an order of magnitude (see Fig. 3 of Ref. 1). The lowest temperature to which Mg has been previously investigated is 0.017 K.[4]

Similar internal checks on the parameters for lithium were not possible for two reasons. First, the pseudo-potential used (selected because it gave the lowest critical temperature) was that derived

from first principles by Goddard[5] who checked it with atomic energy level data but not with Fermi surface data--of which there is very little. Second, there is a martensitic phase transition in lithium at about 80 K which results in some of the sample converting from the high temperature bcc phase to the low temperature hcp phase.[6] The calculations on lithium were made using (a) the Goddard potential, screened by the Lindhard dielectric function; (b) experimental bcc phonon dispersion curves;[7] (c) the phonon renormalized mass m^* derived from specific heat measurements[8] on samples for which the extent of the martensitic transformation was not known and could only be estimated from other data;[6,9] and (d) values for λ, and the band-mass, m_b, derived self-consistently from m^* and λ calculated using $m_b = 1$. Furthermore, the number 0.62 in Eq. (4) may be incorrect for lithium. For the alkali metals, but not for most other metals, direct scattering processes are relatively more important than umklapp processes and the transverse modes are less strongly coupled than the longitudinal modes. This could raise the value of $\langle\omega\rangle/\omega_0$. Although the constant 0.62 was not derived by calculating $\langle\omega\rangle/\omega_0$, an increase in the expected value of $\langle\omega\rangle/\omega_0$ suggests that the constant 0.62 could be larger. The lowest temperature to which Li has been previously investigated is 0.08 K.[10]

These calculations suggest a reasonable probability for the occurrence of superconductivity in magnesium at presently available temperatures and that lithium is the most likely of the alkali metals to become superconducting. The latter result is interesting since earlier calculations of λ suggest the contrary.[11]

B. EXPERIMENTAL

1. Cryostat, field and susceptibility measurements

In this section we discuss all aspects of the experimental procedure except for the nuclear thermometry which is discussed in detail in the next section.

In order to observe a transition, both the temperature and magnetic field must be sufficiently low. In Table IV we give the thermodynamic critical fields at T = 0 calculated from the BCS model assuming the known transition temperatures for beryllium[4] and tungsten[12] and our lowest operating temperature for magnesium and lithium.

The cryostat system used for this experiment was similar to that described by Brewer.[13] It consisted of an outer dewar containing a superconducting solenoid maintained at 4.2 K. Inside this dewar was another dewar of 4.5-inch bore. The inner dewar had a vacuum jacket of copper around its lower portion only--the upper part was cooled by the gas evaporating from both dewars. The superconducting magnet around the inner dewar could be moved from the bottom to the top of the apparatus during a run. The two dewars were separately filled with helium. The inner dewar was pumped, maintaining a temperature of about 1 K.

Figure 1 shows the construction of the lower part of the apparatus that was inserted into the inner dewar. The hot finger (a) in which magnetic field probes could be inserted was of double wall construction with superinsulation between the walls. This insert was introduced into the apparatus through an O-ring seal into the pill vacuum line. The cerium

magnesium nitrate (CMN) pill (b) mounted inside the chromium potassium alum (CrKalum) guard (c) on graphite posts (d) consisted of a slurry of 50 mesh CMN in glycerol. Thermal contact to the slurry was provided by twenty-five 0.005-inch OFHC copper fins (e) with a total surface area of about 2000 cm^2. A stalk (f) of about 5000, 0.0031-inch insulated copper wires was made by potting the wires in Epibond 100A.[14] Thermal contact between the wires and the fins was maintained by electroplating a thick layer of copper on the end of the wires and then electroplating the fins to the layer (g). The upper part (h) of the CrKalum radiation shield was fabricated on a teflon mandrel from strips of 0.005-inch OFHC copper laid lengthwise down the mandrel and from cotton gauze impregnated with Epibond 121,[14] which was wound around the copper strips on the mandrel. Greater detail of the construction techniques of the pumping equipment and pill design is contained in Ref. 13.

Cooling below 1 K was obtained by the simultaneous demagnetization of the CrKalum and CMN from a field of 46 kOe. ^{4}He exchange gas was used to cool the salt pill and to conduct the heat of magnetization to the 1 K bath. Typically, the pill was kept in thermal contact with the 1 K bath for one hour, the exchange gas was pumped for one hour and a half and the demagnetization took forty-five minutes. After demagnetization the ^{60}Co<u>Co</u> thermometer on the copper stalk (j) indicated a temperature of about 3.5 mK. The superconducting solenoid was then slowly raised out of the helium bath to the top of the apparatus; after this it became normal in about fifteen minutes. After raising the solenoid the temperature of the stalk increased to about 4 mK and subsequently warmed at about 0.7 mK/hr at 5 mK and about 2 mK/hr at 10 mK.

The apparatus was designed so that none of the materials used would become superconducting at their operating temperatures. In the parts operating to 1 K cadmium-bismuth eutectic or silver solder was used to make joints. The pill assembly was made of copper, mylar, phenolic plastic, and different types of epoxy. Copper-copper joints on the pill assembly were made by plating the parts together. Most magnesium samples were bonded to gold or copper foils by gold diffusion bonds. Gold was first evaporated onto copper foils, or magnesium speciments, and a gold or gold-coated copper foil was clamped to the specimen and the two heated together for four to twenty-four hours in a hydrogen atmosphere at 400°C. For tungsten specimens, used to test the apparatus, gold previously evaporated on the specimen's surface was diffused into the metal by heating at 1200°C; copper foil was then electroplated to the gold diffusion layer. The foils were then plated to the copper stalk [(i), Fig. 1]. Lithium samples were attached by local melting of one end of a sample onto a copper foil with a spot welder or, for one rather small specimen, by pressing copper wires into the metal. The effectiveness of the diffusion bonds was shown by the results for the critical field curve for tungsten and also by the experiments in which two ^{60}Co thermometers were used connected by a magnesium specimen and two diffusion bonds. (Isolation between the thermometer systems was achieved by shielding each counter with about 30 cm of lead.)

The magnetic field on the specimen was made as small as possible with three pairs of Helmholtz coils. Fields could be measured with a magnetometer[15] or a rotating coil gaussmeter probe[16] and lock-in amplifier. With the apparatus out of the dewar but with the dewars at

liquid nitrogen temperature the field at the specimen site was adjusted to 0 ± 2 mOe and the field gradients, $\partial H_x/\partial x$, etc., to 0 ± 1 mOe/cm. The axial field profile was also measured. The apparatus was then replaced in the dewar. With no specimen or copper stalk on the pill the field probes could be placed at the specimen position; with a specimen, the field probes were placed just outside the measuring coils. With the probes in the specimen position it was found that after demagnetization from 46 kOe, raising the magnet and allowing it to go normal, there was a residual axial field at the sample site of between 10 mOe and 20 mOe. This field, caused by the magnetization of the surrounding laboratory, returned to zero within about a week. In an experiment with a sample in position the field on the sample could be estimated from the field measured some distance away during the experiment and from the field profile measured before the experiment. During an experiment the axial field was swept with a solenoid wound over the mutual inductance coils. The transverse field was also systematically changed by varying the currents in the Helmholtz coils. Superimposed on the static residual field was an 8 mOe pulsed field from the Bevatron with a 6 second period. The estimated field on a sample during an experiment was 0 ± 0.01 Oe.

The onset of superconductivity was detected by the change in susceptibility of the sample, which was measured with a 17-Hz commercial version[17] of the mutual inductance bridge designed by Pillinger et al.[18] The sensitivity of this bridge was improved by using a lock-in amplifier and by replacing the bridge amplifier by a lower noise operational amplifier . The mutual inductance coils, [(k), Fig. 1] had compensated

primaries and 50,000 turns of 0.0063-inch copper wire on each of two secondaries. The secondary circuit was series tuned with 2.2 μF of capacitance. The usual method of operation was to change the field on the sample by sweeping the current in a solenoid wound over the mutual inductance coils.

The mutual inductance system was sufficiently sensitive that at 5 mK the transition of a sample of 1/8-inch diameter tungsten rod of resistivity ratio 17,000 was observed with a signal to noise ratio of 50 (time constant three seconds) when the primary current in the mutual inductance coils produced an rms field of 3 mOe. The volumes of the lithium and magnesium samples used were larger than the tungsten by a factor of two to five. The resistivity ratios of the samples after mounting was not known, but the mounting procedure used strained the samples so that a resistivity ratio comparable with that of the tungsten was unlikely. Thus, even for comparable size specimens, the signal to noise ratio should have been greater than 50. Experiments on a sample of magnesium with a second thermometer mounted above the sample showed that there was no detectable difference in temperature between the two thermometers with the bridge primary field increased to 60 mOe rms.

2. Nuclear orientation thermometry

Temperatures were measured using a nuclear orientation thermometer. A single crystal of hexagonal cobalt was cut into needles with the axis of the needles parallel to the c-axis. The needles were irradiated with neutrons to produce ^{60}Co *in situ*. For a good single crystal the

large anisotropy field of 5 kOe and the small demagnetizing factor ensure that closure domains are small and most of the Co atoms are in domains magnetized along the c-axis, subjecting all the nuclei to the same hyperfine interaction. The ^{60}Co nuclei are thermally distributed among the magnetic sublevels of the ground state split by the hyperfine interaction. Gamma rays emitted from states in ^{60}Ni fed from the ^{60}Co ground state have an anisotropic distribution; the anisotropy depends on the extent of the polarization of the ^{60}Co nuclei, the nature of the gamma transitions and depolarizing effects of intermediate transitions.

The angular distribution of the gamma rays normalized to unity at high temperature is given by[19]

$$W(\theta, T) = 1 + U_2 F_2 Q_2 B_2(T) P_2(\cos\theta) + U_4 F_4 Q_4 B_4(T) P_4(\cos\theta)$$

$$\text{with} \quad U_2 F_2 = -\frac{2}{7}\sqrt{\frac{13}{6}} \quad \text{and} \quad U_4 F_4 = -\frac{\sqrt{26}}{21} \quad \text{for } ^{60}\text{Co}$$

Here Q_2 and Q_4 are solid angle corrections dependent on the experimental geometry. For this experiment $Q_2 = 0.996$ and $Q_4 = 0.985$.[20,21] These corrections differ only slightly from unity because our 3 in. $\times$ 3 in. Na(Tl) detectors were located 24 in. from the thermometer. The P_2 and P_4 functions are Legendre polynomials. The statistical tensors

$$B_k \equiv (2I+1)^{\frac{1}{2}} \sum_{M=-I}^{I} (-1)^M (IMI\text{-}M \mid IIk0)\, \rho_{MM}(T)$$

contain all the temperature dependence. The diagonal elements of the density matrix ρ_{MM} are evaluated from the spin-Hamiltonian for the parent ground state.

In assessing the merits of a thermometer for use at very low temperatures several factors must be considered: freedom from systematic errors, precision, useful temperature range, heating effects, presence or absence of fields, the time required to make a measurement and the experimental complexity of the measuring system. These factors are briefly discussed below with particular reference to ^{60}Co Co.

In principle the temperature derived from an orientation thermometer is very reliable as it comes from the Boltzmann distribution of nuclei in the parent ground state. However, the properties of the parent ground state and its modes of decay must be known. In the case of ^{60}Co Co the decay scheme is particularly simple. The ^{60}Co ground state has a half life of 5.3 yrs, I = 5+ and the splittings are well described by a hyperfine field of 227 kOe parallel to the c-axis.[22] The spin-lattice relaxation time has been measured using magnetic resonance and shown to be temperature independent at about 75 sec below 14 mK.[23] Temperatures were determined from the anisotropy of the 1.17 MeV and 1.33 MeV gamma rays emitted in the decay of ^{60}Co to ^{60}Ni.[24] The observed gamma rays, the 4+(E2)2+(E2)0+ cascade, are fed from the ^{60}Co ground state by a L=1, beta-transition to the ^{60}Ni 4+ state. Only about 1 in 10^4 of the 2+(E2)0+ transitions are fed by another decay. Since the transition is "stretched"[25, 26] the anisotropies of the two gamma rays are the same. Several values of $W(\theta = 0, T)$ are given in Table II for ^{60}Co Co.

The accuracy of a temperature measurement is influenced by the value of $\partial W(\theta, T)/\partial T$, by statistical counting errors, and by systematic errors. The time required for a measurement varies with the desired accuracy and the tolerable rate of radioactive heating. For a counting rate of 6000/min, which can be obtained with a heating rate of 0.1 erg/min, a value of $W(\theta, T)$ can be determined to ± 10 percent in 1 sec and ± 1 percent in 100 sec. It should be noted that most systematic errors tend to give too low an anisotropy; that is, the apparent temperature is too high.

To make measurements with single-crystal hcp cobalt, no electromagnetic fields are required. Since the gamma rays are very penetrating, the detectors can be outside the apparatus. A concomitant disadvantage is that it is difficult to use two thermometers with the same emitting nucleus in close proximity to each other. We have used two ^{60}Co thermometers separated by a few inches by installing lead collimators leading to separate detectors. There is no difficulty in using two thermometers with nuclei emitting gamma-rays at different energies; we have used a ^{60}Co single crystal thermometer and also a ^{54}Mn Fe foil, with polarizing field, in the same apparatus.

The main difficulties in using a gamma ray thermometer are associated with the effects of radioactive heating. (For those thermometers in which the daughter nucleus is formed by electron capture or in which an isomeric state is used, this does not apply.) We used a source giving a high-temperature counting rate of 8000/min for each 3 in. Na(Tl) detector 24 in. from the source. This introduced heat at 2 erg/min into the thermometer; in other applications with counters closer to a weaker source heating of 0.1 erg/min could be obtained for the same counting rate.

For a crystal of thickness d and cross-section A, $d << \sqrt{A}$, the thermal relaxation time of the crystal is $C_v d^2/k\pi^2$, where C_v is the volume heat capacity and k the thermal conductivity. Assuming C_v is a Schottky anomaly due to the splitting of the ^{59}Co ground state, k = T watt/K-cm, and d = 1mm, the thermal relaxation time has a maximum value of about 0.1 sec.

Thermal contact between an orientation thermometer and the surroundings must be sufficiently good that the temperature rise due to radioactive heating is small. If a soft-soldered joint is used in making contact, it has been found that for self-heating of 10^{-2} erg/sec and a contact area of $1cm^2$ at 10mK a temperature difference of order 1mK is to be expected.[27,28] For a metallic joint in which heat is conducted by electrons, such as through a screwed contact[27] or a soft-soldered joint in which trapped flux keeps the solder normal,[27] a temperature difference or order 10^{-4} mK might be expected. In our experiments the thermometer was electroplated with copper to the stalk. We observed that the lowest temperature reached by the apparatus did not change when the heat current density from the thermometer changed by a factor twenty. This suggests that for this method of joining, thermal contact is adequate.

If an orientation thermometer is used in liquid helium, as in a dilution refrigerator, the contact to the helium is relatively poor. For example, if we again assume a heat load of 10^{-2} erg/sec, a contact area of $1cm^2$, a boundary resistance of $10^{-5} / (AT^3)$ K-sec/erg,[29] we find at 10mK, ΔT = 100mK! Thus the thermometer should be attached, using copper plating or a screwed contact, to a large surface area (such as

sintered copper*) in contact with the helium. For a dilution refrigerator the thermometer should not be attached to the walls of the mixing chamber, as they may be hot through heat leaks to the chamber.[30]

To determine the anisotropy of the ^{60}Co gamma rays it is only necessary to count the number of gamma rays in a window including the two gamma photopeaks. If a polar and an equatorial counter are used, a direct measurement of anisotropy is made. If only a polar counter is used, measurements must be taken with the thermometer cold and these must be normalized to counts taken with the thermometer sufficiently warm that there is no anisotropy. The latter option was our normal operating procedure, with the addition of a final series of warm counts after the run. Care must be taken to ensure that the quantities of liquid helium and nitrogen between the thermometer and the counter remains constant during the run or the attenuation of the gamma rays will be slightly changed.

We have checked for complete saturation of the magnetization of the single crystal ^{60}Co thermometer. We compared the measured temperature with and without an external polarizing field and found that for the thermometer used in the experiments there was agreement to within the experimental error of 5 percent. The accuracy was limited by drifts in temperature due to applying the polarizing field.

---

*We have used commercial sintered copper in heat exchangers for dilution refrigerators, in particular Grade H OFHC from Pall Trinity Micro Corp and Feltmetal from Huyck Metals.

C. RESULTS

In order to check that the apparatus was working properly, the critical field curve of a sample of 99.999% tungsten[31] was measured. As described above, the tungsten was attached to the copper stalk by plating copper onto a surface of gold partially diffused into the bulk material. The resistivity ratio (4-300 K) of the sample after diffusion bonding and plating was 17,000. In addition to the transition near 15 mK, a transition was also observed near 2K. A sample which had not been subjected to the gold evaporation, heating and bonding process did not show this high-temperature transition. We attribute this transition to the presence of small amounts of β-tungsten formed during the bonding process which becomes superconducting in that region.[32, 33] The critical field curve measured in two experiments on tungsten to 5 mK gave values of H_c about 10% different from those of Black et al.[12] Furthermore, some hysteresis was observed on changing the polarity of the applied field. We think this was due to the presence of trapped flux in the β-phase. We also found that the transition occurred in a time not exceeding five seconds; occasionally superheating was observed when the transition occurred faster than the response time of the bridge. This may be compared with transition times of several minutes obtained by Black et al. In their experiment thermal contact was limited by the Kapitza boundary resistance between the sample and the ^{3}He used as a thermal contact agent. We found no difficulty in following the transition to a temperature corresponding to a critical field of about one-tenth of that at T = 0. These results show that thermal contact between pill, sample, and thermometer was adequate.

Data for the different samples of magnesium and lithium are given in Table III. We were unable to find a superconducting transition in any of the samples. This does not completely rule out the possibility that T_c is greater than 4 mK, because the samples may have supercooled. For pure, unstrained materials with a transition temperature in the millikelvin range, the coherent length ξ at $T = 0$ is very long, giving a small Ginsberg-Landau κ and type I superconductivity. At a temperature at which the thermodynamic critical field is H_c the lowest field to which the sample can remain normal is $H_{c3} = 2.4\,\kappa H_c$ for surface nucleation, and $H_{c2} = \sqrt{2}\,\kappa H_c$ for bulk nucleation. In Table IV estimates of H_{c2}, H_{c3}, ξ, and κ are given in the clean and dirty limits. Nucleation of the transition above H_{c2} or H_{c3} can occur if nucleation centers exist and are effective. Faber and Pippard[34] have shown that in aluminum and tin the criterion for a flaw of size δ to be effective is $\delta \gg \xi$. In experiments on aluminum they estimated that flaws of 10^{-3} - 10^{-4} cm existed in their specimens. These experiments were made in the middle of carefully made rods of material as nucleation appeared to start at the ends of the rods or at other surface irregularities. This is the usual situation for superconductors with critical temperatures of 1 K or higher--special care is usually necessary to observe appreciable supercooling. For low T_c superconductors it may be more difficult to achieve nucleation since ξ is larger. However, in their experiments on tungsten, Black et al.[12] found that nucleation occurred at about 0.2 H_c unless the surface had been specially prepared; we also found that tungsten did not supercool below 0.2 H_c.

Our magnesium samples were far from homogeneous; parts of the surface were covered with a gold diffusion layer and the clamps used during the diffusion bonding process produced varied strains in the crystals. The lithium samples self-annealed at room temperature after the mounting process but the martensitic transformation severely strained the crystal each time it was cooled. Therefore, it is clear that our lithium and magnesium samples were strained to a greater degree than the tungsten sample. Nevertheless, if T_c is lower than for tungsten, ξ might be longer and it could be more difficult to achieve nucleation in spite of the less perfect state of the samples. Since the mechanism by which defects act as nucleation centers is not understood in detail, it is not possible to predict with any degree of certainty the supercooling behavior of the lithium and magnesium samples from that of tungsten and higher T_c superconductors. However, as a rough guess, it seems probable that a transition would have been observed if T_c were as high as 6 mK. For $T_c = 6$ mK, $H_c(4\text{ mK}) \approx 0.15$ Oe, and between 4 mK and 5 mK the samples would, at some time, have been in a field that was only 4% of H_c. Furthermore, at 4 mK ξ would have a value comparable to its 0 K value.

D. CONCLUSION

We have cooled lithium and magnesium to 4 mK in magnetic fields of 10^{-2} Oe and to 5 mK at 5×10^{-3} Oe without observing superconducting transitions. The possibility that the samples supercooled precludes setting a definite upper limit to T_c, but it seems probable that $T_c < 6$ mK. At best, we have explored 60% of the temperature range predicted for T_c for magnesium; for lithium the theoretical estimates of T_c are so much in doubt that we may still be far from the region of the transition.

APPENDIX

THE HEAT CAPACITY OF TUNGSTEN - IMPLICATIONS FOR THE CERIUM MAGNESIUM NITRATE TEMPERATURE SCALE

Black, Johnson, and Wheatley[12] have recently reported a detailed analysis of the critical field curve for superconducting tungsten. The analysis is of particular interest in relating the thermodynamic temperature T to the magnetic temperature T^* defined by setting $\chi(CMN) = C/T^*$ where $\chi(CMN)$ is the magnetic susceptibility of powdered CMN in the form of a right circular cylinder with height equal to diameter.

The superconducting critical field H_c can be related to the thermodynamic temperature T by the relationship

$$\frac{d(H_c^2)}{dT^2} = \frac{4\pi}{V_m T} [S_s(T) - S_n(T)] \tag{5}$$

where S_s and S_n are the molar entropies of the superconducting and normal states, respectively, and V_m is the molar volume. For sufficiently low temperatures, $S_s \ll S_n = \gamma T$ assuming all other contributions to the entropy are either small or equal in the normal and superconducting state (the lattice entropy for tungsten is negligible at these temperatures so difficulty from this source can be discounted). Therefore, Eq. (5) gives

$$H_c^2 = H_c^2(T = 0) - (4\pi\gamma) T^2 \tag{6}$$

valid as $T \to 0$ (γ/V_m is referred to as γ with the appropriate units - see Table IV).

To first order the effects of magnetic interactions and sample shape may be represented by an "effective Weiss θ" usually referred to as Δ. The authors of Ref. 12 consider the equation

$$T = T^* + \Delta \tag{7}$$

and find that different choices of Δ lead to different values of γ as determined from the slope of H_c^2 versus $(T^* + \Delta)^2$. The choice $\Delta = 0$ was in agreement with the range of values reported in calorimetric determinations of γ, and they note that this choice leads to a critical field curve in good agreement with BCS theory. Lacking any more sensitive test for the true γ value, they chose $\Delta = 0$.

The values of γ reported in the literature[35-37] do not agree well at all, and the discrepancies have been assumed to be partially due to the effect of impurities - especially magnetic impurities - on the low temperature heat capacity. Because of the importance of an accurate value of γ to the analysis and conclusion contained in Ref. 12, the heat capacity of a 1/4" tungsten rod with resistivity ratio 57,000 (see Table III) was measured from 0.3 K to 25 K. The value obtained for the normal state coefficient of the linear term in the heat capacity, $\gamma = (1.005 \pm .005)$ mJ/mole-K,^{2} is not in agreement with the results of the analysis in Ref. 12 and suggests possible corrections to the temperature scale based on powdered CMN.

The tungsten sample weighed 80 g. and was mounted with a threaded copper bushing to the sample holder shown in Fig. 4 of Part I. The tungsten rod was not threaded but was slightly beveled on the mounting end so the bushing could be screwed hand tight over ~1/4" of the end section. No thermal contact agent was used, and relaxation times were essentially instantaneous in spite of the small contact area. The heat capacity of the very high purity copper sample from which the bushing was made was measured in a separate experiment. The contribution from the bushing was subtracted, together with the carefully calibrated calorimeter,

from the total heat capacity measured for the sample plus mounting assembly.

In an attempt to eliminate all extraneous error from impurities, the susceptibility of the tungsten sample was checked from 0.3 K to 15 K. Below 3 K the susceptibility was constant and no evidence was found for the presence of the superconducting β phase of tungsten or localized moments. Above 3 K the susceptibility varied smoothly and increasingly more rapidly as linear thermal expansion of the sample and sample holder changed the volume of the sample sensed by the secondary coil.

In spite of these precautions and the very high resistivity ratio of the sample, it was felt advisable to check for the presence of paramagnetic impurities by making calorimetric measurements in a magnetic field. In Table V the heat capacity data for the tungsten sample are listed. In addition to the zero field data, results are listed for magnetic fields of 1 and 38 kOe. The 38 kOe data have been corrected for the substantial nuclear contribution of the copper (since the field on the calorimeter is highly inhomogeneous, a measured value has been used to derive the appropriate nuclear contribution - see Part I, Section E.2).

The low temperature data for tungsten in 0, 1, and 38 kOe are shown in Fig. 2. The zero field data do shown an anomalous structure below 1 K which is enhanced in 1 kOe but completely suppressed in 38 kOe. Fortunately, the nuclear contribution from ^{183}W is always less than the scatter in our data, and the 38 kOe results define an excellent straight line on the plot of C/T vs T^2. The intercept in Fig. 2 defines $\gamma = (1.005 \pm .005)$ mJ/mole - K^2 and the slope gives $\Theta = (379 \pm 2)$K in excellent agreement with values previously reported.[35,37] The temperature dependence of Θ may be obtained from the higher temperature data listed in Table V and is in agreement with

previously reported behavior.[37] The purity of the sample was high enough so that the total anomalous effects at low T are only ~1% of the electronic heat capacity.

The electronic heat capacity coefficient per unit volume $\gamma = 1056 \pm 5$ erg/K^2/cm^3 allows us to estimate Δ in Eq. (7). Figure 3 shows the data of Black, et al. on a plot of H_c^2 versus $(T^* + \Delta)^2$ for the choices $\Delta = 0$ and $\Delta = -.4$ mK. The straight line through the data for $\Delta = 0$ corresponds to $\gamma = 915$ erg/K^2/cm^3 in poor agreement with our γ value. The choice $\Delta = -.4$ mK, on the other hand, allows a straight line to be drawn through the data with the slope obtained from our calorimetric determination of γ.

The data in Fig.3 deviate from a straight line for both choices of Δ. A correction to the applied magnetic field has been proposed in Ref. 12. Such a correction is expected to arise from the close proximity of the paramagnetic CMN to the tungsten sample, and the authors of Ref. 12 estimate an increase $\Delta H/H = (2 \pm 1)\%$ (1 mK/T) that will correct the low temperature deviations for either choice of Δ in Fig. 3.

Although the value $\Delta = -.4$ mK provides an easy interpretaton of the tungsten results, there have been other experiments done with the same CMN thermometer that provide evidence for $|\Delta| < .2$ mK.[38] While it seems that the interpretation of these experiments would not be altered much and might, in fact, be somewhat more satisfying with the choice $\Delta = -.4$ mK, it is essential to consider possible sources of error in the critical field measurements. The two factors which appear to be relatively unknown are the exact value of the field enhancement produced by the

paramagnetic CMN and the effect of small amounts of magnetic impurities on the critical field curve of tungsten.

Table I. Comparison of theoretical and empirical empirical values of λ.[a]

	Be	Mg	Zn	Cd
Value of λ calculated by Allen and Cohen	0.26	0.31	0.42	0.40
Value of λ derived from heat capacity enhancement	0.25	0.33	0.43	0.36
Value of λ derived from Eq. (4).	0.23	--	0.38	0.38

[a]See Ref. 1.

Table II. Values of W(0, T) for ^{60}Co in Co thermometer (with $Q_2 = Q_4 = 1$)

T(mk)	$B_2(T)$	$B_4(T)$	W(0, T)
1.0	1.6964	1.1721	0.00197
1.5	1.6823	1.1399	0.01574
2.0	1.6517	1.0727	0.04491
2.5	1.6086	0.9831	0.08478
3.0	1.5574	0.8846	0.1303
3.5	1.5015	0.7861	0.1777
4.0	1.4430	0.6928	0.2249
4.5	1.3837	0.6075	0.2706
5.0	1.3244	0.5314	0.3141
5.5	1.2658	0.4630	0.3552
6.0	1.2085	0.4036	0.3938
6.5	1.1528	0.3519	0.4297
7.0	1.0989	0.3069	0.4633
8.0	0.9970	0.2343	0.5238
9.0	0.9037	0.1802	0.5762
10.0	0.8191	0.1396	0.6216
12.0	0.6745	0.0861	0.6954
14.0	0.5591	0.0551	0.7515
16.0	0.4670	0.0364	0.7948
18.0	0.3939	0.0248	0.8283
20.0	0.3352	0.0174	0.8548
25.0	0.2329	0.0080	0.9002
30.0	0.1695	0.0041	0.9277
35.0	0.1283	0.0023	0.9455
40.0	0.1002	0.0014	0.9575
45.0	0.0803	0.0009	0.9660
50.0	0.0657	0.0006	0.9722
100.0	0.0168	0.00004	0.9928

Table III. Samples

	Supplier	Purity	Initial resistivity ratio	Bonding method
Li I	Bram Metallurgical	99.9+%	825	Local welding
Li II	P. H. Schmidt[d]	99.9998%	4×10^3	Metal-metal pressure contact
Mg I	R. A. Stark[e]		$\sim10^6$[b]	Gold diffusion bond
Mg II	Research Organic/ Inorganic Chemical Corporation	99.99%	330[a]	Local welding
Mg III	R. A. Stark		$\sim10^6$[b]	Gold diffusion bond
W	Semi-Elements	99.999%	5.7×10^4[a, c]	Gold diffusion bond-Cu plate

[a]Resistivity ratios determined by the authors by potentiometric and eddy current techniques agreed to within 20% on the samples of tungsten and magnesium.

[b]Mean free path of similar samples grown by the author were ~ 15 cm.

[c]This resistivity ratio was measured on a different sample, from the same supplier, from the one used in the experiment.

[d]J. Electrochemical Soc. 113, 201(1966).

[e]Bull. Am. Phys. Soc. 11, 169(1966).

Table IV. Superconductive parameters for Li, Be, W, and Mg.

	Li	Be	W	Mg	Unit
T_c, superconducting transition temperature (measured)		0.026	0.0154		K
(assumed)	0.004			0.004	
ρ_{300}, resistivity at room temperature	9.4	3.6	5.3	4.3	$\mu\Omega$-cm
γ, electronic specific heat coefficient	1250	470	1056[a]	930	erg $K^{-2}cm^{-3}$
γ/γ_0	2.2	0.428	0.663	1.33	
H_c, thermodynamic critical field at 0 K	0.355	1.3	1.15	0.306	Oe
S/S_0, ratio of Fermi surface area to FEM area	0.787[b]	0.65[b]	0.111[c]	0.60[d]	
$v_F = h/m(3\pi n)^{1/3}$ = Fermi velocity in FEM	1.285×10^8	2.25×10^8	2.20×10^8	1.58×10^8	cm/sec
$v_F^* = (\gamma_0 S/\gamma S_0)v_F$ = renormalized Fermi velocity	0.46×10^8	3.42×10^8	0.369×10^8	0.713×10^8	cm/sec
$\xi_0^* = 0.18(hv_F^*/k_BT_c)$, renormalized coherence distance	0.0158	0.0181	0.0032	0.0245	cm
$\lambda_L^*(0) = (\pi/\gamma)^{1/2}ck_B/2ev_F^*$, renormalized penetration depth	4.69×10^{-6}	1.03×10^{-6}	6.36×10^{-6}	3.52×10^{-6}	cm

Table IV. (Continued)

	Li	Be	W	Mg	Unit
$\kappa_c^* = 0.96\ \lambda_L^*(0)/\xi_0^*$, renormalized GL parameter in clean limit	2.87×10^{-4}	0.55×10^{-4}	1.92×10^{-3}	1.38×10^{-4}	
$\kappa_d = 0.75\ \lambda_L^*(0)/\ell = 7.9\times 10^{-3}\ \rho\gamma^{1/2}$ (ρ in $\mu\Omega$ cm GL parameter in dirty limit[e])	0.0263	0.00617	0.0136	0.0103	
H_{c3} clean $= 2.4\ \kappa_c^* H_c$	2.45×10^{-4}	1.75×10^{-4}	5.30×10^{-3}	1.01×10^{-4}	Oe
H_{c3} dirty[e] $= 2.4\ \kappa_d H_c$	0.022	0.019	0.037	0.0076	Oe

[a] From heat capacity measurements on a sample similar to that used in these experiments (see Appendix).

[b] Estimated from the reduced resistivities--see J. M. Ziman, Electrons and Phonons.

[c] E. Fawcett and D. Griffiths, J. Phys. Chem. Solids 23, 1631 (1962).

[d] E. Fawcett, J. Phys. Chem. Solids 18, 320 (1961).

[e] Resistivity ratio of 100 assumed.

TABLE V. The Heat Capacity of Tungsten

Zero Field

N	T(K)	C(mJ/mole-K)
1	.35162	.36222
2	.38537	.39616
3	.42554	.43424
4	.47486	.48436
5	.52353	.53599
6	.56818	.58127
7	.61956	.63603
8	.67492	.69462
9	.73538	.75967
10	.80147	.83040
11	.87617	.91185
12	.94239	.98538
13	1.02372	1.07522
14	1.10605	1.16389
15	1.18725	1.25292
16	1.27111	1.35089
17	1.36998	1.47167
18	1.47911	1.60670
19	1.61543	1.78222
20	1.75060	1.96599
21	1.92292	2.20500
22	2.11704	2.49093
23	2.32040	2.81369
24	2.53382	3.16520
25	2.76262	3.57554
26	3.03991	4.11021
27	3.34711	4.76321
28	3.69377	5.58499
29	4.05677	6.53906
30	4.42574	7.61742
31	4.85191	9.03339
32	5.35235	10.89780
33	5.91967	13.31875
34	6.23062	14.86947
35	6.85894	18.40091
36	7.45870	22.21969
37	8.09253	26.82660
38	8.87214	33.46471
39	9.74702	42.29505
40	10.64016	53.14511
41	11.59954	66.61240
42	12.52772	82.00677
43	13.80607	107.67655
44	15.27013	144.03637
45	16.87893	195.28311
46	18.69170	268.93572
47	20.51923	364.50038
48	22.35096	490.36847

1.0 kOe Field

N	T(K)	C(mJ/mole-K)
1	.36973	.38357
2	.41574	.42744
3	.46492	.47661
4	.51730	.53024
5	.57702	.59314
6	.63728	.65829
7	.69695	.72484
8	.75889	.79184
9	.83324	.86609
10	.90342	.94042
11	.98450	1.02512
12	1.07937	1.13250
13	1.18738	1.25442
14	1.30961	1.40041
15	1.43715	1.55101
16	1.60222	1.76665
17	1.71041	1.91141
18	1.88440	2.15127
19	2.07845	2.43616
20	2.32846	2.82622
21	2.56274	3.21881
22	2.82544	3.69450
23	3.15905	4.35811
24	3.53142	5.17130
25	3.88230	6.06813
26	4.29320	7.21376
27	4.72493	8.60486
28	5.21103	10.38141
29	5.74961	12.52831

38 kOe Field

N	T(K)	C(mJ/mole-K)
1	.46664	.47292
2	.51794	.52667
3	.56376	.57500
4	.59917	.61007
5	.65906	.67213
6	.72649	.74653
7	.80576	.83012
8	.88955	.91907
9	.95203	.98886
10	1.04127	1.08825
11	1.13883	1.19690
12	1.24760	1.32045
13	1.37046	1.47664
14	1.49816	1.63813
15	1.65352	1.83867

REFERENCES

1. P. B. Allen, M. L. Cohen, Phys. Rev. 187, 525 (1969).
2. W. L. McMillan, Phys. Rev. 167, 331 (1968).
3. P. Morel, P. W. Anderson, Phys. Rev. 125, 1263 (1962).
4. R. L. Falge, N. M. Wolcott, R. A. Hein, J. E. Cox, J. W. Gibson, Bull. Amer. Phys. Soc. 13, 730 (1968).
5. W. A. Goddard, Phys. Rev. 174, 659 (1968).
6. C. S. Barrett, O. R. Trautz, Trans. Amer. Inst. Min. (Metall.) Engr. 175, 579 (1948).
7. H. G. Smith, G. Dolling, R. N. Nicklow, P. R. Vijayazaghavan, M. K. Wilkinson, Proc. Conf. on inelastic neutron scattering, Copenhagen (1968).
8. D. L. Martin, Proc. Roy. Soc. A263, 378 (1961).
9. D. Hill, H. M. Rosenberg, Cryogenics 1, 27 (1960).
10. B. B. Goodman, Nature 167, 111 (1951).
11. A. O. E. Animalu, F. Bonsignori, V. Bortolani, Nuovo Cimento 42B, 83 (1966).
12. W. C. Black, R. T. Johnson, J. C. Wheatley, J. Low Temp. Phys. 1, 641 (1969).
13. W. D. Brewer, Ph. D. Thesis, University of California, Berkeley, UCRL-19533, Dec. 1969.
14. Furane Plastics, 4516 Brazil Street, Los Angeles, California.
15. Magnatest Millioersted Meter Model FM-204, MagnaFlux Corp., Chicago, Ill.

16. Probe Type 720S. Rawson Electrical Instrument Co., Cambrige, Mass.

17. Model ML17B; Cryotronics Inc., High Bridge, New Jersey.

18. W. L. Pillinger, P. S. Jastrum, J. G. Daunt, Rev. Sci. I. 29, 159 (1958).

19. R. J. Blin-Stoyle, M. A. Grace; Handbuch der Physik, ed. S. Flügge (Springer-Verlag, Berlin, 1957), 42, p. 555.

20. A. R. Rutledge, Chalk River Project Report CRP-851 (1959).

21. M. J. L. Yates; Alpha-, beta- and gamma-ray Spectroscopy (1965), ed. K. Siegbahn Vol. II, p. 1691.

22. W. A. Hardy, J. Appl. Phys. 32, 122S(1961).

23. W. D. Brewer, D. A. Shirley, J. E. Templeton, Phys. Letters 27A 81(1968).

24. C. M. Lederer, J. M. Hollander, I. Perlman, Table of Isotopes, Wiley (1967).

25. J. Weneser, D. R. Hamilton, Phys. Rev. 92, 321 (1953).

26. R. W. Grant, D. A. Shirley, Phys. Rev. 130, 1100 (1963).

27. M. Suomi, A. C. Anderson, B. Holmström, Physica 38, 67(1968).

28. W. A. Steyert, Rev. Sci. I. 38, 964 (1967).

29. J. C. Wheatley, O. E. Vilches, W. R. Abel, Physics 4, 1 (1968).

30. H. London, E. Mendoza, Proc. 11th Int. Conf. on L. T. Phys. (1968) ed. J. F. Allen, D. M. Finlayson, D. M. McCall, I p. 89.

31. Semi-Elements Inc., Saxonburg Blvd., Saxonburg, Pa.

32. W. L. Bond, A. S. Cooper, K. Andres, G. W. Hull, T. H. Geballe, B. T. Mathias, Phys. Rev. Lett. 15, 260 (1965).

33. S. Basavaiah, S. R. Pollack, Appl. Phys. Lett. 12, 259 (1968).

34. T. E. Faber, Proc. Roy. Soc. A231, 353 (1955).

35. J. P. Maita, Private communication with the authors of Ref. 12.

36. E. Bucher, F. Heiniger, and J. Muller, Proceedings of the Ninth International Conference on Low Temperature Physics, J. G. Daunt, D. O. Edwards, F. J. Milford and M. Yaqub, eds. (Plenum Press, New York, 1965), p. 1059.

37. T. E. Waite, R. S. Craig, and W. E. Wallace, Phys. Rev. 104, 1240 (1956).

38. J. C. Wheatley, Ann. Acad. Fennicae AVI, No. 210, 15 (1966).

FIGURE CAPTIONS

Fig. 1. Detail of lower section of apparatus.

Fig. 2. Heat capacities of tungsten.

Fig. 3. Plot of the square of the critical field for superconducting tungsten (after W. C. Black, et al., Ref. 12) versus $(T^* + \Delta)^2$ below 20 mK.^{2} Black's data has been plotted for $\Delta = 0$ and $\Delta = -.4$ mK. The straight lines drawn through the data correspond to $\gamma = 915$ erg/K^2/cm^3 and 1056 erg/K^2/cm^3, respectively.

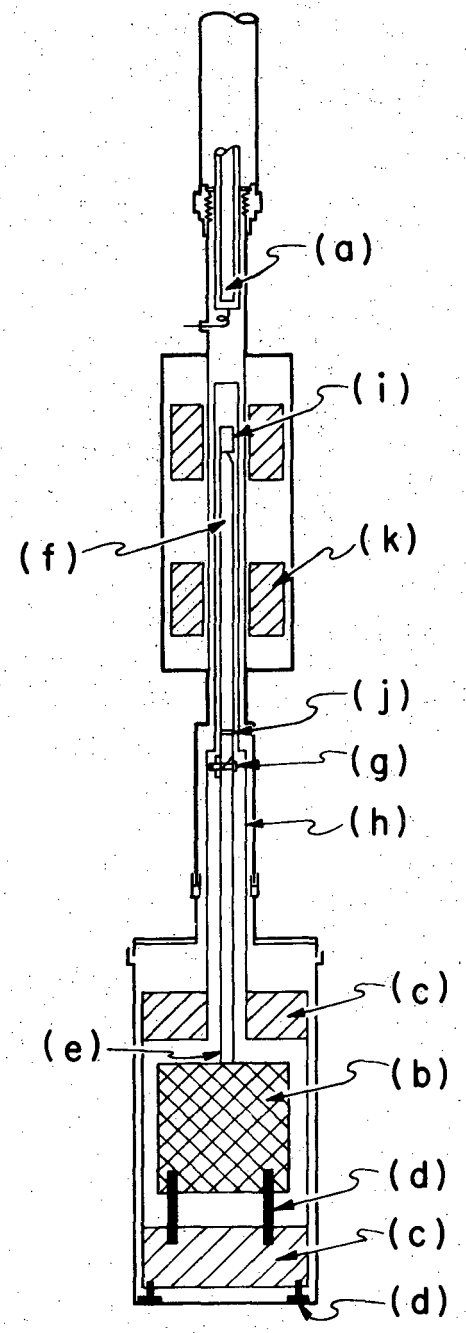

XBL706-3185

Fig. 1

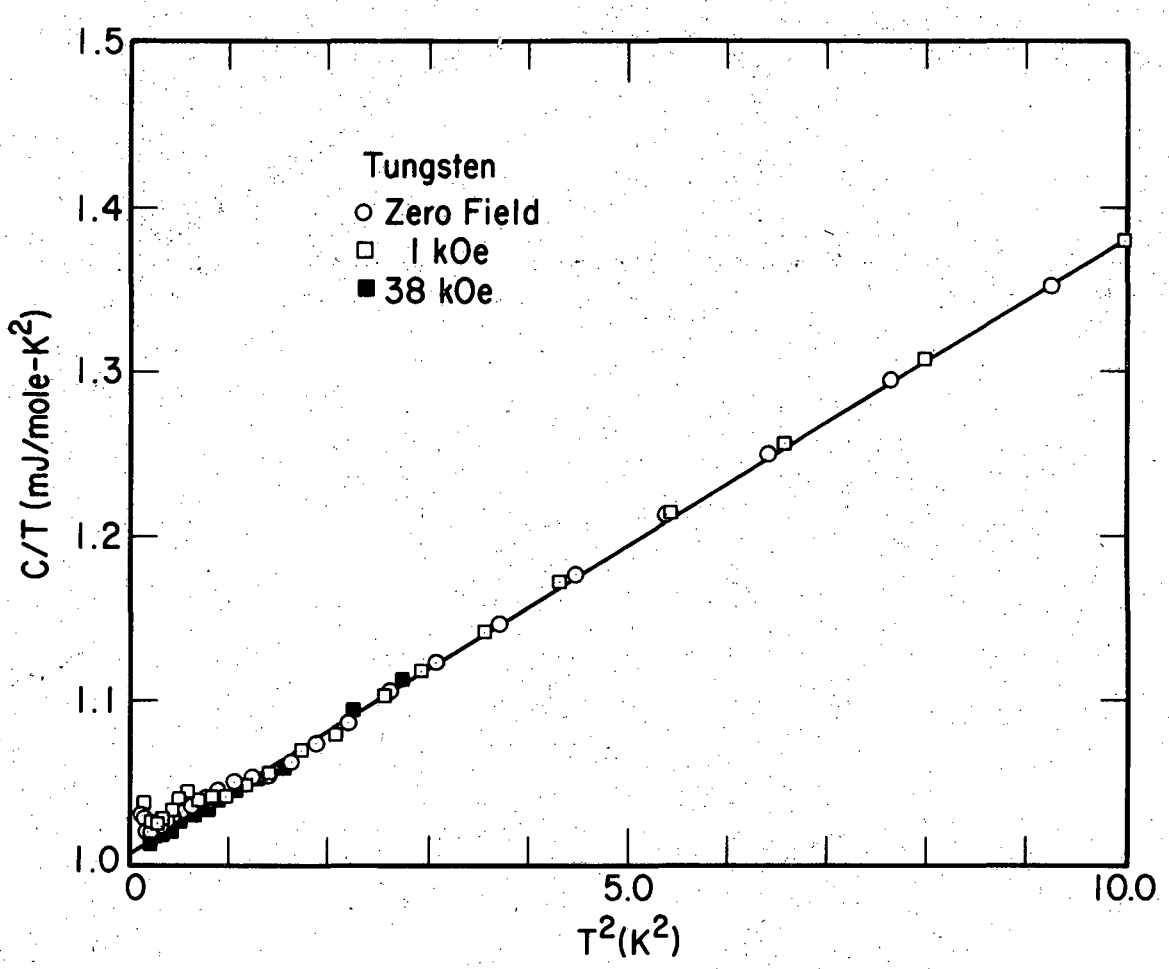

XBL 709-6591

Fig. 2

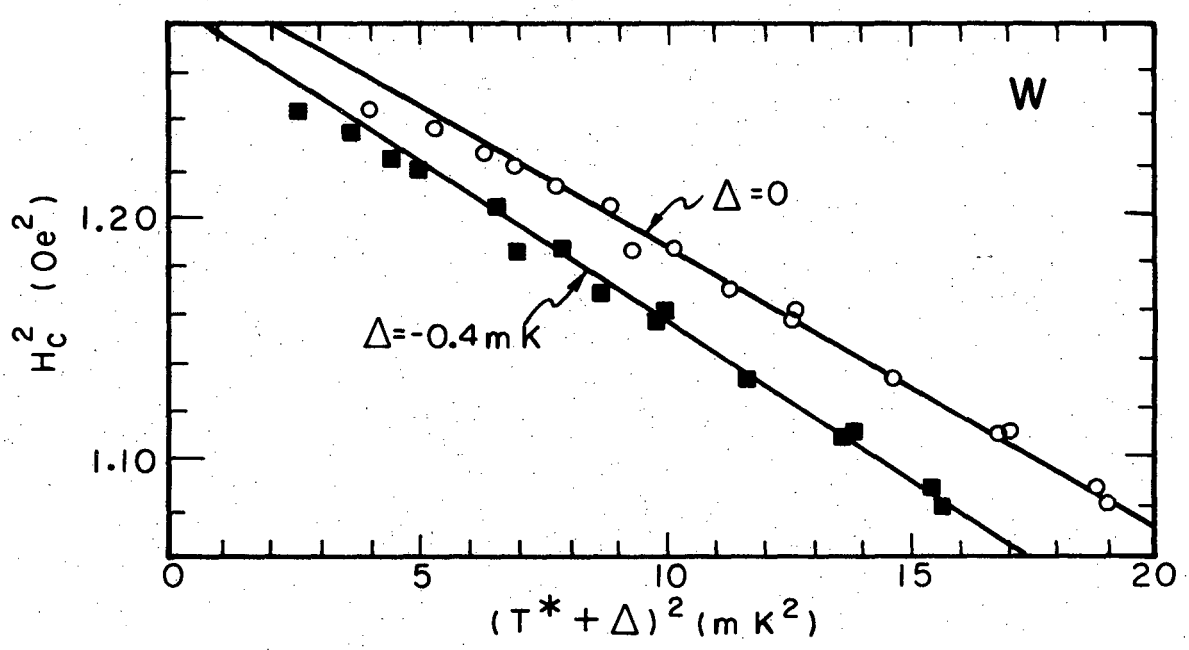

XBL709-3873

Fig. 3

ACKNOWLEDGMENTS

My years of doctoral study at Berkeley have certainly been among the most pleasant and most stimulating of my life. This is certainly due in no small measure to the environment in which I have been able to work.

It is often difficult to believe doctoral theses are worth the effort. Perhaps the most important single factor in making my graduate years so pleasurable was the continuing interest of my friends and colleagues in my thesis research and their willingness to listen to problems associated with it. In particular I wisk to thank Professor Norman E. Phillips for his interest, concern, encouragement, and guidance and all the members of our group who have been able to listen and contribute: Dr. J. K. Hoffer, Dr. C. G. Waterfield, Dr. J. C. F. Brock, Mary Conway, Gary P. Schwartz, Samuel Bader, Howard Simon, David Woody, Robert Estill and Robert Kleinberg.

Special thanks is due to Dr. T. L. Thorp with whom I was privileged to work on the magnesium-lithium project and who taught me to try to approach experimental problems with patience, persistence, and organization. Dr. Thorp and I would like to thank Drs. R. W. Stark and P. H. Schmidt for the high purity magnesium and lithium samples and Dr. W. C. Black for sending us the superconducting critical field data for tungsten. We also wish to extend particular gratitude to Drs. D. A. Shirley, W. D. Brewer, J. E. Templeton, and the rest of Prof. Shirley's group for introducing us to the techniques of nuclear orientation thermometry and single stage demagnetization of CMN into the low millikelvin temperature region.

I wish to thank the support staffs of the Department of Chemistry and the Lawrence Radiation Laboratory for their assistance. Special mention should be made of Mr. Stanley Ross, who prepared the Cu-Cr samples, Mr. Robert Giauque, who did the chemical analysis on them, and Mr. Tom Morrison, who did the chemical analysis on the Cu-Fe system.

The groundwork for my thesis was laid by Dr. J. C. F. Brock and Gary P. Schwartz, who explored the interaction regime of Cu-Fe and anticipated the detection of the dilute impurity limit. I wish to thank Dr. D. H. Hamann for sending me the data from his theoretical calculation on of the Kondo specific heat anomaly and Dr. Albert Narath for imformative discussions.

Lastly, I want to express particular gratitude to my fianceé, Linda Biber, and my sister, Mary Gean Edwards, for their patience, cooperation, and encouragement in helping me complete this thesis.

This work was performed under the auspices of the United States Atomic Energy Commission.

LEGAL NOTICE

This report was prepared as an account of Government sponsored work. Neither the United States, nor the Commission, nor any person acting on behalf of the Commission:

A. Makes any warranty or representation, expressed or implied, with respect to the accuracy, completeness, or usefulness of the information contained in this report, or that the use of any information, apparatus, method, or process disclosed in this report may not infringe privately owned rights; or

B. Assumes any liabilities with respect to the use of, or for damages resulting from the use of any information, apparatus, method, or process disclosed in this report.

As used in the above, "person acting on behalf of the Commission" includes any employee or contractor of the Commission, or employee of such contractor, to the extent that such employee or contractor of the Commission, or employee of such contractor prepares, disseminates, or provides access to, any information pursuant to his employment or contract with the Commission, or his employment with such contractor.

TECHNICAL INFORMATION DIVISION
LAWRENCE RADIATION LABORATORY
UNIVERSITY OF CALIFORNIA
BERKELEY, CALIFORNIA 94720